Spatial heterogeneity tunes the behavior of bacterial genetic circuits

Carlos Barajas[1] and Domitilla Del Vecchio[1*]

[1] Department of Mechanical Engineering, Massachusetts Institute of Technology, Cambridge, Massachusetts

[*] Correspondence: ddv@mit.edu

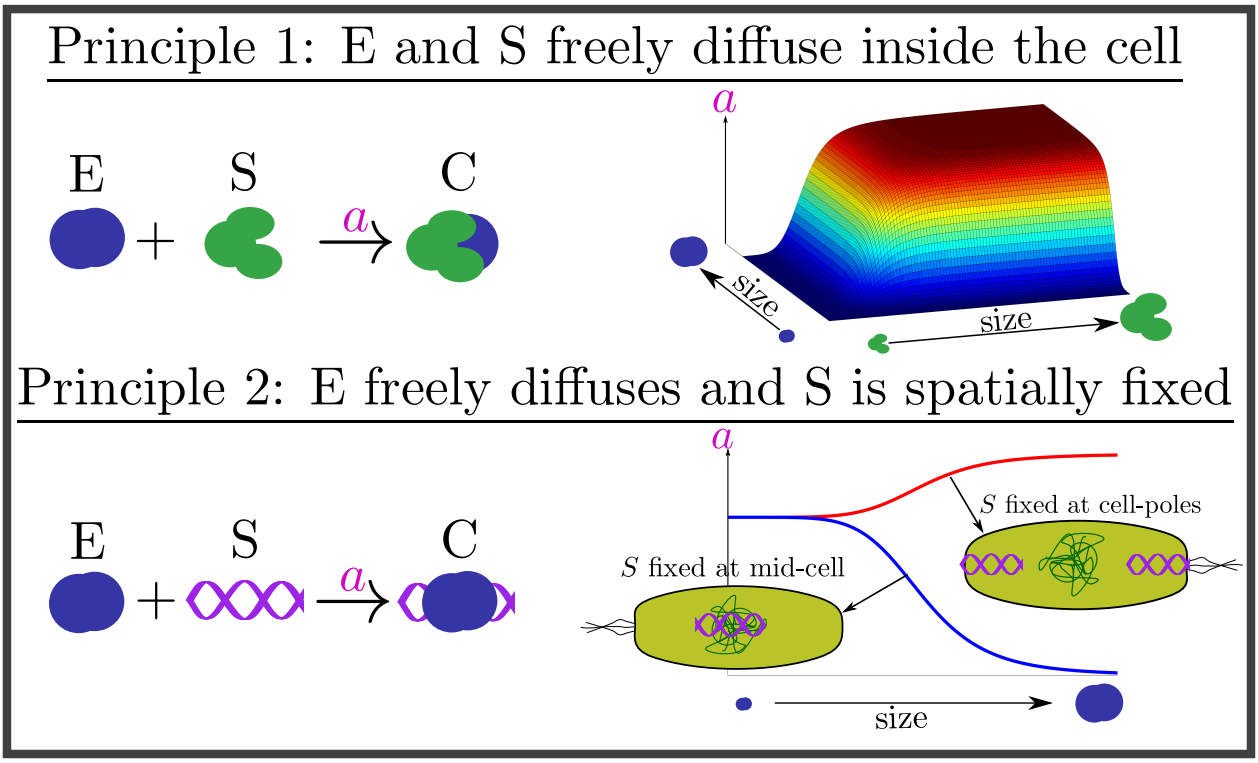

Highlights:

- Intracellular spatial heterogeneity modulates the effective association constant of binding reactions
- A well-mixed model can be appropriate despite spatial heterogeneity
- Chromosome genes are less effectively regulated than pole-localized plasmid genes and this difference increases with regulator size
- Intracellular spatial heterogeneity affects genetic circuit dynamics

Statement of significance: We derive a general and simple ordinary differential equation model that captures spatial heterogeneity in the dynamics of gene networks. This model accounts for freely diffusing species inside bacteria are pushed out of the tightly packed chromosome and localize at the cells poles (*excluded volume effects*). We discover that transcription and its regulation is less effective for genes in the chromosome than is for genes in pole-localized plasmids. Furthermore, the rate at which two freely diffusing molecules bind (e.g, mRNA-ribosome) increases with molecule size. These results indicate that the size of diffusing regulators and the location of regulated genes are important parameters that affect genetic circuit behavior. We illustrate that the operation of well-known genetic circuits is dramatically impacted by these parameters.

Abstract

Deterministic ordinary differential equation (ODE) models of genetic circuits, commonly assume a well-mixed ensemble of species inside the cell. However, intracellular spatial heterogeneity is frequently observed experimentally, with a circuit's DNA location and volume occupied by the chromosome (excluded volume effects) as two primary variables. Here, we derive a reduced ODE model that captures spatial effects, yet has the same structure as commonly used "well-mixed" models. Specifically, the only difference with respect to a well-mixed model, is that the association rate constant of binding reactions is multiplied by a coefficient, which we refer to as the *binding correction factor* (BCF). The BCF depends on the size of interacting molecular species and on their location (poles versus chromosome) if fixed in space. In particular, the effective association rate constant between genes and RNAP (or transcription factors) is lower for genes near mid-cell than for those in the cell poles and thus the transcription rate of genes is less (more) effectively regulated for genes near mid-cell (cell poles). The effective ribosome binding strength (RBS) is always greater relative to a well-mixed model and thus our proposed model predicts higher translation rate. Therefore, location of DNA and transcription factor size determine the behavior of genetic circuits. As an example, we show that for a circuit that produces sustained oscillations according to a well-mixed model may instead result in no oscillations according to our model that accounts for spatial heterogeneity. Our model has broad validity as we derived it from a general reaction-diffusion partial differential equation (PDE) model by only using time scale separation between diffusion and chemical reactions. Since our reduced model is an ODE with the same dimension as a well-mixed model, it is computationally advantageous with respect to PDE also for computational studies. Therefore, this work provides an analysis tool that easily incorporates intracellular heterogeneity in gene network models and also an engineering method to exploit spatial effects in the design of genetic circuits.

Introduction

Deterministic models of gene circuits typically assume a well-mixed ensemble of species inside the cell [1, 2]. However, it is well known that spatial heterogeneity is prevalent inside bacterial cells [3, 4, 5, 6, 7, 8]. Depending on the origin of replication, plasmids tend to localize within bacterial cells [9, 10, 11]. Furthermore, chromosome genes (endogenous and synthetically integrated ones [12]) are distributed in the cell according to the chromosome complex spatial. In bacterial cells, any molecule freely diffusing through the chromosome (e.g., mRNA, ribosome, and protease) experiences what are known as *excluded volume effects*, which capture the tendency of species to be ejected from the nucleoid due to the space occupied by the dense DNA mesh [13]. These excluded volume effects for ribosomes and RNAP in bacteria have been observed experimentally [14].

Despite the strong evidence in support of spatial heterogeneity within bacterial cells, no standard modeling framework exists that captures the spatial-temporal organization of molecules inside the cell. Partial differential equation (PDE) models have been employed on an *ad hoc* basis to numerically capture intracellular spatial dynamics for specific case studies [15, 16, 17]. Although a general PDE model of a gene interaction network (GRN) can be consulted, it is difficult to analyze and impractical for design [18]. Recently matched asymptotic methods were used to simplify the PDEs to a set of ODEs to analyze ribosome-mRNA interactions [19]. Similarly, [20] used a compartmentalized model to capture spatial heterogeneity in sRNA-mRNA interactions. However, these results have not been extended to genetic circuits and relied only on simulation with specific parameter values.

In this paper, we provide a general framework to model spatial heterogeneity without increasing model complexity relative to a well-mixed model. To this end, we first introduce a PDE model to capture spatial dynamics. Next, we exploit the time scale separation between diffusion and the biochemical reaction dynamics to derive a reduced order ODE model of the spaced averaged dynamics. This model accounts for spatial heterogeneity by multiplying the association rate constant of bimolecular interactions by a factor that depends on the size of freely diffusing species (e.g., mRNA) and on the location of spatially fixed species (e.g,. DNA). Thus, this reduced model has similar computational cost as current well-mixed models, yet it captures spatial effects.

We demonstrate the importance of spatial heterogeneity in genetic circuit behavior by modeling and analyzing several core biological processes. We show that the transcription rate of a gene and the affinity at which transcription factors bind to it, is lower (higher) when the gene is located near mid-cell (cell poles) with respect to the well-mixed model. We show that compared to a well-mixed model, translation rate is always higher and increases with mRNA size. Finally, we consider a genetic clock, a circuit that produces sustained oscillations. We show that for a parameter range where a well-mixed model predicts sustained

oscillations, a model that accounts for spatial heterogeneity of DNA may not. All of these phenomena can be captured when diffusion is fast using our reduced ODE model.

Methods

We use mathematical models to investigate the effects of spatial heterogeneity, specifically DNA localization and excluded volume effects. The first part of this section introduces the mathematical model used, a set of nonlinear PDEs. Model reduction is performed on the resulting PDEs to obtain a reduced ODE model.

0.1 Reaction-Diffusion Model

A reaction-diffusion model describes the concentration of a species at a given time and location in the cell. We focus on enzymatic-like reactions since they can be used to capture key processes in the cell.We specialize the model to the cases where the reacting species both freely diffuse or where one freely diffuses while the other one is fixed. For example, mRNA and ribosomes are both freely diffusing, while RNA polymerase and DNA are one freely diffusing and the other one is fixed.

0.1.1 Reaction Models: Enzymatic-like Reactions that Model Key Biological Processes

Let S be a substrate being shared by n enzymes $\mathrm{E_i}$, to form product $\mathrm{P_i}$ where $i = 1, \ldots, n$. The rate at which $\mathrm{E_i}$ and S are produced is given by α_i and α_s, respectively. The decay rates of $\mathrm{E_i}$ and S are given by γ_i and γ_s, respectively. Here, we assume that $\mathrm{E_i}$ and S can be degraded even in complex form, that is, the complex is not protecting them from degradation. Finally, all species are diluted as the cell divides at a rate μ. The biochemical reactions corresponding to this process are given by:

$$\emptyset \xrightarrow{\alpha_\mathrm{i}} \mathrm{E_i} \xrightarrow{\gamma_\mathrm{i}+\mu} \emptyset, \quad \emptyset \xrightarrow{\alpha_\mathrm{s}} \mathrm{S} \xrightarrow{\gamma_\mathrm{s}+\mu} \emptyset, \quad \mathrm{c_i} \xrightarrow{\gamma_\mathrm{i}} \mathrm{S}, \quad \mathrm{c_i} \xrightarrow{\gamma_\mathrm{s}} \mathrm{E_i}, \quad \mathrm{c_i} \xrightarrow{\mu} \emptyset \quad \mathrm{E_i} + \mathrm{S} \underset{\mathrm{d_i}}{\overset{\mathrm{a_i}}{\rightleftharpoons}} \mathrm{c_i} \xrightarrow{\kappa_\mathrm{i}} \mathrm{P_i} + \mathrm{E_i} + \mathrm{S}, \tag{1}$$

where $\mathrm{c_i}$ is the complex formed when $\mathrm{E_i}$ binds to S, a_i is the association rate constant, d_i is the dissociation rate constant, and κ_i is the catalytic rate of product formation. This general set of reaction captures many core biological processes such as genes being transcribed by RNAP polymerase, mRNA translated by ribosomes, or proteins being degraded by a common protease.

E. coli actively regulates its geometry to achieve a near-perfect cylindrical shape [21]. Thus, we model the cell as a cylinder of length $2L$ and radius R_c. This geometry is shown in Figure 1-A. We assume angular and radial homogeneity ($R_c/L \ll 1$) such that the concentration of a species varies only axially (the spatial x direction). Symmetry relative to the mid-cell is assumed and hence only half of the cell is considered, that is, $x \in [0, L]$, where $x = 0$ is at the mid-cell and $x = L$ is at the cell poles. Furthermore, we assume a constant cross-sectional area along the axial direction.

We now specify the model for the flux of a freely diffusing species, which will allow us to capture the effects of a species being repelled from the chromosome via excluded volume effects. For any given biomolecular species in the cell with concentration per unit length given by $y(t, x)$, free to diffuse, let $v(x) \in (0, 1]$ be the volume fraction (dimensionless) available to a species to diffuse within the chromosome (Figure 1-B). The $v(x)$ depends on the local chromosome density at position x and the size of the species. An expression for the flux term, derived in [13] and more generally discussed in the the ecology literature as the attractive dispersal (AD) [26, 27], is given by:

$$J(x, y) \propto \Bigg(\underbrace{-\frac{\partial y(t,x)}{\partial x} v(x)}_{\text{towards low concentration}} + \underbrace{y(t,x) \frac{\partial v(x)}{\partial x}}_{\text{towards high available volume}} \Bigg) = -v(x)^2 \frac{d}{dx}\left[\frac{y(t,x)}{v(x)}\right]. \tag{2}$$

The flux is driven by two mechanisms: the first is concentration gradient, which pushes molecules from high to low concentrations and the second drives molecules to regions with a higher volume fraction. This second term is referred to as the excluded volume effect [13]. From (2), if $\left|\frac{\partial y(t,x)}{\partial x} v(x)\right| < \left|y(t,x)\frac{\partial v(x)}{\partial x}\right|$ and $\frac{\partial y(t,x)}{\partial x}\frac{\partial v(x)}{\partial x} > 0$, then the net flux is from low to high concentration, which is the case when species are repelled from the chromosome to high concentration areas in the cell poles. As we will show, this mechanism is responsible for intracellular heterogeneity in the limit of fast diffusion.

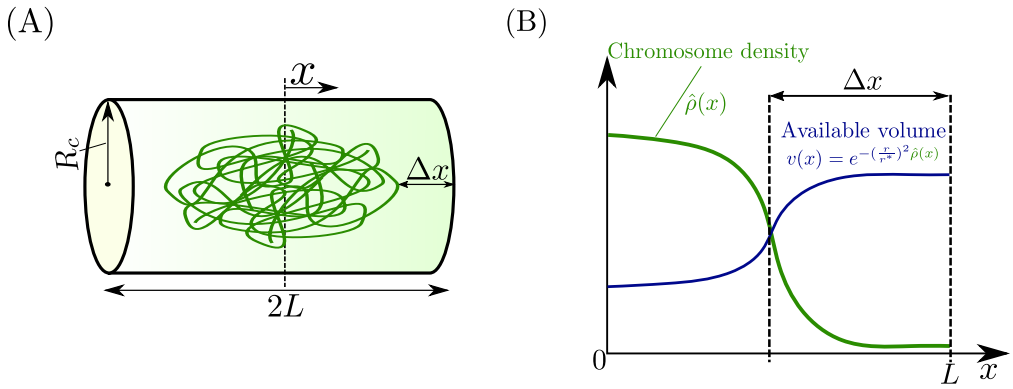

Figure 1: **Intracellular spatial geometry.** (A) We model the cell as a cylinder of radius R_c and length $2L$. The distance between the end of the chromosome and the cell poles is Δx. (B) The spatial profiles for the normalized local density of DNA length ($\hat{\rho}(x)$) and the fraction of available volume ($v(x)$) of a freely diffusing species within the chromosomal mesh with radius of gyration (r). These two quantities are related by $v(x) = e^{-(r/r^*)^2\hat{\rho}(x)}$, where r^* is a length scale dependent on the averaged chromosome density in the cell. The chromosome density is assumed to be monotonically decreasing from mid-cell to the cell poles (as in [13]), thus the available volume profile are monotonically increasing.

As discussed in SI Section 1.5, the available volume profile of a species with a radius of gyration r, takes the form

$$v(x) = e^{-(r/r^*)^2\hat{\rho}(x)} \tag{3}$$

where r^* is a length scale that is proportional to the square root of the total length of the chromosome DNA divided by the total volume occupied by the chromosome within the cell and $\hat{\rho}(x)$ is the normalized local density of DNA length such that $\int_0^L \hat{\rho}(x)dx/L = 1$ and it is assumed to be monotonically decreasing (i.e, the chromosome is more dense near mid-cell than the cell poles). Therefore, the available volume is higher near mid-cell than the cell poles (see Figure 1-B) and the discrepancy between the two increases with r/r^*.

For species S, we denote by $S(t,x)$ its concentration per length at time t at location x (similarly for $\mathrm{E_i}$ and $\mathrm{c_i}$). Assuming sufficently high molecular counts, the reaction-diffusion dynamics corresponding to (1) describing the rate of change of the species concentrations at position x, are given by [22] :

$$\begin{aligned}
\frac{\partial E_i(t,x)}{\partial t} &= -\frac{d}{dx}\big[J_{E_i}(x,E_i)\big] + \alpha_i(t,x) - a_iE_i(t,x)S(t,x) + (\gamma_i + d_i + \kappa_i)c_i(t,x) - (\gamma_i + \mu)E_i(t,x) \\
\frac{\partial c_i(t,x)}{\partial t} &= -\frac{d}{dx}\big[J_{c_i}(x,c_i)\big] + a_iE_i(t,x)S(t,x) - (\gamma_i + \gamma_s + d_i + \kappa_i + \mu)c_i(t,x), \\
\frac{\partial S(t,x)}{\partial t} &= -\frac{d}{dx}\big[J_S(x,S)\big] + \alpha_s(t,x) + \sum_{j=1}^{n}\big[-a_jE_j(t,x)S(t,x) + (\gamma_j + d_j + \kappa_j)c_j(t,x)\big] - (\gamma_s + \mu)S(t,x),
\end{aligned} \tag{4}$$

where J_{E_i}, J_{c_i}, and J_S are the fluxes per unit area per unit time of species $\mathrm{E_i}$, $\mathrm{c_i}$ and S, respectively, within the cell. The boundary conditions associated with (4) are zero flux at the cell poles and cell center due to the assumed left-right symmetry, which corresponds to:

$$J_{E_i}(0,E_i) = J_{E_i}(L,E_i) = 0, \quad J_{c_i}(0,c_i) = J_{c_i}(L,c_i) = 0, \quad J_S(0,S) = J_S(L,S) = 0. \tag{5}$$

Notice that none of the parameters in (4) corresponding to (1) depend explicitly on time and space except for the production terms $\alpha_i(t,x)$ and $\alpha_s(t,x)$. The explicit time dependence of the production terms allows us to capture how genes can be activated or repressed externally with a time varying signal [23]. The explicit dependence of the production terms on x allows us to capture where the species is produced within the cell (e.g., DNA in the chromosome vs DNA in pole localized plasmid genes).

Dimensionless Model: We work with variables and parameters in their dimensionless form to identify the underlying time and length scales that govern the physics of the system (4). We nondimensionalize the system variables using dilution ($1/\mu$) as the characteristic time scale, the length of the cell (L) as the characteristic length, and μ/a_1 as the characteristic concentration per length scale: $t^* = t\mu$, $y^* = y\frac{a_1}{\mu}$, $x^* = \frac{x}{L}$, where

y denotes some general concentration per unit length and the superscript "$*$" is used on the dimensionless variable. All concentrations are related to the a_1 because it contains a concentration scale, it is fixed in time, and it is assumed to exist and be nonzero. The dimensionless form of (4) is given by

$$\begin{aligned}
\frac{\partial E_i^*(t^*,x^*)}{\partial t^*} &= -\frac{d}{dx}\big[J^*_{E_i}(x^*,E_i^*)\big] + \alpha_i^*(t^*,x^*) + \frac{1}{\eta_i}\Big[-E_i^*(t^*,x^*)S^*(t^*,x^*)\frac{\tilde{a}_i}{\tilde{d}_i} + c_i^*(t^*,x^*)\Big] \\
&\qquad - (\gamma_i^*+1)(E_i^*(t^*,x^*)+c_i^*(t^*,x^*)), \\
\frac{\partial c_i^*(t^*,x^*)}{\partial t^*} &= -\frac{d}{dx}\big[J^*_{c_i}(x^*,c_i^*)\big] + \frac{1}{\eta_i}\Big[E_i^*(t^*,x^*)S^*(t^*,x^*)\frac{\tilde{a}_i}{\tilde{d}_i} - c_i^*(t^*,x^*)\Big], \\
\frac{\partial S^*(t^*,x^*)}{\partial t^*} &= -\frac{d}{dx}\big[J^*_{s}(x^*,S^*)\big] + \alpha_s^*(t^*,x^*) + \sum_{j=1}^{n}\frac{1}{\eta_j}\Big[-E_j^*(t^*,x^*)S^*(t^*,x^*)\frac{\tilde{a}_j}{\tilde{d}_j} + c_j^*(t^*,x^*)\Big] \\
&\qquad - (\gamma_s^*+1)(S^*(t^*,x^*)+\sum_{j=1}^{n}c_j^*(t^*,x^*)),
\end{aligned} \tag{6}$$

where $\tilde{a}_i = a_i/a_1$, $\gamma_s^* = \gamma_s/\mu$, $\gamma_i^* = \gamma_i/\mu$, $d_i^* = d_i/\mu$, $\kappa_i^* = \kappa_i/\mu$, $\alpha_i^* = \alpha_i a_1/\mu^2$, $\alpha_s^* = \alpha_s a_1/\mu^2$, $\tilde{d}_i = \gamma_i^*+\gamma_s^*+d_i^*+\kappa_i^*+1$, $\eta_i = 1/\tilde{d}_i$, $J^*_{E_i} = J_{E_i}a_1/(\mu^2 L)$, $J^*_{c_i} = J_{c_i}a_1/(\mu^2 L)$, and $J_s^* = J_s a_1/(\mu^2 L)$. From hereon, unless otherwise specified, we work with variables in their dimensionless form and drop the star superscript for simplifying notation.

Concentrations per cell: Concentrations per cell are usually the quantities measured experimentally [24] and are the primary quantities of interest. We now provide the space averaged dynamics corresponding to (6). We define $\bar{E}_i(t)$, $\bar{S}(t)$, and $\bar{c}_i(t)$ to be the space averaged enzyme, substrate, and complex concentrations, respectively (e.g., $\bar{E}_i(t) = \int_0^1 E_i(t,x)dx$). The dynamics governing these space averaged variables are derived by integrating (6) in space and applying the boundary conditions (5) and are given by:

$$\begin{aligned}
\frac{d\bar{E}_i(t)}{dt} &= \bar{\alpha}_i(t) - \frac{1}{\eta_i}\big[\bar{E}_i(t)\bar{S}(t)\frac{\tilde{a}_i\theta_i(t)}{\tilde{d}_i} - \bar{c}_i(t)\big] - (\gamma_i+1)(\bar{E}_i(t)+\bar{c}_i(t)) \\
\frac{d\bar{c}_i(t)}{dt} &= \frac{1}{\eta_i}\big[\bar{E}_i(t)\bar{S}(t)\frac{\tilde{a}_i\theta_i(t)}{\tilde{d}_i} - \bar{c}_i(t)\big] \\
\frac{d\bar{S}(t)}{dt} &= \bar{\alpha}_s(t) - \sum_{j=1}^{n}\frac{1}{\eta_j}\Big[\bar{E}_j(t)\bar{S}(t)\frac{\tilde{a}_j\theta_j(t)}{\tilde{d}_j} - \bar{c}_j(t)\Big] - (\gamma_s+1)(\bar{S}(t)+\sum_{j=1}^{n}\bar{c}_j(t))
\end{aligned} \tag{7a}$$

where overbars denote spatially averaged variables and

$$\theta_i(t) = \frac{\int_0^1 E_i(t,x)S(t,x)dx}{\big[\int_0^1 E_i(t,x)dx\big]\big[\int_0^1 S(t,x)dx\big]}. \tag{7b}$$

Therefore, to calculate concentrations per cell, one could integrate the outputs of the full PDE (6) directly or use (7) along with (7b), illustrated in Figure 2. Notice that calculating θ_i in (7b) requires solving the full PDE system (6) because of its dependence on the product $E_i(t,x)S(t,x)$. Therefore, in general, there is no obvious benefit in working with (7). However, the modeling framework provided by (7) will be leveraged in this work to provide methods to calculate θ_i without solving the PDEs (6).

Well-mixed model: Next, we define what we have been informally referring to as a "well-mixed" model [25]. A standard well-mixed model is derived starting from (1) assuming mass action kinetics, that molecular counts are sufficiently large, and that the intracellular environment is spatially homogeneous (well-mixed) [1]. We let $\bar{E}_i^{\mathrm{wm}}(t)$, $\bar{S}^{\mathrm{wm}}(t)$ and $c_i^{\mathrm{wm}}(t)$, denote the well-mixed concentrations per cell of $\mathrm{E_i}$, S, and $\mathrm{c_i}$, respectively, and their dynamics are given by

$$\begin{aligned}
\frac{d\bar{E}_i^{\mathrm{wm}}(t)}{dt} &= \bar{\alpha}_i(t) - \frac{1}{\eta_i}\big[\bar{E}_i^{\mathrm{wm}}(t)\bar{S}^{\mathrm{wm}}(t)\frac{\tilde{a}_i}{\tilde{d}_i} - \bar{c}_i^{\mathrm{wm}}(t)\big] - (\gamma_i+1)(\bar{E}_i^{\mathrm{wm}}(t)+\bar{c}_i^{\mathrm{wm}}(t)) \\
\frac{d\bar{c}_i^{\mathrm{wm}}(t)}{dt} &= \frac{1}{\eta_i}\big[\bar{E}_i^{\mathrm{wm}}(t)\bar{S}^{\mathrm{wm}}(t)\frac{\tilde{a}_i}{\tilde{d}_i} - \bar{c}_i^{\mathrm{wm}}(t)\big] \\
\frac{d\bar{S}^{\mathrm{wm}}(t)}{dt} &= \bar{\alpha}_s(t) - \sum_{j=1}^{n}\frac{1}{\eta_j}\Big[\bar{E}_j^{\mathrm{wm}}(t)\bar{S}^{\mathrm{wm}}(t)\frac{\tilde{a}_j}{\tilde{d}_j} - \bar{c}_j^{\mathrm{wm}}(t)\Big] - (\gamma_s+1)(\bar{S}^{\mathrm{wm}}(t)+\sum_{j=1}^{n}\bar{c}_j^{\mathrm{wm}}(t)).
\end{aligned} \tag{8}$$

Comparing (7) and (8), motivates us to define $a_i' = \tilde{a}_i\theta_i$, which can be thought of as the effective association rate constant between E_i and S in (7). Therefore, we refer to $\theta_i(t)$ as the *binding correction factor* (BCF). The space averaged concentrations (7) coincide with the well-mixed model (8) when $\theta_i(t) = 1$ (thus $a_i' = \tilde{a}_i$) for all time and for all $i = 1, \ldots, n$. However, if $S(t, x)$ is spatially constant while $E_i(t, x)$ has any arbitrary spatial profile (or *vice-versa*), then $\theta_i(t) = 1$, thus the space average concentrations can coincide with those of a well-mixed model despite severe spatial heterogeneity. This insight exemplifies the utility of the framework given by (7). In this work, we provide an approximation of $\theta_i(t)$ given by a constant θ_i^* that depends on spatial variables (molecule size and location of expression). The spaced-averaged dynamics (7) with $\theta_i(t)$ replaced by θ_i^* provide a reduced ODE model that captures spatial information without having to solve (6). We will compare how solutions to (7) with (7b) calculated from the full PDE (6) and with the proposed reduced model compare to the well-mixed model (8) to highlight the importance of modeling spatial heterogeneity. Furthermore, as predicted from our theory, we show that solutions from the full PDE and the reduced model are in agreement with each other.

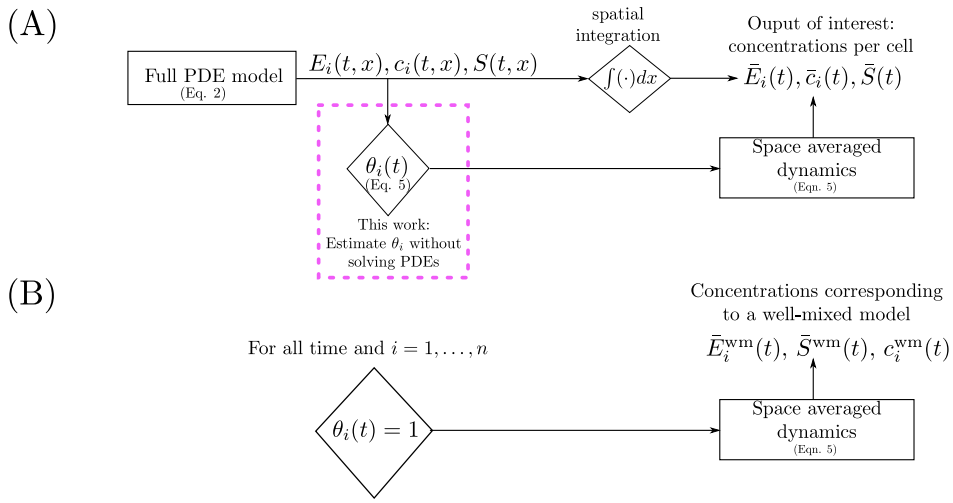

Figure 2: **Methods to calculate concentrations per cell.** (A) The time and space dependent states from the full PDE (6) are integrated spatially to yield concentrations per cell. Alternatively, concentrations per cell can be calculated by considering the space average dynamics (7), which depend on the BCF ($\theta_i(t)$ (7b)). In general, calculating $\theta_i(t)$ requires solving the full PDE. In this work we provide a reduced model to approximate $\theta_i(t)$ without solving (6). (B) The space averaged concentrations coincide with the well-mixed model (8) when $\theta_i(t) = 1$ for all time and for all $i = 1, \ldots, n$.

0.1.2 Three Diffusion Cases Considered to Capture Several Biological Processes

To apply model (6) to a wide range of biological relevant problems, we consider three cases. In Case I, we model both E_i and S freely diffusing within the cell; in Case II, we model E_i to be spatially fixed ($J_{E_i}(x, E_i) = 0$ for all $x \in [0, 1]$) and S freely diffusing; in Case III, we model E_i freely diffusing and S to be spatially fixed ($J_S(x, S) = 0$ for all $x \in [0, 1]$). Case I may represent n mRNA molecules (E_i) competing for ribosomes (S), both freely diffusing in the cell. Case II captures n genes (E_i), which are spatially fixed being transcribed by RNA polymerase (S), which freely diffuses.Case III models n transcription factors (E_i), which freely diffuse regulating the same gene (S), which is spatially fixed.

The flux dynamics, the boundary conditions, and the biological relevance of each case are summarized in Table. 1. A species being spatially fixed mathematically translated to the flux dynamics being zero throughout the whole spatial domain. Fast diffusion corresponds to $\epsilon \gg 1$. The available volume profiles for the enzyme, complex, and substrate are given by $v_{E_i}(x)$, $v_{c_i}(x)$, and $v_S(x)$, respectively. The available volume profile for the complex $v_{c_i}(x)$, represent the probability that the complex has enough free volume to hop into the DNA mesh at position x and it equals the product of the probability of the two independent events of the enzyme and the substrate hopping into the DNA mesh [13], thus

$$v_{c_i}(x) = v_{E_i}(x)v_S(x). \tag{9}$$

Furthermore, we define the normalized available volume profiles as

$$\hat{v}_{E_i}(x) = \frac{v_{E_i}(x)}{\int_0^1 v_{E_i}(x)dx}, \quad \hat{v}_{c_i}(x) = \frac{v_{c_i}(x)}{\int_0^1 v_{c_i}(x)dx}, \quad \hat{v}_S(x) = \frac{v_S(x)}{\int_0^1 v_S(x)dx}. \tag{10}$$

Case	I: All species diffuse	II: Substrate diffuses and enzymes fixed	III: Enzymes diffuses and substrate fixed
Dimensionless Flux	$J^*_{E_i} = -\frac{1}{\epsilon}\chi_{E_i} v^2_{E_i} \frac{d}{dx^*}[\frac{E^*_i}{v_{E_i}}]$ $J^*_s = -\frac{1}{\epsilon} v^2_S \frac{d}{dx^*}[\frac{S}{v_s}]$ $J^*_{c_i} = -\frac{1}{\epsilon}\chi_{c_i} v^2_{c_i} \frac{d}{dx^*}[\frac{c_i}{v_{c_i}}]$	$J^*_{E_i} = 0$ $J^*_s = -\frac{1}{\epsilon} v^2_s \frac{d}{dx^*}[\frac{S^*}{v_s}]$ $J^*_{c_i} = 0$	$J^*_{E_i} = -\frac{1}{\epsilon} v^2_{E_i} \frac{d}{dx^*}[\frac{E^*_i}{v_{E_i}}]$ $J^*_s = 0$ $J^*_{c_i} = 0$
Boundary conditions	$J^*_{E_i}(0, E^*_i) = J^*_{E_i}(1, E^*_i) = 0$ $J^*_{c_i}(0, c^*_i) = J^*_{c_i}(1, c^*_i) = 0$ $J^*_s(0, S^*) = J^*_s(1, S^*) = 0$	$J^*_s(0, S^*) = J^*_s(1, S^*) = 0$	$J^*_{E_i}(0, E^*_i) = J^*_{E_i}(1, E^*_i) = 0$
ϵ	$(\mu L^2)/D_s$	$(\mu L^2)/D_s$	$(\mu L^2)/D_{E_1}$
Dimensionless diffusion	$\chi_{E_i} = D_{E_i}/D_s, \chi_{c_i} = D_{c_i}/D_s$		
Case bio example	mRNA's competing for ribosomes	RNAP transcribing several DNA	Transcription factors competing for promoter

Table 1: The flux dynamics and the boundary conditions corresponding to (6) for each case of interest along with the the biological relevance. The parameters D_{E_i}, D_{c_i}, and D_s, are the enzyme, complex, and substrate diffusion coefficients, respectively, ϵ is a dimensionless parameter that captures the speed of diffusion (with respect to dilution). A species being spatially fixed translates to the flux being zero throughout the whole spatial domain.

0.2 Numerical Method: Finite Difference

In general, a closed form solution to (6) is not readily available. Therefore, we rely on numerical solutions to directly integrate the PDE. In particular, we utilize a finite difference method that is a widely used to simulate PDEs [28]. For a general diffusing species with its concentration given by $y(t, x)$, and available volume profile $v(x)$, we make the following coordinate transformation $u(t, x) := y(t, x)/v(x)$. In this coordinate, the boundary conditions (if applicable) are Neumann [29]: $\frac{\partial u}{\partial x}\Big|_{x=0,1} = 0$. We discretized the spatial domain into $N+1$ equidistant points such that $\Delta x = 1/N$. Using a second order finite difference method, we approximate the derivatives as:

$$\frac{\partial u}{\partial x}\bigg|_{x=x_i} \approx \frac{u(t, x_{i+1}) - u(t, x_{i-1})}{2\Delta x} \text{ and } \frac{\partial^2 u}{\partial x^2}\bigg|_{x=x_i} \approx \frac{u(t, x_{i+1}) - 2u(t, x_i) + u(t, x_{i-1})}{\Delta x^2}.$$

The boundary conditions under this new set of coordinates give rise to the following constraints:

$$\frac{\partial^2 u}{\partial x^2}\bigg|_{x=0} \approx 2\frac{u(t, x_2) - u(t, 0)}{\Delta x^2} \text{ and } \frac{\partial^2 u}{\partial x^2}\bigg|_{x=1} \approx 2\frac{u(t, x_N) - u(t, 1)}{\Delta x^2}.$$

This discretization leads to a system of $N+1$ ODEs. The resulting set of ODEs are then simulated with MATLAB, using the numerical ODE solvers ode23s and ode15s. To calculate the space averaged concentrations $\left(\bar{y}(t) := \int_0^1 y(t, x)dx\right)$, we implement a second oder trapezoidal integration scheme [29] given by:

$$\bar{y}(t) \approx \frac{\Delta x}{2}\sum_{j=1}^{N}\big[y(t, x_j) + y(t, x_{j+1})\big].$$

The convergence rate of our numerical method is demonstrated in Section 1.9. For all simulations in this paper $N = 200$.

0.3 Model Reduction Via Time Scale Separation

Numerical solutions of (6) are computationally expensive, especially when compared to the commonly used well-mixed model (8). Furthermore, it is difficult to achieve a mechanistic understanding of the system's behavior based on simulation. Therefore, to study the effects of spatial heterogeneity we exploit the time scale

separation between diffusion and the reaction dynamics in (6). Diffusion occurs in the order of mili-seconds compared to minutes for dilution and mRNA degradation [2]. We leverage this time scale separation to derive an approximation for the BCF ($\theta_i(t)$ (7b)) that does not require solving the PDE (6). The approximate BCF is constant in time and can be treated as a parameter that contains spatial heterogeneity. Therefore, this approximation provides a simple method to calculate concentrations per cell and incorporate spatial heterogeneity in models while maintaining the same complexity as a well-mixed model.

Results

0.4 Time Scale Separation

In this section, we provide a time independent approximation of the BCF (7b) in the limit of fast diffusion that depends solely on the size of diffusing species, chromosome density profiles, and the spatial localization of non-diffusing species. With this approximation, we can compute space averaged solutions in (7) without solving the PDEs in (6).

0.4.1 Reduced Spaced Averaged Dynamics When Diffusion is Fast and Fixed Species are Localized

The following assumption will make mathematically precise what we refer to as localization of a fixed species.

Assumption 1. (Localization of spatially fixed species) Assume that there exists $x_i, x_s \in (0,1)$ and $L_i, L_s > 0$ such that for $t \geq 0$

- for Case II: $\alpha_i(t,x) \leq L_i\delta$, for all $x \notin [x_i - \delta, x_i + \delta]$,
- for Case III: $\alpha_s(t,x) \leq L_s\delta$, for all $x \notin [x_s - \delta, x_s + \delta]$,

where $\delta > 0$ is such that $[x_i - \delta, x_i + \delta] \subset [0,1]$ and $[x_s - \delta, x_s + \delta] \subset [0,1]$ and Cases II-III correspond to those described in Table 1. Furthermore, assume that $\bar{\alpha}_i(t) = \int_0^1 \alpha_i(t,x)dx$ and $\bar{\alpha}_s(t) = \int_0^1 \alpha_s(t,x)dx$ are independent of δ.

The latter part of Assumption 1 ensures that the spaced averaged production rates are independent of localization. Biologically, this is consistent with the fact that the total amount of DNA in the cell is independent of where the DNA is concentrated. The following definition will provide the candidate reduced model that approximates (7) well when diffusion is fast ($\epsilon \ll 1$) and the production of spatially fixed species is localized to a small region (Assumption 1 holds for $\delta \ll 1$).

Definition 1. (Reduced spaced-averaged dynamics) Let $\hat{\bar{E}}_i(t)$, $\hat{\bar{S}}(t)$, and $\hat{\bar{c}}_i(t)$ be given by (7) where $\theta_i(t)$ in (7b) is replaced by

$$\theta_i^* = \begin{cases} \int_0^1 \hat{v}_{E_i}(x)\hat{v}_S(x)dx & \text{for Case I} \\ \hat{v}_S(x_i) & \text{for Case II} \\ \hat{v}_{E_i}(x_s) & \text{for Case III} \end{cases}, \tag{11}$$

where x_i and x_s are as in Assumption 1, Case I-III correspond to those described in Table 1, and $\hat{v}_{E_i}(x)$ and $\hat{v}_S(x)$ are given by (10).

Theorem 1. *Let $\epsilon > 0$ be defined for Case I-III by Table 1, $\bar{E}_i(t)$, $\bar{c}_i(t)$, and $\bar{S}(t)$ be given by (7), and $\hat{\bar{E}}_i(t)$, $\hat{\bar{S}}(t)$, and $\hat{\bar{c}}_i(t)$ be as in Definition 1, and suppose Assumption 1 holds for $\delta > 0$, then, there exists $\epsilon^* > 0$ such that for all $\epsilon < \epsilon^*$ and $t \geq 0$, we have that*

$$\bar{E}_i(t) = \hat{\bar{E}}_i(t) + \mathcal{O}\left(\frac{\epsilon}{1-\epsilon/\epsilon^*}\right) + \mathcal{O}(\delta), \quad \bar{c}_i(t) = \hat{\bar{c}}_i(t) + \mathcal{O}\left(\frac{\epsilon}{1-\epsilon/\epsilon^*}\right) + \mathcal{O}(\delta), \quad \bar{S}(t) = \hat{\bar{S}}(t) + \mathcal{O}\left(\frac{\epsilon}{1-\epsilon/\epsilon^*}\right) + \mathcal{O}(\delta).$$

Proof: The complete proof is provided in Section 1.3. The proof consists of decomposing the state variables of (6) that are freely diffusing into two components: their projection onto the functional space spanned by their available volume profiles and the left over infinite dimensional component. We show that the infinite dimensional component is order ϵ after a fast transient with respect to a weighted $L^2[(0,1)]$-norm via Lyapunov methods. We then show that (7) has the form described by Definition 1, but with additional

"disturbance" terms of order ϵ and δ. We demonstrate the system described in Definition 1 is contracting [30] and apply the robustness property of contracting systems [31] to show closeness between its solutions and those of (7). ■

Remark 1. *The result of Theorem 1 holds under Assumption 1, which only applies to Cases II-III. The result is independent of this assumption for Case I and thus one can let $\delta = 0$ for this case.*

Remark 2. *As discussed in SI Section 1.3, as $\epsilon \to 0^+$, the spatial profile of diffusing molecules approaches that of their available volume profile (independently of δ), that is,*

$$\underbrace{E_i(t,x) \approx \bar{E}_i(t)\hat{v}_{E,i}(x)}_{\textit{Case I and Case III}}, \quad \underbrace{c_i(t,x) \approx \bar{c}_i(t)\hat{v}_{c,i}(x)}_{\textit{Case I}}, \quad \underbrace{S(t,x) \approx \bar{S}(t)\hat{v}_S(x)}_{\textit{Case I and Case II}},$$

Remark 3. *It was assumed in Theorem 1 that the timescales associated with diffusion were much fast faster than any other time scales in (6), however in Section 1.4.1 we motivate why our result holds even if $\eta_i/\epsilon = \mathcal{O}(1)$ (biding and unbinding between $\mathrm{E_i}$ and S occurs at a similar timescale as diffusion). Furthermore, we confirm our hypothesis numerically in Section 0.5.*

The parameter θ_i^* as in Definition 1, is temporally constant and thus the reduced model has the same complexity as the well-mixed model (8), yet provides physical insight to the role of spatial heterogeneity in the interactions between cellar species. Therefore, θ_i^* is a practical and accurate approximation of the BCF when $\epsilon \ll 1$ and if applicable (Remark 1) $\delta \ll 1$.

0.4.2 Dependence of the BCF on Species Size and Localization

When diffusion is fast and the expression of spatially fixed species is localized (Assumption 1), the BCF is well approximated by θ_i^*. Using (3) and (11) and denoting r_e and r_s as the radius of gyration of $\mathrm{E_i}$ and S, respectively, we can recast θ_i^* as

$$\theta_i^* = \begin{cases} \frac{\int_0^1 e^{-(r_{e,i}^2+r_s^2)/(r^*)^2\hat{\rho}(x)}dx}{[\int_0^1 e^{-(r_{e,i}/r^*)^2\hat{\rho}(x)}dx][\int_0^1 e^{-(r_s/r^*)^2\hat{\rho}(x)}dx]} & \text{for Case I} \\ \frac{e^{-(r_s/r^*)^2\hat{\rho}(x_i)}}{\int_0^1 e^{-(r_s/r^*)^2\hat{\rho}(x)}dx} & \text{for Case II} \\ \frac{e^{-(r_{e,i}/r^*)^2\hat{\rho}(x_s)}}{\int_0^1 e^{-(r_{e,i}/r^*)^2\hat{\rho}(x)}dx} & \text{for Case III} \end{cases}. \tag{12}$$

From (12), we observe that θ_i^*, depends on the spatial localization of spatially fixed species (i.e,. x_i and x_s), the radius of gyration of diffusing species, r^* (a length scale associated with the average chromosome density in the cell), and the nominalized local density of DNA length $\hat{\rho}(x)$. Using (12), we graphically illustrate the dependence of θ_i^* on these parameter in Figure 3.

For Case I, the BCF is always greater than or equal to that of the well-mixed model (8) (where $\theta_i = 1$ for all i) and this discrepancy increases with the size of $\mathrm{E_i}$ and S. Intuitively, as the size of $\mathrm{E_i}$ and S increases, they are pushed out of the chromosome and colocalize near the cell poles, thus they are confined to to a smaller volume to interact and hence their effective binding strength increases. The upper bound for θ_i^* is $1/\Delta x$ (where Δx is the distance between the end of the chromosome and the cell poles) when $\hat{\rho}(x)$ is assumed to be a step function as derived in SI Section 1.5. If only one of the species is large (with respect to r^*), while the other one is small, then the large species will be ejected from the chromosome and thus will not be homogeneously distributed throughout the cell, however $\theta_i^* \approx 1$, and thus a well-mixed model is valid despite this spatial heterogeneity.

For Case II and III, when the size of the diffusing species is sufficiently large, then $\theta_i^* < 1$ (even zero) when the fixed species is localized near mid-cell and $\theta_i^* > 1$ (upper bounded by $1/\Delta x$ when $\hat{\rho}(x)$ is assumed to be a step function) when the fixed species is localized near the cell-poles. This occurs because as the size of the diffusing species increases, it is ejected from the chromosome onto the cell poles and therefore it is more likely to interact with species fixed at the cell-poles than those near mid-cell. In the special case where $x^* \approx 0.5$, then $\theta_i^* \approx 1$ independently of the size of the diffusing species. Thus, this provides additional evidence that a well-mixed model may be appropriate despite severe intracellular heterogeneity.

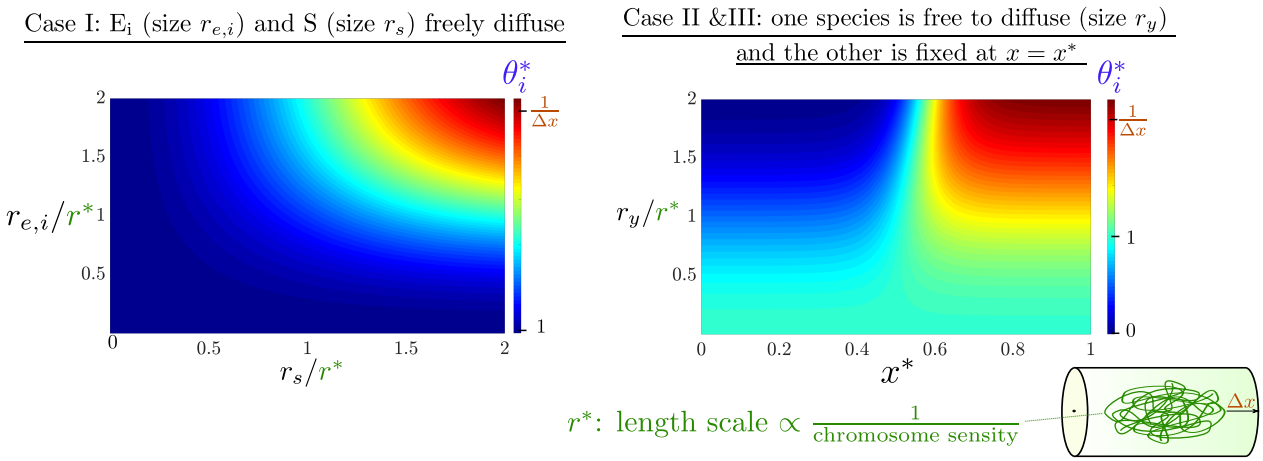

Figure 3: **The BCF in the limit of fast diffusion and assuming localization of spatially fixed species**. An approximation of the BCF (θ_i in (7b)) denoted by θ_i^* (12) is provided for Case I and for Case II/Case III. For Case I, $\theta_i \geq 1$ and increases when both the size of E_i ($r_{e,i}$) and S (r_s) are sufficiently large (with respect to r^*, which is a length scale dependent on the chromosome density). For Case II and III, where one of the species diffuses (size r_y) and the other is fixed at $x = x^*$, θ_i^* is different than unity when $r_y/r^* \geq 1$. For $r_y/r^* \geq 1$, $\theta_i < 1$ (can be even zero) for $x^* \approx 0$ and $\theta_i > 1$ (bounded by $1/\Delta x$) for $x^* \approx 1$. Here, Δx is the distance between the end of the chromosome and the cell poles.

0.5 Biological Examples and Applications

In the following section we apply the results of the time scale separation analysis from Section 0.4 to several core processes in the cell to determine the effects of intracellular heterogeneity on genetic circuit dynamics. We focus on the transcription and translation process, gene regulation via transcription factors, and a biological clock.

0.5.1 Application of the reduced ODE model to core biological processes

In this section, we investigate how intracellular heterogeneity affects the core biological processes of transcription and translation, which are responsible for protein production. The biochemical reactions pertaining to n genes ($\mathrm{D_i}$) being transcribed by RNAP (S) to form a DNA-RNAP complex ($\mathrm{c_{s,i}}$) to produce mRNA ($\mathrm{m_i}$) which is translated by ribosomes (R) to form mRNA-ribosome complex ($\mathrm{c_{m,i}}$) which produces protein $\mathrm{P_i}$, are given by:

$$\underbrace{\mathrm{D_i} + \mathrm{S} \underset{\mathrm{d_{s,i}}}{\overset{\mathrm{a_{s,i}}}{\rightleftharpoons}} \mathrm{c_{s,i}} \xrightarrow{\kappa_{\mathrm{s,i}}} \mathrm{m_i} + \mathrm{S} + \mathrm{D_i}}_{\text{transcription, Case II}}, \quad \underbrace{\mathrm{m_i} + \mathrm{R} \underset{\mathrm{d_{m,i}}}{\overset{\mathrm{a_{m,i}}}{\rightleftharpoons}} \mathrm{c_{m,i}} \xrightarrow{\kappa_{\mathrm{m,i}}} \mathrm{P_i} + \mathrm{R} + \mathrm{m_i}}_{\text{translation, Case I}}, \tag{13}$$

where $a_{s,i}$ and $d_{s,i}$ are the association and disassociation rate constants, respectively, between RNAP and the gene $\mathrm{D_i}$, $\kappa_{s,i}$ is the catalytic rate of formation of mRNA $\mathrm{m_i}$, $a_{m,i}$ and $d_{m,i}$ are the association and disassociation rate constants, respectively, between ribosomes and mRNA , $\kappa_{m,i}$ is the catalytic rate of formation of protein $\mathrm{P_i}$. The transcription reaction is in the form of Case II in (Table 1) since the gene does not freely diffuse and the RNAP freely diffuses. The translation process falls under Case I, since both mRNA and ribosomes freely diffuse. The space averaged dynamics corresponding to (13) (as in (7)) are given by

$$
\begin{aligned}
\frac{d\bar{D}_i(t)}{dt} &= \bar{\alpha}_{D,i}(t) - a_{s,i}\theta_{s,i}(t)\bar{D}_i(t)\bar{S}(t) + (d_{s,i} + \kappa_{s,i})\bar{c}_{s,i}(t) - \mu D_i(t),\\
\frac{d\bar{c}_{s,i}(t)}{dt} &= a_{s,i}\theta_{s,i}(t)\bar{D}_i(t)\bar{S}(t) - (d_{s,i} + \kappa_{s,i} + \mu)\bar{c}_{s,i}(t),\\
\frac{d\bar{S}(t)}{dt} &= \bar{\alpha}_s(t) + \sum_{j=1}^{n}\Big(- a_{s,j}\theta_{s,j}(t)\bar{D}_j(t)\bar{S}(t) + (\kappa_{s,j} + d_{s,j})\bar{c}_j(t)\Big) - \mu\bar{S}(t),\\
\frac{d\bar{m}_i(t)}{dt} &= \kappa_{s,i}\bar{c}_{s,i}(t) - a_{m,i}\theta_{r,i}(t)\bar{R}(t)\bar{m}_i(t) + (d_{m,i} + \kappa_{m,i})\bar{c}_i(t) - (\gamma_i + \mu)\bar{m}_i(t) \qquad (14a)\\
\frac{d\bar{c}_{m,i}(t)}{dt} &= a_{m,i}\theta_{r,i}(t)\bar{R}(t)\bar{m}_i(t) - (d_{m,i} + \kappa_{m,i} + \mu + \gamma_i)\bar{c}_i(t),\\
\frac{d\bar{R}(t)}{dt} &= \bar{\alpha}_r(t) + \sum_{j=1}^{n}\Big(- a_{m,j}\theta_{r,j}(t)\bar{R}(t)\bar{m}_j(t) + (\gamma_j + d_{m,j} + \kappa_{m,j})\bar{c}_{m,j}(t)\Big) - \mu\bar{R}(t),\\
\frac{d\bar{P}_i(t)}{dt} &= \kappa_{m,i}\bar{c}_{m,i}(t) - \mu\bar{P}_i(t).
\end{aligned}
$$

where it was assumed that P_i was only diluted via cell growth and not actively degraded. Here $\bar{\alpha}_{D,i}$ is the space averaged production rate of gene $\mathrm{D_i}$, $\bar{\alpha}_s$ is the space averaged production rate of RNAP , $\bar{\alpha}_r$ is the ribosome space averaged production rate, μ is the cell growth rate, and γ_i is the mRNA degradation rate. Assuming that the production rate of $\mathrm{D_i}$ given by $\alpha_{D,i}(t,x)$ (such that $\int_0^1 \alpha_{D,i}(t,x)dx = \bar{\alpha}_{D,i}(t)$) is localized at $x = x_i$ (as in Assumption 1) and applying the result from Theorem 1 to the translation and transcription dynamics separately, implies that the BCF's are given by

$$
\underbrace{\theta_{s,i} = \hat{v}_s(x_i) = \frac{e^{-(r_s/r^*)^2\hat{\rho}(x_i)}}{\int_0^1 e^{-(r_s/r^*)^2\hat{\rho}(x)}dx}}_{\text{RNAP excluded volume effects and localization of } D_i}, \qquad (15a)
$$

$$
\underbrace{\theta_{r,i} = \int_0^1 \hat{v}_{m_i}(x)\hat{v}_R(x)dx = \frac{\int_0^1 e^{-(r_{m,i}^2 + r_R^2)/(r^*)^2\hat{\rho}(x)}dx}{[\int_0^1 e^{-(r_{m,i}/r^*)^2\hat{\rho}(x)}dx][\int_0^1 e^{-(r_R/r^*)^2\hat{\rho}(x)}dx]}}_{\text{mRNA and ribosome excluded volume effects}}. \qquad (15b)
$$

where $\hat{v}_s(x)$, $\hat{v}_{m_i}(x)$, $\hat{v}_R(x)$, and $\hat{v}_{c_i}(x)$ are the normalized available volume profiles of RNAP, mRNA, ribosomes, and the mRNA-ribosome complex (i.e,. $\hat{v}_s(x) = v_s(x)/\int_0^1 v_s(x)dx$), respectively, and r_s, $r_{m,i}$, and r_R are the radius of gyration of RNAP, mRNA, and ribosomes, respectively.

mRNA production: The steady state mRNA levels of (13) are given by

$$
m_i = \frac{\kappa_{s,i}\bar{c}_{s,i}/(\gamma_i + \mu)}{1 + \bar{R}/K_{R,i}\theta_{R,i}}, \quad \text{with} \quad \bar{c}_{s,i} = \bar{D}_{i,T}\underbrace{\frac{\bar{S}\theta_{S,i}/K_{s,i}}{1 + \bar{S}\theta_{S,i}/K_{s,i}}}_{\text{RNAP dependence}}, \qquad (16)
$$

where $\bar{D}_{i,T} = \frac{\bar{\alpha}_{D,i}}{\mu}$, $K_{s,i} = d_{s,i}/a_{s,i}$. If $\theta_{S,i} = 1$ for all i in (16), then the predicted mRNA production rate will be identical to that of a well-mixed model (as in (8)). If the RNAP radius of gyration is sufficiently large with respect to a length scale dependent on the local chromosome density at $x = x_i$ (i.e., $r_s/r^*\hat{\rho}(x_i) \gtrsim 1$), then spatial effects are considerable since $\theta_{S,i}$ will be different than unity. If the DNA is localized near the mid-cell ($x_i \approx 0$), then it implies a lower transcription rate ($\theta_{S,i} < 1$) and for for very large values of $r_s/r^*\hat{\rho}(x_i)$, this rate can even be zero ($\theta_{S,i} \approx 0$). Similarly, if the DNA is localized near the cell-poles ($x_i \approx 1$), then it implies a higher transcription rate ($\theta_{S,i} > 1$). This phenomena occurs because as the excluded volume effects of RNAP are amplified (large $r_s/r^*\hat{\rho}(x_i)$), RNAP will localize primarily in the cell poles and hence transcribe pole-localized DNA more efficiently than DNA near mid-cell (or any region where the local chromosome density is high). When designing genetic circuits, a plasmid backbone is chosen to provide a certain DNA copy number, however the backbone also determines where in the cell the plasmid localizes [9, 10, 11], and therefore, based on our results, localization should also be taken into consideration. If instead the DNA is integrated directly into the chromosome, then the local chromosome density of the

integration site should be a parameter to consider. Figure 4 (A) shows numerical results of simulating the expression of a single type of gene ($n = 1$). As predicted, expression is higher for pole localized genes than those near mid-cell and the discrepancy increases with the size of RNAP relative to r^*. The agreement in the simulations between the full PDE model ((66) in SI Section 1.6) and the reduced ODE model (14) provides numerical validation in the model reduction results (Theorem 1). In the SI Section 1.6, we show in Figure 8 the transient response corresponding to Figure 4, for which the full-PDE and reduced model agree well. We verify that as the size of RNAP increases, it is indeed ejected from the chromosome and adopts its available volume profile (Remark 2). Furthermore, in SI-Figure 9, we demonstrate that these results hold independently of the binding and unbinding speed between RNAP and DNA (Remark 3).

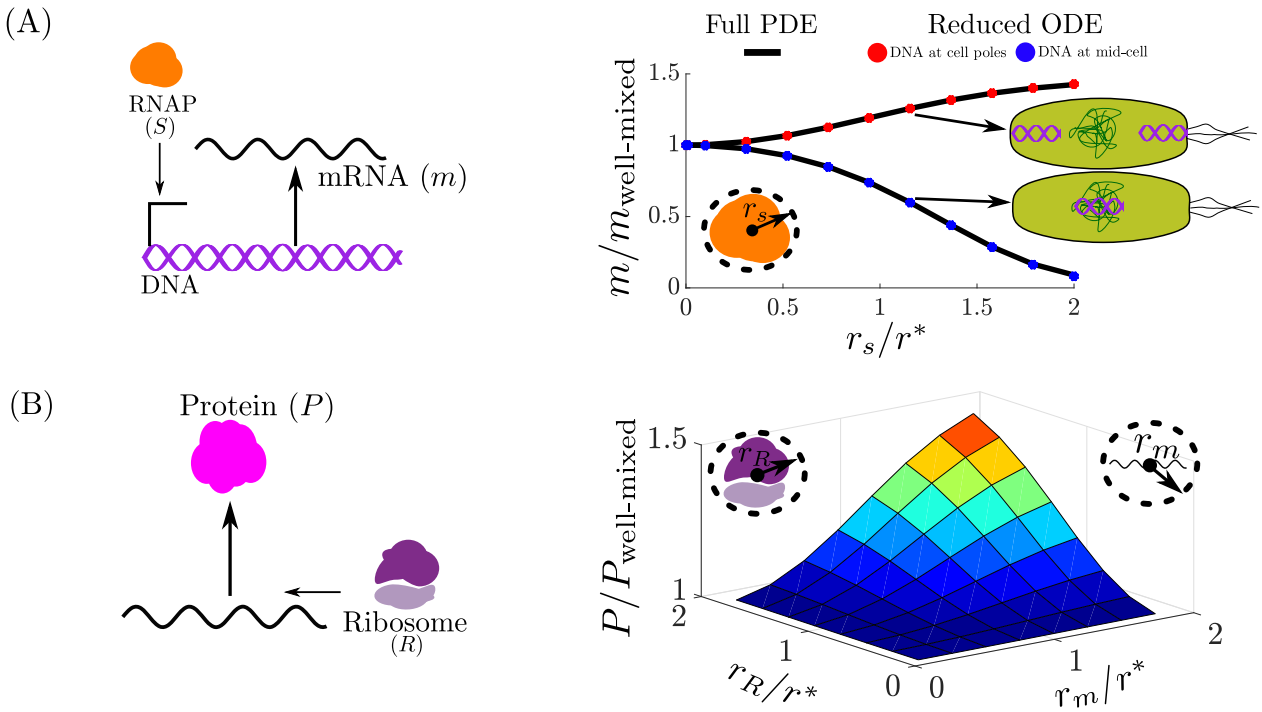

Figure 4: **Spatial heterogeneity controls transcription and translation rate via the BCF** For the following we refer to the well-mixed model as (14) with (15) given by $\theta_{s,i} = 1$ and $\theta_{r,i} = 1$ for all i. (A) The mRNA concentration per-cell predicted by the full PDE model ((66) in SI Section 1.6) and the reduced ODE model (14) normalized by that of the well-mixed model as the size of the RNAP (r_s) varies with respect to r^*. With respect to the well-mixed modl, the amount of mRNA decreases (increases) when the DNA is localized near mid-cell (cell poles). (B) The protein concentration per-cell predicted by the full PDE model ((66) in SI Section 1.6) normalized by that of the well-mixed model as the size of the of mRNA (r_m) and ribosome (r_R) varies with respect to r^*. The amount of protein increases when both the mRNA and ribosome size increases. The parameter values and full simulation details are provided in SI Section 1.6

A potential experiment to test our hypothesis is to measure the rate of transcription (via Quantitative PCR) of a gene under the control of the T7 promoter. This promoter is solely transcribed by the T7 RNAP which specifically targets the promoter, thus this system can be considered orthogonal to the endogenous transcription machinery [32]. By appending random base pairs (BPs) to the sequence of T7 RNAP that do not effect its functionally, we can control its size and thus how much excluded volume effects it experiences. We can then measure the transcription rate of the gene when it is localized in the cell-poles and mid-cell. The results of this experiment should look similar to Figure 4-A, as the size of the T7 RNAP increases the mid-cell (pole) gene has lower (higher) transcription rate. For the mid-cell localized gene, this can be repeated in parts of the chromosome which are known to be dense to amplify these effects.

mRNA translation: The steady state protein levels of (13) for $i = 1, \ldots, n$, are given by

$$\bar{P}_i = \frac{\kappa_{m,i}\bar{c}_{m,i}}{\mu}, \quad \text{with} \quad \bar{c}_{m,i}(t) = \bar{m}_{i,T} \underbrace{\frac{\bar{R}/K_{R,i}\theta_{R,i}}{1 + \bar{R}/K_{R,i}\theta_{R,i}}}_{\text{Ribosome dependence}}, \tag{17}$$

where $\bar{m}_{i,T} = \kappa_{s,i}\bar{c}_{s,i}/(\gamma_i + \mu)$, $K_{m,i} = d_{m,i}/a_{m,i}$. From (17), if $\theta_{R,i} = 1$, for all i, then the rate of translation will be identical to that of a well-mixed model. From (15) and Figure 3, we conclude that $\theta_{R,i} \geq 1$ and it will substantially differ from unity if both $r_s, r_{m,i} \gtrsim 1$, because both species will be excluded from the chromosome onto the cell poles. Once localized at the cell-poles, the mRNA and ribosomes are more likely to bind. This prediction is verified by simulating the translation rate of a single gene $n = 1$ with $\theta_S = 1$ (same transcription rate as a well-mixed model) as we vary the size of mRNA and ribosomes. The results of the simulation are shown in Figure 4 for the full PDE model ((66) in SI Section 1.6). As predicted, the amount of protein with respect to a well-mixed model increases when both the mRNA and ribosome size are sufficiently large. In SI-Figure 11, we show the reduced ODE model (14) is within 2% of the full PDE model (SI (66)) for the result in Figure 4-B. In the SI Section 1.6 we show in Figure 10 the transient response corresponding to Figure 4, for which the full-PDE and reduced model agree well. We verify that as the size of ribosome (mRNA) increases, it is indeed ejected from the chromosome and adopts its available volume profile (Remark 2). Furthermore, in SI-Figure 12-13, we demonstrate that these results hold independently of the binding and unbinding speed between ribosomes and mRNA (Remark 3).

To experientially validate our analytical predictions, we propose expressing a florescence protein from a plasmid with an appended sequence of base pairs added downstream of the stop codon. The appended sequence should have a low affinity to recruit ribosome such that the amount of ribosomes sequestered by the mRNA are the same as without the appended sequence. Assuming this appended sequence does not affect the lifetime of the mRNA, then it should yield the same functional protein which can be used to quantify the mRNA excluded volume effects. This appended sequence of base pairs will allow us to control the size of the mRNA without increasing its ribosome usage. From our theory, for longer appended sequences, more protein expression is expected.

0.5.2 Transcription factors: Gene Regulation

Intracellular signaling to control gene expression is often done via transcription factors (TFs). In this section we model a general transcription factor architecture where the repressor $\mathrm{P_r}$ dimerizes to form $\mathrm{c_1}$ (e.g., TetR dimerizes before targeting gene [33]) and then blocks the transcription of gene D that produces protein P. The biochemical reactions corresponding to this process are:

$$\emptyset \xrightarrow{\alpha} \mathrm{P_r}, \quad \underbrace{\mathrm{P_r} + \mathrm{P_r} \underset{\mathrm{d_1}}{\overset{\mathrm{a_1}}{\rightleftharpoons}} \mathrm{c_1}}_{\text{Case I}}, \quad \underbrace{\mathrm{c_1} + \mathrm{D} \underset{\mathrm{d_2}}{\overset{\mathrm{a_2}}{\rightleftharpoons}} \mathrm{c_2}}_{\text{Case II}}, \quad \mathrm{D} \xrightarrow{\kappa} \mathrm{P}, \tag{18}$$

where α is the production rate of $\mathrm{P_r}$, a_1 (d_1) is the association (disassociation) constant to form the $\mathrm{c_1}$ complex, a_2 (d_2) is the association (disassociation) constant to form the the $\mathrm{c_2}$ complex, and κ is the catalytic rate to produce protein P. Since the repressor $\mathrm{P_r}$, freely diffuses, the dimerization reaction belongs to Case I. The gene D is spatially fixed and it is repressed by the freely diffusing $\mathrm{c_1}$, thus this interaction falls under Case II. We assume that the total concentration of D is conserved, so that $D_T(x) = D(t,x) + c_2(t,x)$ and that that $D_T(x)$ is localized at $x = x^*$. The space averaged dynamics corresponding to (18) obey

$$\frac{d\bar{P}_r(t)}{dt} = \bar{\alpha}(t) - \gamma_r \bar{P}_r(t), \quad \frac{d\bar{c}_1(t)}{dt} = a_1\theta_1(t)\bar{P}_r^2(t) - d_1 c_1(t) - a_2\theta_2(t)\bar{c}_1(t)\bar{D}(t) + d_2\bar{c}_2(t), \tag{19a}$$

$$\frac{d\bar{c}_2(t)}{dt} = a_2\theta_2(t)\bar{D}(t)\bar{c}_i(t) - d_2\bar{c}_2(t), \quad \bar{D}(t) = \bar{D}_T - \bar{c}_2(t), \quad \frac{d\bar{P}(t)}{dt} = \kappa\bar{D}(t) - \gamma_p\bar{P}(t), \tag{19b}$$

where overbars correspond to space averaged quantities, γ_r and γ_p are the degradation rates of P_r and P, respectively, and from Theorem 1, the BCF's are given by

$$\underbrace{\theta_1 = \int_0^1 \hat{v}_{P_r}^2(x)dx = \frac{\int_0^1 v_{P_r}^2(x)dx}{[\int_0^1 v_{P_r}(x)dx]^2}}_{\text{excluded volume effects on } \mathrm{P_r}}, \quad \underbrace{\theta_2 = \hat{v}_{c_1}(x^*) = \frac{v_{c_1}(x^*)}{\int_0^1 v_{c_1}(x)dx}}_{\text{excluded volume effects on } \mathrm{c_1} \text{ and localization of D}}, \quad v_{P_r}(x) = e^{-(r/r^*)^2\hat{\rho}(x)} \tag{19c}$$

where r is the radius of gyration of $\mathrm{P_r}$, $v_{P_r}(x)$ and $v_{c_1}(x)$ are the available volume profiles of $\mathrm{P_r}$ and $\mathrm{c_1}$, respectively, and from (9), $v_{c_1}(x) = v_{P_r}^2(x)$. Figure 3 alongside (19c) may be leveraged to visualize the relationship between r and θ_1 and θ_2.

From setting (19) to steady state, we obtain

$$\bar{P} = \frac{\kappa}{\gamma_p}\bar{D}, \quad \text{where} \quad \bar{D} = \frac{\bar{D}_T}{1 + \frac{\bar{P}_r^2}{K}\theta}, \quad \theta = \theta_1\theta_2 = \hat{v}^2_{P_r}(x^*) \tag{20}$$

where $K = K_{d,1}K_{d,2}$ and $K_{d,i} = d_i/a_i$ for $i = 1, 2$. From (20) and (19c), we observe as that θ contains all the spatial information which includes the size of P_r and the location of the target gene D. If $\theta = 1$, then the protein concentration would be the same as the well-mixed model. The ratio K/θ can be thought of as a an effective dissociation constant of the repressor. If D is located near the mid-cell ($x^* \approx 0$ in (19c)), then for $r/r^* \ll 1$ we have $\theta \approx 1$ (see Figure 3), but as r/r^* increases, we have that $\theta < 1$ and asymptotically approaches zero. Similarly, if D is located near the cell poles ($x^* \approx 1$ in (19c)), then for $r/r^* \ll 1$ we have $\theta \approx 1$ (see Figure 3), but as r/r^* increases, we have that $\theta > 1$. Thus, the efficacy of TFs regulating genes in the chromosome (cell-poles) decreases (increases) with TF size. Physically, this occurs because as the TF size increases, excluded volume effects will push it out of the chromosome onto the cell-poles (see Remark 2), thus interacting with DNA near the cell-poles more frequently than with DNA near mid-cell. We perform numerical simulations to validate our predictions as shown in Figure 5, where increasing the transcription factor size implies higher (lower) repression when the target DNA is localized at the cell poles (mid-cell) with respect to a well-mixed model. The simulation results suggest an excellent agreement between the predictions of the full PDE ((68) in SI Section 1.7) and reduced ODE model (19). Figure 14 in SI Section 1.7, show the temporal curves corresponding to Figure 5, we observe excellent agreement between the full PDE model and the reduced ODE model. Furthermore, we show that all our results hold independently of the binding and unbinding speeds of the transcription factor dimerizing and of the dimer binding to the DNA (Figure 15 in SI Section 1.7).

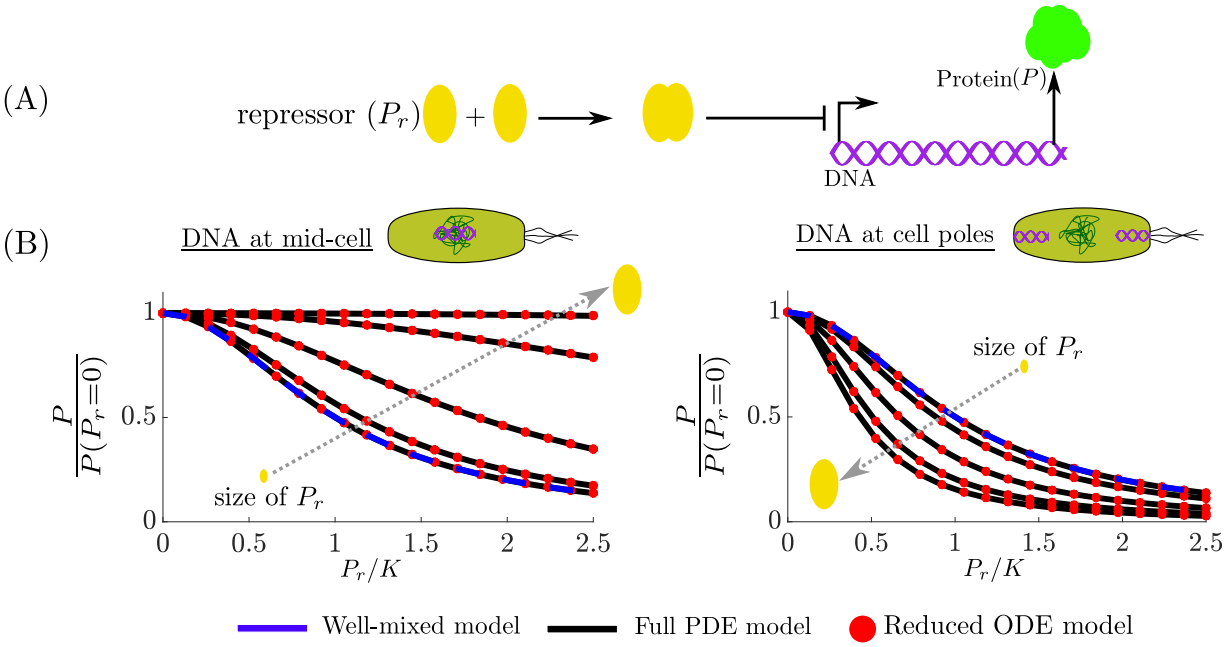

Figure 5: **Spatial heterogeneity dictates transcriptional regulation**. (A) The repressor P_r dimerizes and regulates the production of protein P. (B) The steady state spaced average concentration per-cell of $\bar{P}$ normalized by its value when $\bar{P}_r = 0$ (20) for the PDE model ((68) in SI Section 1.7), the well-mixed model ((19) with $\theta_1 = \theta_2 = 1$), and the reduced ODE model (19) when the DNA is located near mid-cell ($x^* \approx 0$ in (20)) and when the DNA is located at the cell-poles ($x^* \approx 1$). The parameter values and full simulation details are provided in SI Section 1.7.

The reactions in (18) can be easily extended to CRISPRi repression [34], where instead of two identical species dimerizing, we have two distinct freely diffusing species bind (dCas9 and guide RNA) to form the complex gRNA-dCas9 complex which can target a desired DNA sequence. Exploiting the insight gained from analyzing (18), we expect that due to the large size of dCas9 [35] (which is further emphasized as it forms a complex with the gRNA), it will regulate pole localized DNA (e.g,. ColE1 plasmid integrated DNA [9]) more

efficiently than mid-cell DNA (e.g,. chromosomally integrated) and thus spatial effects should be taken into account when using CRISPRi in genetic circuit design. Furthermore, this motivates the search for methods to systematically vary the size of the dCas9 protein or the guide RNA without effecting functionality, to leverage size as a tuning parameters to control gene expression.

To validate this hypothesis in a wet lab setting we propose a genetic circuit on a plasmid expressing a repressor that targets a gene expressing a florescence protein. The transcription factor chosen should be large enough or dimerize to have considerate excluded volume effects. The target DNA expressing protein should be placed on several axial locations in the cell (under the same promoter) achieved by using backbones with different localization profiles and/or different chromosomal integration sites. We should observe that the effective disassociation constant of the repression curve increases as the target genes location is closer to the mid-cell. The disassociation constant is proportional to the amount of repressor necessary to cause the genes expression to decrease by half.

0.5.3 Genetic Oscillator

Now we consider the repressor activator clock genetic circuit [36]. This circuit produces sustained oscillations if tuned within an appropriate parameter range [37, 1]. The circuit consists of two proteins $\mathrm{P_a}$ and $\mathrm{P_r}$. Protein $\mathrm{P_a}$, is an activator which dimerizes to form $\mathrm{P_{a,2}}$ and then binds to its own gene $\mathrm{D_a}$ to form complex $\mathrm{c_{a,1}}$ to initiate transcription. The dimer $\mathrm{P_{a,2}}$ also finds to the gene $\mathrm{D_r}$, which transcribes $\mathrm{P_r}$ to form complex $\mathrm{c_{a,2}}$ and initiates transcription. Protein $\mathrm{P_r}$, dimerizes to form $\mathrm{P_{r,2}}$ and then represses $\mathrm{P_a}$ by binding to $\mathrm{D_a}$ to form complex $\mathrm{c_r}$. The biochemical equations corresponding to this circuit are:

$$\underbrace{\mathrm{P_a} + \mathrm{P_a} \underset{\mathrm{d_1}}{\overset{\mathrm{a_1}}{\rightleftharpoons}} \mathrm{P_{a,2}},}_{\text{Case I, } \mathrm{P}_a \text{ diffuses}} \quad \underbrace{\mathrm{P_r} + \mathrm{P_r} \underset{\mathrm{d_2}}{\overset{\mathrm{a_2}}{\rightleftharpoons}} \mathrm{P_{r,2}},}_{\text{Case II, } \mathrm{P}_r \text{ diffuses}} \quad \underbrace{\mathrm{P_{a,2}} + \mathrm{D_a} \underset{\mathrm{d_3}}{\overset{\mathrm{a_3}}{\rightleftharpoons}} \mathrm{c_{a,1}}, \quad \mathrm{P_{r,2}} + \mathrm{D_a} \underset{\mathrm{d_5}}{\overset{\mathrm{a_5}}{\rightleftharpoons}} \mathrm{c_r},}_{\text{Case III, } \mathrm{P}_{a,2} \text{ and } \mathrm{P}_{r,2} \text{ diffuse and } \mathrm{D_a} \text{ fixed}} \quad \underbrace{\mathrm{P_{a,2}} + \mathrm{D_r} \underset{\mathrm{d_4}}{\overset{\mathrm{a_4}}{\rightleftharpoons}} \mathrm{c_{a,2}},}_{\text{Case II, } \mathrm{P}_{a,2} \text{ diffuse and } \mathrm{D_r} \text{ fixed}}$$

$$\mathrm{D_a} \xrightarrow{\kappa_1} \mathrm{P_a}, \quad \mathrm{D_r} \xrightarrow{\kappa_2} \mathrm{P_r}, \quad \mathrm{P_a} \xrightarrow{\gamma_a} \emptyset, \quad \mathrm{P_r} \xrightarrow{\gamma_r} \emptyset, \quad \mathrm{c_{a,1}} \xrightarrow{\kappa_3} \mathrm{P_a}, \quad \mathrm{c_{a,2}} \xrightarrow{\kappa_4} \mathrm{P_r}, \tag{21a}$$

where a_i (d_i) for $i = 1, \ldots, 5$ are association (disassociation) rate constants, γ_a (γ_r) is the degradation rate of $\mathrm{P_a}$ ($\mathrm{P_r}$) κ_1 (κ_2) is the basal rate at which gene $\mathrm{D_a}$ ($\mathrm{D_r}$) is transcribed, and κ_3 (κ_4) is the rate at which the DNA-transcription-factor complexes are transcribed for $\mathrm{D_a}$ ($\mathrm{D_r}$). We assume that the total concentration of $\mathrm{D_a}$ is conserved, so that $D_{a,T}(x) = D_a(t,x) + c_{a,1}(t,x) + c_r(t,x)$ and that $D_{a,T}(x)$ is localized at $x = x_a$. Similarly, we assume that the total concentration of $\mathrm{D_r}$ is conserved, so that $D_{r,T}(x) = D_r(t,x) + c_{a,2}(t,x)$ and that $D_{r,T}(x)$ is localized at $x = x_r$. The space averaged dynamics corresponding to (21) are given by:

$$\begin{aligned}
\frac{d\bar{P}_a(t)}{dt} =& \kappa_1 \bar{D}_a(t) + \kappa_3 \bar{c}_{a,1}(t) - \gamma_a \bar{P}_a(t), \quad \frac{d\bar{P}_r(t)}{dt} = \kappa_2 \bar{D}_r(t) + \kappa_4 \bar{c}_{a,2}(t) - \gamma_r \bar{P}_r(t), \\
\frac{d\bar{P}_{a,2}(t)}{dt} =& a_1\theta_1(t)\bar{P}_a^2(t) - d_1\bar{P}_{a,2}(t) - a_3\theta_3(t)\bar{P}_{a,2}(t)\bar{D}_a(t) + d_3\bar{c}_{a,1}(t) - a_4\theta_4(t)\bar{P}_{a,2}(t)\bar{D}_r(t) + d_4\bar{c}_{a,2}(t),
\end{aligned} \tag{22a}$$

$$\begin{aligned}
\frac{d\bar{P}_{r,2}(t)}{dt} =& a_2\theta_2(t)\bar{P}_r^2(t) - d_2\bar{P}_{r,2}(t) - a_5\theta_5(t)\bar{P}_{r,2}(t)\bar{D}_a(t) + d_5\bar{c}_r(t), \quad \frac{d\bar{c}_{a,1}(t)}{dt} = a_3\theta_3(t)\bar{P}_{a,2}(t)\bar{D}_a(t) - d_3\bar{c}_{a,1}(t), \\
\frac{d\bar{c}_{a,2}(t)}{dt} =& a_4\theta_4(t)\bar{P}_{a,2}(t)\bar{D}_r(t) - d_4\bar{c}_{a,2}(t), \quad \frac{d\bar{c}_r(t)}{dt} = a_5\theta_5(t)\bar{P}_{r,2}(t)\bar{D}_a(t) - d_5\bar{c}_r(t), \\
\bar{D}_a(t) =& \bar{D}_{a,T} - \bar{c}_{a,1}(t) - \bar{c}_r(t), \quad \bar{D}_r(t) = \bar{D}_{r,T} - \bar{c}_{a,2}(t),
\end{aligned}$$

and applying Theorem 1, the BCF's are given by

$$\theta_1 = \int_0^1 \hat{v}_{P_a}^2(x)dx, \quad \theta_2 = \int_0^1 \hat{v}_{P_r}^2(x)dx, \quad \theta_3 = \hat{v}_{P_{a,2}}(x_a), \quad \theta_4 = \hat{v}_{P_{a,2}}(x_r), \quad \theta_5 = \hat{v}_{P_{r,2}}(x_a). \tag{22b}$$

where $\hat{v}_{P_a}(x)$, $\hat{v}_{P_r}(x)$, $\hat{v}_{P_{a,2}}(x)$, and $\hat{v}_{P_{r,2}}$ are the normalized available volume profiles (i.e,. $\hat{v}_{P_a}(x) = v_{P_a}(x))/\int_0^1 v_{P_a}(x)dx)$ of $\mathrm{P_a}$, $\mathrm{P_r}$, $\mathrm{P_{a,2}}$, and $\mathrm{P_{r,2}}$, respectively. From (9), notice that $v_{P_{a,2}}(x) = v_{P_a}^2(x)$ and $v_{P_{r,2}}(x) = v_{P_r}^2(x)$. The available volume profiles are given by

$$v_{P_a}(x) = e^{-(r_a/r^*)^2\hat{\rho}(x)}, \quad v_{P_r}(x) = e^{-(r_r/r^*)^2\hat{\rho}(x)} \tag{23}$$

where r_a and r_r are the radius of gyration of $\mathrm{P_a}$ and $\mathrm{P_r}$, respectively. If the complexes $\bar{P}_{a,2}(t)$, $\bar{P}_{r,2}(t)$, $\bar{c}_{a,1}(t)$, $\bar{c}_{a,2}(t)$ and $\bar{c}_r(t)$ are in their quasi-steady state (i.e, $d_i \gg \gamma_a, \gamma_r$ for $i = 1, \ldots, 5$, [1]), that is

$$\bar{P}_{a,2}(t) = \frac{a_1\theta_1}{d_1}\bar{P}_a^2(t), \quad \bar{P}_{r,2}(t) = \frac{a_2\theta_2}{d_2}\bar{P}_r^2(t),$$

$$\bar{c}_{a,1}(t) = \frac{a_3\theta_3}{d_3}\bar{P}_{a,2}(t)\bar{D}_a(t), \quad \bar{c}_{a,2}(t) = \frac{a_4\theta_4}{d_4}\bar{P}_{a,2}(t)\bar{D}_r(t), \quad \bar{c}_r(t) = \frac{a_5\theta_5}{d_5}\bar{P}_{r,2}(t)\bar{D}_a(t),$$

then we can simplify (22) to

$$\frac{d\bar{P}_a}{dt} = \frac{\alpha_{0,A} + \Delta\alpha_A\left(\frac{\bar{P}_a}{K_{d,1}}\right)^2}{1 + \left(\frac{\bar{P}_a}{K_{d,1}}\right)^2 + \left(\frac{\bar{P}_r}{K_{d,2}}\right)^2} - \gamma_A\bar{P}_a, \quad \frac{d\bar{P}_r}{dt} = \frac{\alpha_{0,R} + \Delta\alpha_R\left(\frac{\bar{P}_a}{K_{d,3}}\right)^2}{1 + \left(\frac{\bar{P}_a}{K_{d,3}}\right)^2} - \gamma_R\bar{P}_r \tag{24a}$$

where $\alpha_{0,A} = \kappa_1\bar{D}_{a,T}$ ($\alpha_{0,R} = \kappa_2\bar{D}_{r,T}$) is the basal production rate of $\mathrm{P_a}$ ($\mathrm{P_r}$), $\Delta\alpha_A = \kappa_3\bar{D}_{a,T}$ ($\Delta\alpha_R = \kappa_4\bar{D}_{r,T}$) is the additional production rate of $\mathrm{P_a}$ ($\mathrm{P_r}$) due to activation from $\mathrm{P_a}$, and

$$K_{d,1} = \frac{d_1 d_3}{\theta_{A,1}a_1a_3}, \quad K_{d,2} = \frac{d_2 d_5}{\theta_R a_2 a_5}, \quad K_{d,3} = \frac{d_1 d_4}{\theta_{A,2}a_1a_4}, \tag{24b}$$

$$\theta_{A,1} = \theta_1\theta_3 = \hat{v}_{P_a}(x_a), \quad \theta_R = \theta_2\theta_5 = \hat{v}_{P_r}(x_a), \quad \theta_{A,2} = \theta_1\theta_4 = \hat{v}_{P_a}(x_r). \tag{24c}$$

The form of the dynamics given by (24) was theoretically analyzed in [37, 1], and it was shown that the values of $K_{d,i}$ for $i = 1, 2, 3$, were critical in determining if sustained oscillation occur. From (24b), these bifurcation parameters depend on (24c) and thus the size of $\mathrm{P_a}$ and $\mathrm{P_r}$ (23) and the location of $\mathrm{D_a}$ and $\mathrm{D_r}$ (x_a and x_r). We perform numerical experiments to demonstrate how these spatial parameters affect the circuits behavior. In our simulation setup, the parameters are chosen such that the associated well-mixed model ($\theta_R = \theta_{A,1} = \theta_{A,2} = 1$) oscillates, the DNA of $\mathrm{P_a}$ and $\mathrm{P_r}$ are localized at the cell poles and have the same copy number (e.g., they are on the same pole-localized plasmid), the size of $\mathrm{P_r}$ is chose to be small $r_r/r^* \ll 1$ (thus $\theta_R \approx 1$), and the size of $\mathrm{P_a}$ is varied (thus varying $\theta_{A,1}$ and $\theta_{A,2}$). Since $\mathrm{D_a}$ is localized at the cell poles, it implies $x_a \approx 1$ and from (24c), (12), and Figure 3, we observe that if $r_a/r^* \ll 1 \implies \theta_{A,1} \approx \theta_{A,2} \approx 1$ and $\theta_{A,1}, \theta_{A,2}$ increase as r_a/r^* increases. The results of these simulations are shown in Figure 6. As predicted, when $r_a/r^* \ll 1$, the full PDE model ((70) in SI Section 1.8), the reduced ODE model (22), and the well-mixed model are all in agreement and sustained oscillations are observed. When $r_a/r^* = 1$, the well-mixed model still predicts oscillations while the PDE and reduced model (which are in excellent agreement) predict oscillations will no longer occur. Furthermore, in SI Section 1.8 we demonstrate in Figure 17 that indeed as the size of $\mathrm{P_a}$ increases it is excluded from the chromosome onto the cell poles while the spatial profile of $\mathrm{P_r}$ is homogeneously distributed throughout the cell since $r_r/r^* \ll 1$ (Remark 2). These results imply that the qualitative behavior of circuits depends on spatial parameters (DNA location and molecule size) and highlights the importance of modeling spatial effects to ensure desired behavior.

Discussion

In this work, we modeled intracellular spatial heterogeneity that is usually neglected by standard models of genetic circuits but observed experimentally. Primarily, we accounted for genetic circuit spatial location and the tendency for diffusing species to be ejected outside the chromosome (excluded volume effects). Previous spatial-temporal models were solely solved numerically and for a very specific set of reactions based on the context [38, 8, 15]. In contrast, we analyzed a general set of enzymatic like reactions which can be extended to a wide range of biological problems. Furthermore, we performed model reduction to minimize the computational cost of acquiring numerical solutions to the model and to gain insight into the physics that spatial heterogeneity plays in genetic circuit dynamics.

Our model consists of a set of semilinear partial differential equations (PDEs) that capture n enzymes competing for a common substrate. These set of reactions are applicable to many biological processes in the cell. The reactions were considered in three cases: (1) all enzymes and substrate are allowed to diffuse (2) the enzymes are spatially fixed and the substrate is allowed to diffuse (3) the enzymes are allowed to diffuse and the substrate is fixed. For all cases, we accounted for DNA localization and excluded volume effects. We gather numerical solutions to this nonlinear PDE model via a second order finite difference scheme.

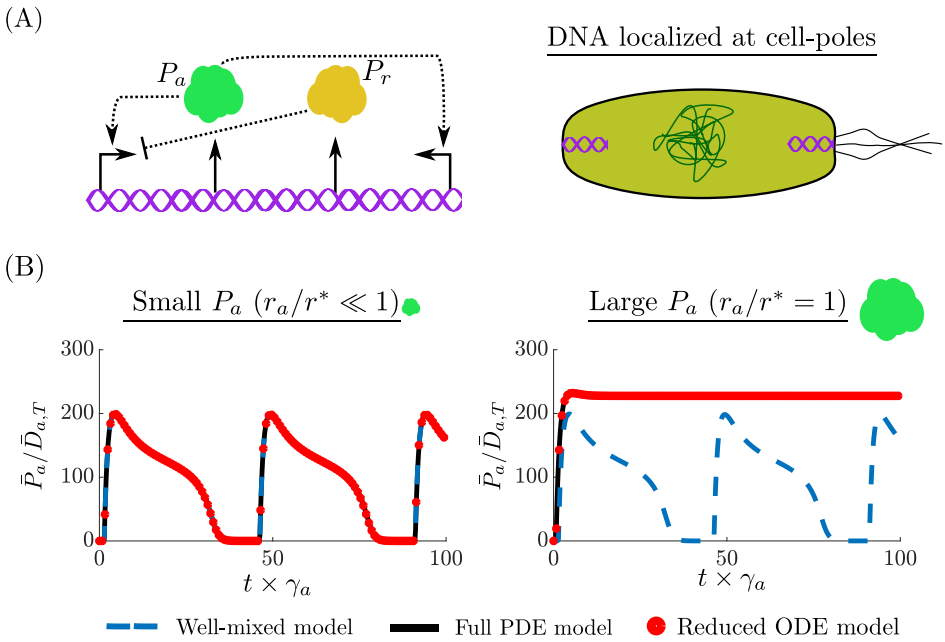

Figure 6: **Genetic circuit qualitative behavior changes due to spatial heterogeneity**. (A) The activator-repressor clock where P_r represses P_a and P_a activates itself and P_r. Both proteins are expressed from the same cell-pole localized plasmid. (B) The temporal evolution of P_a is given for the full-PDE model ((70) in SI Section 1.8), the reduced ODE model (22), and the well-mixed model (same as (22) with $\theta_{A,1} = \theta_{A,2} = \theta_R = 1$). When P_a is small ($r_a/r^* \ll 1$), all three models predict sustained oscillations. When P_a is large ($r_a/r^* = 1$), the full-PDE model and the reduced ODE model predict the oscillations will cease. For both simulations $r/r^* \ll 1$. The full simulation details and parameter values are given in SI Section 1.8.

However, it is hard to gain insight on the physics by solely relying on numerical simulations. Furthermore, these simulations are computationally more expensive than those corresponding to current ODE models.

To overcome the computational expense of solving the full PDE model, we exploit the timescale separation between diffusion and other processes in the cell (such as mRNA degradation and cell growth). We show that under certain assumptions, to model concentration per cell, a modified ODE model may be sufficient. This modified ODE model is very similar to standard "well-mixed" models, but contains a correction coefficient multiplying the association rate constant of bimolecular interactions. The correction coefficient carries all the information relating to spatial heterogeneity, specifically DNA localization and excluded volume effects. Note that this correction factor depends on the spatial distribution of the nucleoid density, which was assumed to be fixed in time. However, it has been shown that nucleoid may actively regulate its shape [4, 39], hence in future work this correction factor may be treated as a time varying parameter. A similar approach of exploiting time scale separation and analyzing space averaged dynamics ("spatial aggregation methods") was proposed in [40, 41] in the population dynamics literature.

Equipped with the tool this reduced modeling framework provides, we analyzed several biological processes of interest. Motivated by the fact that DNA, ribosomes, and mRNA have been shown to localize [4, 14, 5], we look at the transcription and translation processes. We determined that the transcriptional activity of a genetic circuits is lower (higher) when the gene is localized near the mid-cell (cell poles). This discrepancy is greatest when the size of RNAP is larger than a critical value, which depends on the chromosome density near mid-cell. We also considered a transcription factor targeting a gene of interest. We showed that when the target gene is near the mid-cell (cell poles) the effective repression is lower (higher) with respect to the well-mixed model. This discrepancy is amplified as the size of the transcription factor increases. These results add a new perspective on know biological phenomena such as:

- Why the expression of chromosome genes depends on the locus where the gene is inserted [42]
- How the nucleoid actively changes shape (thus local density) to regulate gene expression and transcription factor regulation [4, 39]

- Coregulation and coexpression among genes depends on their spatial distance [43]

For a fixed amount of mRNA, we showed that our model predicts higher translational activity since both mRNA and ribosome are pushed out of the chromosome into a small region near the cell-poles and thus have a greater binding affinity. We showed that the effective ribosome binding strength (RBS) increases with the size of the mRNA.

Our framework can be easily extended to other aspects of gene expression. For example, we may consider co-transcriptional translation [44], in which now the effective RBS will also depend on gene location. We may also consider the role of spatial heterogeneity on orthogonal translational machinery [45]. From our insight, we predict that one can tune the rate at which orthogonal ribosomes are formed by creating larger synthetic 16S rRNA. Furthermore, once the production of orthogonal ribosomes is put in a feedback form to decouple genetic circuits, our framework suggests that the feedback efficiency may depend on the spatial location of the synthetic 16S rRNA gene.

Leveraging our insight from the transcription factor example, we next look at the oscillator circuit which depends on the interaction between an activator and a repressor via transcription factor. This circuit can produce sustained oscillations if the circuit parameters are chosen within an appropriate range. We show that if we consider a parameter set such that the well-mixed model predicts sustained oscillations, then these oscillations may no longer occur depending on DNA localization and size of the transcription factors. Thus these key parameters should be considered in the circuit design process as they can significantly change the qualitative behavior of the circuit.

To conclude, this paper provided a general framework to easily account for DNA localization and excluded volume effects in intracellular species dynamics. While other phenomena attributing to intracellular spatial heterogeneity, such as crowding [46], sliding and hoping, and dimensionality [17], exist, this is a first step towards creating a general framework to modify current models to capture spatial information. The results were shown carefully for a set of enzymatic like reactions. We showed via examples that they could be extended to a more general class of reactions, including those of the oscillator which don't have a fixed steady state. Furthermore, in this work we detailed why our main results hold even though the time scales associated with binding and unbinding of species are comparable to those of diffusion. In future work, we would like to rigorously treat the case where trajectories do not a have a fixed steady state (oscillator) and binding and unbinding are fast. Furthermore, we proposed experimental set ups to test our predictions for the biological examples provided. We would like to carry out these experiments in the near future.

Author Contributions

C.B. performed the research, developed the mathematical analysis, and wrote the article. D.D.V. designed the research, assisted with the mathematical analysis, and edited the article.

Acknowledgments

This work was supported in part by AFOSR grant FA9550-14-1-0060, the NSF Graduate Research Fellowships Program , and the Ford Foundation Predoctoral Fellowship.

References

[1] D. Del Vecchio and R. M. Murray, *Biomolecular Feedback Systems*. 2014.

[2] U. Alon, "An Introduction to Systems Biology: Design Principles of Biological Circuits," 2007.

[3] N. S. Wingreen and K. C. Huang, "Physics of Intracellular Organization in Bacteria," *Annu. Rev. Microbiol.*, vol. 69, no. 1, pp. 361–379, 2015.

[4] X. Weng and J. Xiao, "Spatial organization of transcription in bacterial cells," *Trends Genet.*, vol. 30, no. 7, pp. 287–297, 2014.

[5] L. A. van Gijtenbeek, A. Robinson, A. M. van Oijen, B. Poolman, and J. Kok, "On the Spatial Organization of mRNA, Plasmids, and Ribosomes in a Bacterial Host Overexpressing Membrane Proteins," *PLoS Genet.*, vol. 12, no. 12, pp. 1–28, 2016.

[6] S. Saberi and E. Emberly, "Non-Equilibrium Polar Localization of Proteins in Bacterial Cells," *PLoS One*, vol. 8, no. 5, pp. 1–9, 2013.

[7] C. A. Brackley, S. Taylor, A. Papantonis, P. R. Cook, and D. Marenduzzo, "Nonspecific bridging-induced attraction drives clustering of DNA-binding proteins and genome organization," *Proc. Natl. Acad. Sci.*, vol. 110, no. 38, pp. E3605–E3611, 2013.

[8] C. K. Macnamara and M. A. J. Chaplain, "Spatio-temporal models of synthetic genetic oscillators," *Math. Biosci. Eng.*, vol. 14, no. 1, pp. 249–262, 2016.

[9] S. Yao, D. R. Helinski, and A. Toukdarian, "Localization of the naturally occurring plasmid ColE1 at the cell pole," *J. Bacteriol.*, vol. 189, no. 5, pp. 1946–1953, 2007.

[10] G. Ebersbach and K. Gerdes, "Plasmid Segregation Mechanisms," *Annu. Rev. Genet.*, vol. 39, no. 1, pp. 453–479, 2005.

[11] Y. Wang, P. Penkul, and J. N. Milstein, "Quantitative Localization Microscopy Reveals a Novel Organization of a High-Copy Number Plasmid," *Biophys. J.*, vol. 111, no. 3, pp. 467–479, 2016.

[12] J. A. Englaender, J. A. Jones, B. F. Cress, T. E. Kuhlman, R. J. Linhardt, and M. A. Koffas, "Effect of Genomic Integration Location on Heterologous Protein Expression and Metabolic Engineering in E. coli," *ACS Synth. Biol.*, vol. 6, no. 4, pp. 710–720, 2017.

[13] M. Castellana, S. Hsin-Jung Li, and N. S. Wingreen, "Spatial organization of bacterial transcription and translation," *Proc. Natl. Acad. Sci.*, vol. 113, no. 33, pp. 9286–9291, 2016.

[14] S. Bakshi, A. Siryaporn, M. Goulian, and J. C. Weisshaar, "Superresolution imaging of ribosomes and RNA polymerase in live Escherichia coli cells," *Mol. Microbiol.*, vol. 85, no. 1, pp. 21–38, 2012.

[15] R. Stoof, A. Wood, and A. Goni-Moreno, "A model for the spatio-temporal design of gene regulatory circuits," *bioRxiv*, p. 522946, 2019.

[16] J. Halatek and E. Frey, "Rethinking pattern formation in reaction-diffusion systems," *Nat. Phys.*, vol. 14, no. 5, pp. 507–514, 2018.

[17] S. Soh, M. Byrska, K. Kandere-Grzybowska, and B. A. Grzybowski, "Reaction-diffusion systems in intracellular molecular transport and control," *Angew. Chemie - Int. Ed.*, vol. 49, no. 25, pp. 4170–4198, 2010.

[18] H. de Jong, "Modeling and Simulation of Genetic Regulatory Systems: A Literature Review," *J. Comput. Biol.*, vol. 9, no. 1, pp. 67–103, 2002.

[19] C. Barajas and D. D. Vecchio, "Genetic Circuit-Host Ribosome Transactions : Diffusion-Reaction Model," *Acc*, pp. 1533–1540, 2019.

[20] H. Teimouri, E. Korkmazhan, J. Stavans, and E. Levine, "Sub-cellular mRNA localization modulates the regulation of gene expression by small RNAs in bacteria," *Phys. Biol.*, vol. 14, no. 5, 2017.

[21] A. Amir and S. van Teeffelen, "Getting into shape: How do rod-like bacteria control their geometry?," *Syst. Synth. Biol.*, vol. 8, no. 3, pp. 227–235, 2014.

[22] Leah Edelstein-Keshet, "Mathematical Models in Biology," *Siam*, vol. XXXIII, no. 2, pp. 81–87, 2012.

[23] D. Mishra, P. M. Rivera, A. Lin, D. Del Vecchio, and R. Weiss, "A load driver device for engineering modularity in biological networks," *Nat. Biotechnol.*, vol. 32, no. 12, pp. 1268–1275, 2014.

[24] S. H. Cho, J. M. Godin, C.-H. Chen, W. Qiao, H. Lee, and Y.-H. Lo, "Review Article: Recent advancements in optofluidic flow cytometer," *Biomicrofluidics*, vol. 4, p. 043001, dec 2010.

[25] W. Chen, M. Niepel, and P. Sorger, "Classic and contemporary approaches to modeling biochemical reactions," *Genes Dev.*, vol. 24, pp. 1861–1875, 2010.

[26] A. Okubo and P. Kareiva, "Diffusion and ecological problems," *Interdiscip. Appl. Math.*, pp. 190–195, 2001.

[27] A. Potapov, U. E. Schlägel, and M. A. Lewis, "Evolutionarily stable diffusive dispersal," *Discret. Contin. Dyn. Syst. - Ser. B*, vol. 19, no. 10, pp. 3319–3340, 2014.

[28] C. Grossmann, H.-G. Roos, and M. Stynes, *Numerical Treatment of Partial Differential Equations*. 2007.

[29] G. Strang, *Computational science and engineering*. Wellesley-Cambridge Press Wellesley, 2007.

[30] W. Lohmiller and J. J. E. Slotine, "On Contraction Analysis for Non-linear Systems," *Automatica*, vol. 34, no. 6, pp. 683–696, 1998.

[31] D. Del Vecchio and J. J. E. Slotine, "A contraction theory approach to singularly perturbed systems," *IEEE Trans. Automat. Contr.*, vol. 58, no. 3, pp. 752–757, 2013.

[32] S. Tabor, "Expression Using the T7 RNA Polymerase/Promoter System," *Curr. Protoc. Mol. Biol.*, 2004.

[33] J. L. Ramos, M. Mart, A. J. Molina-henares, W. Tera, R. Brennan, and R. Tobes, "TetR family of transcriptional," vol. 69, no. 2, pp. 1–31, 2005.

[34] M. H. Larson, L. A. Gilbert, X. Wang, W. A. Lim, J. S. Weissman, and L. S. Qi, "CRISPR interference (CRISPRi) for sequence-specific control of gene expression," *Nat. Protoc.*, vol. 8, no. 11, pp. 2180–2196, 2013.

[35] G. J. Gibson and M. Yang, "What rheumatologists need to know about CRISPR/Cas9," *Nat. Rev. Rheumatol.*, vol. 13, no. 4, pp. 205–216, 2017.

[36] M. R. Atkinson, M. A. Savageau, J. T. Myers, and A. J. Ninfa, "Development of genetic circuitry exhibiting toggle switch or oscillatory behavior in Escherichia coli," *Cell*, vol. 113, no. 5, pp. 597–607, 2003.

[37] D. Del Vecchio, "Design and analysis of an activator-repressor clock in E. Coli," in *Proc. Am. Control Conf.*, pp. 1589–1594, 2007.

[38] Q. Zhao, M. Yi, and Y. Liu, "Spatial distribution and dose-response relationship for different operation modes in a reaction-diffusion model of the MAPK cascade," *Phys. Biol.*, vol. 8, no. 5, 2011.

[39] J. K. Fisher, A. Bourniquel, G. Witz, B. Weiner, M. Prentiss, and N. Kleckner, "Four-dimensional imaging of E. coli nucleoid organization and dynamics in living cells," *Cell*, vol. 153, no. 4, pp. 882–895, 2013.

[40] P. Auger, J. C. Poggiale, and E. Sánchez, "A review on spatial aggregation methods involving several time scales," *Ecol. Complex.*, vol. 10, pp. 12–25, 2012.

[41] R. S. Cantrell, C. Cosner, M. A. Lewis, and Y. Lou, "Evolution of dispersal in spatial population models with multiple timescales," *J. Math. Biol.*, vol. 1514752, no. 11571364, 2018.

[42] M.-A. Sánchez-Romero, D. Lee, E. Sánchez-Morán, and S. Busby, " Location and dynamics of an active promoter in Escherichia coli K-12 ," *Biochem. J.*, vol. 441, no. 1, pp. 481–485, 2012.

[43] L. Pannier, E. Merino, K. Marchal, and J. Collado-Vides, "Effect of genomic distance on coexpression of coregulated genes in E. coli," *PLoS One*, vol. 12, no. 4, pp. 1–20, 2017.

[44] S. Bakshi, H. Choi, and J. C. Weisshaar, "The spatial biology of transcription and translation in rapidly growing Escherichia coli," *Front. Microbiol.*, vol. 6, no. JUL, pp. 1–15, 2015.

[45] A. P. Darlington, J. Kim, J. I. Jiménez, and D. G. Bates, "Dynamic allocation of orthogonal ribosomes facilitates uncoupling of co-expressed genes," *Nat. Commun.*, vol. 9, no. 1, 2018.

[46] M. Tabaka, T. Kalwarczyk, J. Szymanski, S. Hou, and R. Holyst, "The effect of macromolecular crowding on mobility of biomolecules, association kinetics, and gene expression in living cells," *Front. Phys.*, vol. 2, no. September, pp. 1–14, 2014.

[47] M. Renardy and R. C. Rogers, "An Introduction to Partial Differential Equations," *Differ. Equations*, vol. 13, no. 2, pp. 1–5, 2003.

[48] H. Weinberger, "Invariant sets for weakly coupled parabolic and elliptic systems," *Rend. Mat. Univ. Roma*, vol. 8, no. l, pp. 295–310, 1975.

[49] W. F. Trench, *Trench_Real_Analysis*. 2010.

[50] A. Gyorgy, J. I. Jiménez, J. Yazbek, H. H. Huang, H. Chung, R. Weiss, and D. Del Vecchio, "Isocost Lines Describe the Cellular Economy of Genetic Circuits," *Biophys. J.*, vol. 109, no. 3, pp. 639–646, 2015.

[51] B. P. Bratton, R. A. Mooney, and J. C. Weisshaar, "Spatial distribution and diffusive motion of rna polymerase in live Escherichia coli," *J. Bacteriol.*, vol. 193, no. 19, pp. 5138–5146, 2011.

[52] T. E. Kuhlman and E. C. Cox, "Gene location and DNA density determine transcription factor distributions in Escherichia coli," *Mol. Syst. Biol.*, vol. 8, no. 610, pp. 1–13, 2012.

Supplementary Material

1 Time Scale Separation Proofs

In this section we provide the mathematical analysis used to proof the results in Section 0.4. First, we provide some preliminary definitions and results that will be frequently used in our analysis. Then, we show our model reduction scheme for a general system. This general result is then applied to (6) in all three diffusion cases when the diffusion dynamics are much faster than the reaction dynamics. Finally, we motivate why our results still holds for the cases when binding and unbinding of species is comparably fast with respect to diffusion.

1.1 Preliminaries:

Notation: Let $\boldsymbol{z} = [z_1, \ldots, z_n]^T \in \mathbb{R}^n$ (where superscript T denotes the transpose operation) and the j-th component of $\boldsymbol{z}$ is denoted by $\boldsymbol{z}^j$. A vector of zeros is denoted as $\boldsymbol{0}_n = [0, \ldots, 0]^T \in \mathbb{R}^n$ and we use $\boldsymbol{A} = \text{diag}(\boldsymbol{v}) \in \mathbb{R}^{n\times n}$ to refer to a square matrix with all zeros in the off-diagonals and diagonal elements specified by the vector $\boldsymbol{v}$. The (j,k)-th element of matrix $\boldsymbol{A}$ is denoted by $\boldsymbol{A}^{j,k}$ and $\boldsymbol{I}_{n,n}$ is the identity matrix in $\mathbb{R}^n$. Let $\mathbb{R}^n_+ = \{[z_1, \ldots, z_n]^T : z_i > 0, i = 1, \ldots, n\}$ denote the positive orthant of $\mathbb{R}^n$. Let $\Omega = (0,1)$, $\overline{\Omega} = [0,1]$, $\partial\Omega = \{0,1\}$. Finally, let over bars denote spatial integration $\bar{u} := \int_\Omega u$. For a Hilbert space H with inner product $\langle \cdot, \cdot \rangle_H$, we denote the norm as $|| \cdot ||_H = \sqrt{\langle \cdot, \cdot \rangle_H}$.

Definition 2. (Linear Differential Operator) Let $v(x) : \bar{\Omega} \to \mathbb{R}_+$ be a smooth function, and consider the following linear differential operator:

$$\mathcal{L}_v(y) := \frac{d}{dx}\left[v^2(x)\frac{d}{dx}\left[\frac{y}{v(x)}\right]\right], \tag{25}$$

with domain $D(\mathcal{L}_v) = \{u \in L^2(\Omega) : v^2 \frac{d}{dx}\left[\frac{u}{v}\right]\big|_{\partial\Omega} = 0\}$:

Next, we introduce the Hilbert space H suitable for our analysis, for which the operator (25) is self-adjoint and negative semi-definite. Thus, its eigenfunctions form a complete orthonormal basis for H and hence we can decompose any elements in this space into a linear sum (possibly infinite) of eigenfunctions.

Definition 3. (Weighted L^2 space) For smooth $v : \bar{\Omega} \to \mathbb{R}_+$ we denote $L^2_v(\Omega)$ as a weighted space of the square integrable functions such that $f \in L^2_v(\Omega)$ if and only if $: \frac{f}{\sqrt{v(x)}} \in L^2(\Omega)$. The inner-product is defined as $\langle f, g\rangle_v := \int_\Omega \frac{f(x)g(x)}{\hat{v}}$, for $f, g \in L^2_v$ and $\hat{v}(x) = \frac{v(x)}{\bar{v}}$. Furthermore, let $\boldsymbol{v} = [v_1(x), \ldots, v_n(x)]^T$, where $v_i(x) : \bar{\Omega} \to \mathbb{R}_+$ is smooth, then $\boldsymbol{z} \in L^2_{\boldsymbol{v}}(\Omega, \mathbb{R}^n)$ if $\boldsymbol{z}^i \in L^2_{v_i}(\Omega)$ for $i = 1, \ldots, n$, and the inner product in this space is defined as $\langle \boldsymbol{f}, \boldsymbol{g}\rangle_{\boldsymbol{v}} := \int_\Omega \boldsymbol{f}^T(x)[\text{diag}(\hat{\boldsymbol{v}})]^{-1}\boldsymbol{g}(x)$, for $\boldsymbol{f}, \boldsymbol{g} \in L^2_{\boldsymbol{v}}(\Omega, \mathbb{R}^n)$, where $\hat{\boldsymbol{v}}^i(x) = \frac{\boldsymbol{v}^i(x)}{\bar{\hat{\boldsymbol{v}}}^i}$.

Lemma 1. *(Negative semi-definite and self-adjoint Operator) The operator in Definition 2, has the following properties:*

1. *Has countably many, real, and distinct eigenvalues such that $\lambda_1 > \ldots > \lambda_n > \ldots$ and $\lambda_n \to -\infty$ as $n \to \infty$*

2. *The set of corresponding eigenfunctions* $\{\psi_i(x)\}$ *form an orthonormal basis for* $L^2_v(\Omega)$ *(Definition 3)*

3. $\lambda_1 = 0$ *and* $\psi_1 = \hat{v}(x) = \frac{v(x)}{\bar{v}}$

4. *From orthogonality* $\bar{\psi}_i = 0, \forall i > 1$

Proof: The proof of (1) and (2) follow from Sturm-Liouville theory [47]. To prove (3), notice $\mathcal{L}_v \psi_i = \lambda_i \psi_i$ and taking the weighted inner product of both sides with ψ_i, using orthonormality, integration by parts, and applying the boundary conditions:

$$\begin{aligned} \lambda_i &= \langle \psi_i, \mathcal{L}_v(\psi_i) \rangle_v \\ &= \int_\Omega \frac{\psi_i}{\hat{v}} \frac{\partial}{\partial x}\left(v^2 \frac{\partial}{\partial x}(\frac{\psi_i}{v}) \right) \\ &= \cancelto{0}{\left[\frac{\psi_i}{\hat{v}} v^2 \frac{\partial}{\partial x}(\frac{\psi_i}{v}) \right]_{\partial\Omega}} - \int_\Omega \bar{v} \left(v \frac{\partial}{\partial x}(\frac{\psi_i}{v}) \right)^2 \\ &\leq 0. \end{aligned} \tag{26}$$

The maximum of (26) is achieved ($\lambda_1 = 0$) for $\psi_1 = \hat{v}(x)$, since $\mathcal{L}_v(\psi_1) = 0$ and $||\psi_1||_{L^2_v} = \sqrt{\langle \psi_1, \psi_1 \rangle_v} = 1$ and therefore $\lambda_i < 0, \forall i > 1$. To show (4), let $i > 1$ and recall from orthonormality $\langle \psi_1, \psi_i \rangle_v = 0$, and thus

$$0 = \langle \psi_1, \psi_i \rangle_v = \langle \hat{v}, \psi_i \rangle_v = \int_\Omega \frac{\hat{v}}{\hat{v}} \psi_i = \int_\Omega \psi_i = \bar{\psi}_i,$$

as desired. ■

Definition 4. (Decomposition onto operator spectrum) Let $\{\psi_i\}$ be the set of complete orthonormal eigenfunctions in $L^2_v(\Omega)$ generated by the operator in Definition 2. We define $\bar{L}^2_v(\Omega) = \text{span}(\psi_1)$ and $L^{2,\perp}_v(\Omega) = \text{span}(\{\psi_i\}_{i=2}^\infty)$ then $L^2_v(\Omega) = \bar{L}^2_v(\Omega) \oplus L^{2,\perp}_v(\Omega)$. Furthermore, if $u \in L^2_v(\Omega)$, then

$$P^1_v : L^2_v(\Omega) \to \bar{L}^2_v(\Omega), \quad u^1_v := P^1_v(u) = \langle u, \psi_1 \rangle_v \psi_1 = \langle u, \hat{v} \rangle_v \hat{v} = \bar{u}\hat{v},$$

$$P^\perp_v : L^2_v(\Omega) \to L^{2,\perp}_v(\Omega), \quad u^\perp_v := P^\perp_v(u) = \sum_{i=2}^\infty \langle u, \psi_i \rangle_v \psi_i,$$

and therefore $u = u^1_v + u^\perp_v = \bar{u}\hat{v} + u^\perp_v$ from completeness. More generally, if $\boldsymbol{u} \in L^2_{\boldsymbol{v}}(\Omega, \mathbb{R}^n)$, then $\boldsymbol{u} = \boldsymbol{V}(x)\bar{\boldsymbol{u}} + \boldsymbol{u}^\perp$, where $\boldsymbol{V}(x) = \text{diag}(\boldsymbol{v}(x))$ and $\boldsymbol{u}^{\perp,i} = P^\perp_{\boldsymbol{v}^i}(\boldsymbol{u}^i)$. Notice $L^2_{\boldsymbol{v}}(\Omega, \mathbb{R}^n) = \bar{L}^2_{\boldsymbol{v}}(\Omega, \mathbb{R}^n) \oplus L^{2,\perp}_{\boldsymbol{v}}(\Omega, \mathbb{R}^n)$, where $\bar{L}^2_{\boldsymbol{v}}(\Omega, \mathbb{R}^n) = \bar{L}^2_{\boldsymbol{v}^1}(\Omega) \times \ldots \times \bar{L}^2_{\boldsymbol{v}^n}(\Omega)$ and $L^{2,\perp}_{\boldsymbol{v}}(\Omega, \mathbb{R}^n) = L^{2,\perp}_{\boldsymbol{v}^1}(\Omega) \times \ldots \times L^{2,\perp}_{\boldsymbol{v}^n}(\Omega)$.

The following will introduce the notion of contracting dynamical systems. A dynamical system is said to be contracting within an open and connected subspace of the state space, if all trajectories starting within this region converge exponentially to each other. We provide an exact mathematical definition of contraction, then provide sufficient conditions to guarantee that a dynamical system has this property, and finally show that contracting systems have what is known as the robustness property. The robustness property will be exploited several times in our analysis to perform our model reduction.

Definition 5. (Contracting systems in $\mathbb{R}^n$) Let $\dot{\boldsymbol{z}} = \boldsymbol{f}(t, \boldsymbol{z})$ be a dynamical system in the Hilbert space $H = \mathbb{R}^n$ with inner product $\langle \cdot, \cdot \rangle_H : H \times H \to \mathbb{R}$ where $\boldsymbol{f}$ is a smooth nonlinear function. An open and connected subset of the state space $\chi \subseteq H$ is contracting if there exists $C \in \mathbb{R}_+$ and $\lambda \in \mathbb{R}_+$ such that for any two trajectories of the dynamical system, $\boldsymbol{z}_1(t)$ and $\boldsymbol{z}_2(t)$, satisfy:

$$||\boldsymbol{z}_2(t) - \boldsymbol{z}_1(t)||_H \leq C||\boldsymbol{z}_2(0) - \boldsymbol{z}_1(0)||_H e^{-\lambda t}, \quad \forall t \geq 0, \quad \forall \boldsymbol{z}_2(0), \boldsymbol{z}_1(0) \in \chi.$$

The scalar λ defines the contraction rate of the system.

Theorem 2. *A sufficient condition for a system to be contracting as in Definition 5, is the existence of a uniformly positive definite matrix* $\boldsymbol{P}(\boldsymbol{z}) \in \mathbb{R}^{n \times n}$ *such that*

$$\frac{1}{2}\left[\frac{\partial \boldsymbol{f}}{\partial \boldsymbol{z}}^T \boldsymbol{P} + \boldsymbol{P}\frac{\partial \boldsymbol{f}}{\partial \boldsymbol{z}} + \dot{\boldsymbol{P}}\right] \leq -\lambda \boldsymbol{P}, \forall \boldsymbol{z} \in \chi, \forall t \geq 0$$

where the constant $\lambda > 0$ *defines the contraction rate of the system.*

Proof: See Theorem 2 in [30]. ■

Lemma 2. *(Robustness property of contracting systems) Assume that $\dot{\boldsymbol{z}} = \boldsymbol{f}(t, \boldsymbol{z})$ satisfies the conditions of Theorem 2, for some $\boldsymbol{P} = \boldsymbol{P}^T > 0$ in a region $\chi \subseteq H$, and thus it is contracting with some contraction rate λ. Consider the perturbed system $\dot{\boldsymbol{z}}_{\boldsymbol{p}} = \boldsymbol{f}(t, \boldsymbol{z}_p) + \boldsymbol{d}(t, \boldsymbol{z}_p)$, and suppose there exists $L_1, L_2, \zeta, \epsilon > 0$ such that $\zeta/\epsilon > \lambda$ and $||\boldsymbol{d}(t, \boldsymbol{z}_p)||_H \leq L_1 e^{-\zeta/\epsilon t} + L_2\epsilon$, then*

$$||\boldsymbol{z}(t) - \boldsymbol{z}_p(t)||_H \leq M\left(||\boldsymbol{z}(0) - \boldsymbol{z}_p(0)||_H e^{-\lambda t} + \frac{L_1}{\zeta}\frac{\epsilon}{1-\epsilon\lambda/\zeta} + \frac{L_2\epsilon}{\lambda}\right),$$

where M is the ratio of the maximum and minimum eigenvalues of $\boldsymbol{P}$.

Proof: Building on the proof of lemma 1 in [31], we have

$$\begin{aligned}||\boldsymbol{z}(t) - \boldsymbol{z}_p(t)||_H &\leq M\left(||\boldsymbol{z}(0) - \boldsymbol{z}_p(0)||_H e^{-\lambda t} + \int_0^t L_1 e^{-\zeta/\epsilon\tau} e^{-\lambda(t-\tau)} d\tau + \frac{L_2\epsilon}{\lambda}\right)\\ &\leq M\left(||\boldsymbol{z}(0) - \boldsymbol{z}_p(0)||_H e^{-\lambda t} + \frac{L_1}{\zeta}\frac{\epsilon}{1-\epsilon\lambda/\zeta} + \frac{L_2\epsilon}{\lambda}\right).\end{aligned}$$

■

1.2 Solutions of diffusing states converge to the null space of the differential operator $\mathcal{L}$

Let $\boldsymbol{v} : \bar{\Omega} \to \mathbb{R}_+^{n_d}$ be a smooth vector-valued function and $\boldsymbol{V}(x) = \text{diag}(\boldsymbol{v}(x))$. For the state vectors $\boldsymbol{z}_s(t, x) \in H_s := L^2(\Omega, \mathbb{R}^{n_s})$ and $\boldsymbol{z}_d(t, x) \in H_d := L^2_{\boldsymbol{v}}(\Omega, \mathbb{R}^{n_d})$, consider the following reaction diffusion system:

$$\begin{aligned}&\frac{\partial \boldsymbol{z}_s(t,x)}{\partial t} = \boldsymbol{f}_s(t, x, \boldsymbol{z}_s, \boldsymbol{z}_d), \quad t > 0, x \in \bar{\Omega},\\ &\frac{\partial \boldsymbol{z}_d(t,x)}{\partial t} = \frac{1}{\epsilon}\boldsymbol{\mathcal{L}}(\boldsymbol{z}_d) + \boldsymbol{f}_d(t, x, \boldsymbol{z}_s, \boldsymbol{z}_d), \quad t > 0, x \in \Omega,\\ &\boldsymbol{V}(x)\frac{d}{dx}\left[\boldsymbol{V}^{-1}(x)\boldsymbol{z}_d(t,x)\right] = \boldsymbol{0}_n \quad t > 0, x \in \partial\Omega\\ &\boldsymbol{z}_s(0,x) = \boldsymbol{z}_{s,0}(x), \quad x \in \Omega,\\ &\boldsymbol{z}_d(0,x) = \boldsymbol{z}_{d,0}(x), \quad x \in \Omega,\end{aligned} \tag{27a}$$

where $\boldsymbol{\mathcal{L}}^i$ in the form of the operator introduced in Definition 2, that is

$$\boldsymbol{\mathcal{L}}^i(\boldsymbol{z}_d) = D_i \frac{d}{dx}\left[\boldsymbol{v}^i(x)\frac{d}{dx}\left[\frac{\boldsymbol{z}_d^i(t,x)}{\boldsymbol{v}^i(x)}\right]\right], \tag{27b}$$

$D_i \in \mathbb{R}_+$, $\epsilon \in \mathbb{R}_+$, $\boldsymbol{f}_s : [0, \infty) \times \bar{\Omega} \times \mathbb{R}^{n_s} \times \mathbb{R}^{n_d} \to \mathbb{R}^{n_s}$ and $\boldsymbol{f}_d : [0, \infty) \times \bar{\Omega} \times \mathbb{R}^{n_s} \times \mathbb{R}^{n_d} \to \mathbb{R}^{n_d}$ are smooth nonlinear functions, $\boldsymbol{z}_{s,0}^i : \bar{\Omega} \to \mathbb{R}+$, and $\boldsymbol{z}_{d,0}^i : \bar{\Omega} \to \mathbb{R}_+$. The elements of $\boldsymbol{z}_d$ may be thought of as "freely diffusing" and those of $\boldsymbol{z}_s$ as "spatially fixed". For the general system (27), we show in this section that as $\epsilon \to 0^+$, the spatial profiles of the diffusing species $\boldsymbol{z}_d$ approaches that of $\boldsymbol{v}(x)$, that is, the null space of $\boldsymbol{\mathcal{L}}$.

<u>Assumption</u> 2.

I There exists a positively invariant compact set $\chi \subset \mathbb{R}^{n_s+n_d}$ such that if $[\boldsymbol{z}_s^T(0,x), \boldsymbol{z}_d^T(0,x)]^T \in \chi, \forall x \in \bar{\Omega}$, then $[\boldsymbol{z}_s^T(t,x), \boldsymbol{z}_d^T(t,x)]^T \in \chi, \forall x \in \bar{\Omega}, \forall t \geq 0$

II There exists a smooth function $\boldsymbol{f} : \bar{\Omega} \times \mathbb{R}^{n_s} \times \mathbb{R}^{n_d} \to \mathbb{R}^{n_s+n_d}$ such that for $i = 1, \ldots, n_s + n_d$

$$|[f_s^T(t, x, \boldsymbol{z}_s, \boldsymbol{z}_d), f_d^T(t, x, \boldsymbol{z}_s, \boldsymbol{z}_d)]^{i,T}| \leq |\boldsymbol{f}^i(x, \boldsymbol{z}_s, \boldsymbol{z}_d)|, \forall t \geq 0, \forall x \in \bar{\Omega}, \forall [\boldsymbol{z}_s^T, \boldsymbol{z}_d^T]^T \in \chi,$$

which implies uniform boundedness of the nonlinearities with respect to all arguments (recall compactness of χ and $\bar{\Omega}$).

We decompose $\boldsymbol{z}_d$ onto the spectra of $\boldsymbol{\mathcal{L}}$ as in Definition 4. Let

$$\boldsymbol{z}_d(t,x) = \hat{\boldsymbol{V}}(x)\bar{\boldsymbol{z}}_d(t)+\boldsymbol{z}_d^{\perp}(t,x), \quad \text{where} \quad \boldsymbol{z}_d^{\perp,i}(t,x) = P_{\boldsymbol{v}^i}^{\perp}(\boldsymbol{z}_d^i(t,x)) \quad \text{and} \quad \hat{\boldsymbol{V}}(x) = \left[\int_0^1 \boldsymbol{V}(x)dx\right]^{-1}\boldsymbol{V}(x),$$

$P_{\boldsymbol{v}^i}^{\perp}$ is given by Definition 4. The dynamics given in (27) can then be expressed as

$$\begin{aligned}
&\frac{\partial \boldsymbol{z}_s(t,x)}{\partial t} = \boldsymbol{f}_s(t,x,\boldsymbol{z}_s,\hat{\boldsymbol{V}}(x)\bar{\boldsymbol{z}}_d) + \Delta\boldsymbol{f}_s(t,x,\boldsymbol{z}_s,\bar{\boldsymbol{z}}_d,\boldsymbol{z}_d^{\perp}), \quad t>0, x\in\bar{\Omega},\\
&\frac{d\bar{\boldsymbol{z}}_d(t)}{dt} = \bar{\boldsymbol{f}}_d(t,\boldsymbol{z}_s,\bar{\boldsymbol{z}}_d) + \Delta\bar{\boldsymbol{f}}_d(t,\boldsymbol{z}_s,\bar{\boldsymbol{z}}_d,\boldsymbol{z}_d^{\perp}) \quad t>0,\\
&\frac{\partial \boldsymbol{z}_d^{\perp}(t,x)}{\partial t} = \frac{1}{\epsilon}\boldsymbol{\mathcal{L}}(\boldsymbol{z}_d^{\perp}) + \boldsymbol{f}_d^{\perp}(t,x,\boldsymbol{z}_s,\bar{\boldsymbol{z}}_d,\boldsymbol{z}_d^{\perp}), \quad t>0, x\in\Omega,\\
&\boldsymbol{V}(x)\frac{d}{dx}\left[\boldsymbol{V}^{-1}(x)\boldsymbol{z}_d^{\perp}(t,x)\right] = \boldsymbol{0}_n \quad t>0, x\in\partial\Omega\\
&\boldsymbol{z}_s(0,x) = \boldsymbol{z}_{s,0}(x), \quad x\in\Omega,\\
&\bar{\boldsymbol{z}}_d(0) = \int_0^1 \boldsymbol{z}_{d,0}(x)dx,\\
&\boldsymbol{z}_d^{\perp}(0,x) = \boldsymbol{z}_{d,0}(x) - \hat{\boldsymbol{V}}(x)\bar{\boldsymbol{z}}_d(0), \quad x\in\Omega,
\end{aligned} \tag{28}$$

where

$$\begin{aligned}
&\Delta\boldsymbol{f}_s(t,x,\boldsymbol{z}_s,\bar{\boldsymbol{z}}_d,\boldsymbol{z}_d^{\perp}) = \boldsymbol{f}_s(t,x,\boldsymbol{z}_s,\hat{\boldsymbol{V}}(x)\bar{\boldsymbol{z}}_d+\boldsymbol{z}_d^{\perp}) - \boldsymbol{f}_s(t,x,\boldsymbol{z}_s,\hat{\boldsymbol{V}}(x)\bar{\boldsymbol{z}}_d),\\
&\bar{\boldsymbol{f}}_d(t,\boldsymbol{z}_s,\bar{\boldsymbol{z}}_d) = \int_0^1\left[\boldsymbol{f}_d(t,x,\boldsymbol{z}_s,\hat{\boldsymbol{V}}(x)\bar{\boldsymbol{z}}_d)\right]dx,\\
&\Delta\bar{\boldsymbol{f}}_d(t,x,\boldsymbol{z}_s,\bar{\boldsymbol{z}}_d,\boldsymbol{z}_d^{\perp}) = \int_0^1\left[\boldsymbol{f}_d(t,x,\boldsymbol{z}_s,\hat{\boldsymbol{V}}(x)\bar{\boldsymbol{z}}_d+\boldsymbol{z}_d^{\perp}) - \boldsymbol{f}_d(t,x,\boldsymbol{z}_s,\hat{\boldsymbol{V}}(x)\bar{\boldsymbol{z}}_d)\right]dx,\\
&\boldsymbol{f}_d^{\perp}(t,x,\boldsymbol{z}_s,\bar{\boldsymbol{z}}_d,\boldsymbol{z}_d^{\perp}) = \boldsymbol{f}_d(t,x,\boldsymbol{z}_s,\hat{\boldsymbol{V}}(x)\bar{\boldsymbol{z}}_d+\boldsymbol{z}_d^{\perp}) - \hat{\boldsymbol{V}}(x)\bar{\boldsymbol{f}}_d(t,\boldsymbol{z}_s,\bar{\boldsymbol{z}}_d).
\end{aligned} \tag{29}$$

Remark 4. *The smoothness and the temporal boundedness properties of $\boldsymbol{f}_s$ and $\boldsymbol{f}_d$, the compactness of χ, and the structure shown in (29) imply the existence of constants $L_s\in\mathbb{R}_+$, $L_d\in\mathbb{R}_+$, and $M\in\mathbb{R}_+$ such that*

$$\begin{aligned}
&||\Delta\boldsymbol{f}_s(t,x,\boldsymbol{z}_s,\bar{\boldsymbol{z}}_d,\boldsymbol{z}_d^{\perp})||_{H_s} \le L_s||\boldsymbol{z}_d^{\perp}||_{H_d},\\
&||\Delta\bar{\boldsymbol{f}}_d(t,x,\boldsymbol{z}_s,\bar{\boldsymbol{z}}_d,\boldsymbol{z}_d^{\perp})||_{H_d} \le L_d||\boldsymbol{z}_d^{\perp}||_{H_d},\\
&||\boldsymbol{f}_d^{\perp}(t,x,\boldsymbol{z}_s,\bar{\boldsymbol{z}}_d,\boldsymbol{z}_d^{\perp})||_{H_d} \le M,
\end{aligned} \tag{30}$$

holds locally in χ.

The following theorem is a direct consequence of the operator $\boldsymbol{\mathcal{L}}$ from Definition 2 being self-adjoint and negative semi-definite. This result will show that the infinite dimensional left over dynamics $\boldsymbol{z}_d^{\perp}(t,x)$ become $\mathcal{O}(\epsilon)$ after a fast transient.

Theorem 3. *For $\boldsymbol{z}_d^{\perp}(t,x)$ given by (28), if $[\boldsymbol{z}_{s,0}^T(x),\boldsymbol{z}_{d,0}^T(x)]^T\in\chi, \forall x\in\bar{\Omega}$, where $[\boldsymbol{z}_{s,0}^T(x),\boldsymbol{z}_{d,0}^T(x)]^T$ is defined in (27) and χ from Assumption 2, then there exists $\zeta>0$ such that for $t\ge 0$*

$$||\boldsymbol{z}_d^{\perp}(t,x)||_{H_d} = ||\boldsymbol{z}_d^{\perp}(0,x)||_{H_d}e^{-\zeta t/\epsilon} + \mathcal{O}(\epsilon) = \mathcal{O}(e^{-\zeta t/\epsilon}) + \mathcal{O}(\epsilon).$$

Proof:

Let $\psi(t) = ||\boldsymbol{z}_d^{\perp}(t,x)||_{H_d}^2/2$ and $\tau = t/\epsilon$ thus

$$\frac{d\psi(\tau)}{d\tau} = \langle \boldsymbol{z}_d^{\perp}, \frac{\partial \boldsymbol{z}_d^{\perp}}{\partial\tau}\rangle_{\boldsymbol{v}} = \langle \boldsymbol{z}_d^{\perp}, \mathcal{L}(\boldsymbol{z}_d^{\perp})\rangle_{\boldsymbol{v}} + \epsilon\langle \boldsymbol{z}_d^{\perp}, \boldsymbol{f}_d^{\perp}(t,x,\boldsymbol{z}_s,\bar{\boldsymbol{z}}_d,\boldsymbol{z}_d^{\perp})\rangle_{\boldsymbol{v}}.$$

Let $\lambda_{i,j}$ and $\psi_{i,j}$ denote the j-th eigenvalue and eigenfunction, respectively, of $\boldsymbol{\mathcal{L}}^i(\cdot)$ (i.e,. $\boldsymbol{\mathcal{L}}^i(\psi_{i,j}) = \lambda_{i,j}\psi_{i,j}$). Recall that $\{\psi_{i,j}\}$ forms a complete orthonormal eigenfunctions of $L^2_{\boldsymbol{v}^i}(\Omega)$ generated by (25) guaranteed by

Lemma 1. From the orthonormality of the eigenfunctions, linearity of $\boldsymbol{\mathcal{L}}^i(\cdot)$, and the ordering of eigenvalues, notice that:

$$\begin{aligned}
\langle \boldsymbol{z}_d^{\perp}, \mathcal{L}(\boldsymbol{z}_d^{\perp})\rangle_{\boldsymbol{v}} &= \sum_{i=1}^{n_d} \langle \boldsymbol{z}_d^{\perp,i}, \boldsymbol{\mathcal{L}}^i(\boldsymbol{z}_d^{\perp,i})\rangle_{\boldsymbol{v}^i} \\
&= \sum_{i=1}^{n_d} \Big\langle \sum_{j=2}^{\infty} \langle \boldsymbol{z}_d^{\perp,i}, \psi_{i,j}\rangle_{\boldsymbol{v}^i} \psi_{i,j}, \boldsymbol{\mathcal{L}}^i\big(\sum_{j=2}^{\infty} \langle \boldsymbol{z}_d^{\perp,i}, \psi_{i,j}\rangle_{\boldsymbol{v}^i} \psi_{i,j}\big)\Big\rangle_{\boldsymbol{v}^i} \\
&= \sum_{i=1}^{n_d} \Big\langle \sum_{j=2}^{\infty} \langle \boldsymbol{z}_d^{\perp,i}, \psi_{i,j}\rangle_{\boldsymbol{v}^i} \psi_{i,j}, \sum_{j=2}^{\infty} \langle \boldsymbol{z}_d^{\perp,i}, \psi_{i,j}\rangle_{\boldsymbol{v}^i} \boldsymbol{\mathcal{L}}^i\big(\psi_{i,j}\big)\Big\rangle_{\boldsymbol{v}^i} \\
&= \sum_{i=1}^{n_d} \Big\langle \sum_{j=2}^{\infty} \langle \boldsymbol{z}_d^{\perp,i}, \psi_{i,j}\rangle_{\boldsymbol{v}^i} \psi_{i,j}, \sum_{j=2}^{\infty} \lambda_{i,j} \langle \boldsymbol{z}_d^{\perp,i}, \psi_{i,j}\rangle_{\boldsymbol{v}^i} \psi_{i,j}\Big\rangle_{\boldsymbol{v}^i} \\
&= \sum_{i=1}^{n_d} \sum_{j=2}^{\infty} \lambda_{i,j} \langle \boldsymbol{z}_d^{\perp,i}, \psi_{i,j}\rangle_{\boldsymbol{v}^i}^2 \\
&\leq \sum_{i=1}^{n_d} \lambda_{i,2} \sum_{j=2}^{\infty} \langle \boldsymbol{z}_d^{\perp,i}, \psi_{i,j}\rangle_{\boldsymbol{v}^i}^2 \\
&= \sum_{i=1}^{n_d} \lambda_{i,2} \langle \boldsymbol{z}_d^{\perp,i}, \boldsymbol{z}_d^{\perp,i}\rangle_{\boldsymbol{v}^i} \\
&\leq -|\bar{\lambda}_2| \langle \boldsymbol{z}_d^{\perp}, \boldsymbol{z}_d^{\perp}\rangle_{\boldsymbol{v}} \\
&= -2|\bar{\lambda}_2| \psi(\tau)
\end{aligned}$$

where $\bar{\lambda}_2 = \max_{i=1,\ldots n_d}(\{\lambda_{2,i}\})$. Recall from Remark 4 that $||\boldsymbol{f}_d^{\perp}||_{H_d} \leq M, \forall z \in \chi$ and the cauchy-Schwarz inequality $|\langle \boldsymbol{z}_d^{\perp}, \boldsymbol{f}_d^{\perp}\rangle_{\boldsymbol{v}}| \leq ||\boldsymbol{f}_d^{\perp}||_{H_d} ||\boldsymbol{z}_d^{\perp}||_{H_d}$ and let $\nu \in (0,1)$ thus

$$\begin{aligned}
\frac{d\psi(\tau)}{d\tau} &\leq -2|\bar{\lambda}_2|\psi(\tau) + \epsilon M \psi^{1/2}(\tau) \\
&\leq -2(1-\nu)|\bar{\lambda}_2|\psi(\tau) - 2\nu|\bar{\lambda}_2|\psi(\tau) + \epsilon M \psi^{1/2}(\tau) \\
&\leq -2(1-\nu)|\bar{\lambda}_2|\psi(\tau), \quad \forall \psi > \big[\frac{\epsilon M}{2\nu|\bar{\lambda}_2|}\big]^2.
\end{aligned}$$

Therefore, if $\psi(0) > \big[\frac{\epsilon M}{2\nu|\bar{\lambda}_2|}\big]^2$ it implies that

$$\psi(\tau) \leq \psi(0) e^{-2(1-\nu)|\bar{\lambda}_2|\tau}.$$

This implies that

$$\psi(\tau) \leq \psi(0) e^{-2(1-\nu)|\bar{\lambda}_2|\tau} + \big[\frac{\epsilon M}{2\nu|\bar{\lambda}_2|}\big]^2, \forall \tau \geq 0.$$

Finally,

$$||\boldsymbol{z}_d^{\perp}(t,x)||_{H_d} \leq ||\boldsymbol{z}_d^{\perp}(0,x)||_{H_d} e^{-\zeta t/\epsilon} + \frac{\epsilon M}{2\nu|\bar{\lambda}_2|},$$

where $\zeta = (1-\nu)|\bar{\lambda}_2|$. ■

Remark 5. *The following nominal system*

Definition 6. (Reduced slow dynamics) Let the state vectors $\hat{\boldsymbol{z}}_s(t,x) \in \mathbb{R}^{n_s}$ and $\hat{\boldsymbol{z}}_d(t,x) \in \mathbb{R}^{n_d}$ satisfy

$$\begin{aligned}
\frac{\partial \hat{\boldsymbol{z}}_s(t,x)}{\partial t} &= \boldsymbol{f}_s(t,x,\hat{\boldsymbol{z}}_s,\hat{\boldsymbol{z}}_d), \quad t>0, x\in\bar{\Omega},\\
\frac{\partial \hat{\boldsymbol{z}}_d(t,x)}{\partial t} &= \boldsymbol{V}(x)\int_0^1 \boldsymbol{f}_d(t,x,\hat{\boldsymbol{z}}_s,\hat{\boldsymbol{z}}_d)dx, \quad t>0, x\in\bar{\Omega},\\
\hat{\boldsymbol{z}}_s(0,x) &= \boldsymbol{z}_{s,0}(x), \quad x\in\Omega,\\
\hat{\boldsymbol{z}}_d(0,x) &= \boldsymbol{V}(x)\int_0^1 \boldsymbol{z}_{d,0}(x)dx.
\end{aligned} \tag{31}$$

corresponds to (28) *when* $\Delta\boldsymbol{f}_s(t,x,\boldsymbol{z}_s,\bar{\boldsymbol{z}}_d,\boldsymbol{z}_d^{\perp}) = \boldsymbol{0}$ *and* $\Delta\bar{\boldsymbol{f}}_d(t,\boldsymbol{z}_s,\bar{\boldsymbol{z}}_d,\boldsymbol{z}_d^{\perp}) = \boldsymbol{0}$*, which occurs when* $\boldsymbol{z}_d^{\perp} = \boldsymbol{0}$*. Thus, one could show that the solutions of* (31) *are close to those of* (28)*, if exponential stability of* (31) *is shown around some equilibrium point or if the system is shown to be contracting (to treat the time varying case).*

1.3 Model Reduction of Enzymatic-like Reaction In the Limit of Fast diffusion

The spatial-temporal dynamics of the enzymatic-like reactions provided in the main text are given in dimensionless form by

$$\frac{\partial E_i(t,x)}{\partial t} = -\frac{d}{dx}\big[J_{E_i}(x,E_i)\big] + \alpha_i(t,x) + \frac{1}{\eta_i}\Big[-E_i(t,x)S(t,x)\frac{\tilde{a}_i}{\tilde{d}_i} + c_i(t,x)\Big] - (\gamma_i+1)(E_i(t,x)+c_i(t,x)), \tag{32a}$$

$$\frac{\partial c_i(t,x)}{\partial t} = -\frac{d}{dx}\big[J_{c_i}(x,c_i)\big] + \frac{1}{\eta_i}\Big[E_i(t,x)S(t,x)\frac{\tilde{a}_i}{\tilde{d}_i} - c_i(t,x)\Big], \tag{32b}$$

$$\frac{\partial S(t,x)}{\partial t} = -\frac{d}{dx}\big[J_s(x,S)\big] + \alpha_s(t,x) + \sum_{j=1}^{n}\frac{1}{\eta_j}\Big[-E_j(t,x)S(t,x)\frac{\tilde{a}_j}{\tilde{d}_j} + c_j(t,x)\Big] - (\gamma_s+1)(S(t,x)+\sum_{j=1}^{n}c_j(t,x)), \tag{32c}$$

where the flux term and the boundary conditions are given in Table 2 for three cases of interest. Fast diffusion corresponds to $\epsilon \ll 1$, where ϵ is provided in Table 2.

Case	I: All species diffuse	II: Substrate diffuses and enzymes fixed	III: Enzymes diffuses and substrate fixed
Dimensionless Flux	$J^*_{E_i} = -\frac{1}{\epsilon}\chi_{E_i}v^2_{E_i}\frac{d}{dx^*}[\frac{E^*_i}{v_{E_i}}]$ $J^*_s = -\frac{1}{\epsilon}v^2_S\frac{d}{dx^*}[\frac{S}{v_s}]$ $J^*_{c_i} = -\frac{1}{\epsilon}\chi_{c_i}v^2_{c_i}\frac{d}{dx^*}[\frac{c_i}{v_{c_i}}]$	$J^*_{E_i} = 0$ $J^*_s = -\frac{1}{\epsilon}v^2_s\frac{d}{dx^*}[\frac{S^*}{v_s}]$ $J^*_{c_i} = 0$	$J^*_{E_i} = -\frac{1}{\epsilon}v^2_{E_i}\frac{d}{dx^*}[\frac{E^*_i}{v_{E_i}}]$ $J^*_s = 0$ $J^*_{c_i} = 0$
Boundary conditions	$J^*_{E_i}(0,E^*_i) = J^*_{E_i}(1,E^*_i) = 0$ $J^*_{c_i}(0,c^*_i) = J^*_{c_i}(1,c^*_i) = 0$ $J^*_s(0,S^*) = J^*_s(1,S^*) = 0$	$J^*_s(0,S^*) = J^*_s(1,S^*) = 0$	$J^*_{E_i}(0,E^*_i) = J^*_{E_i}(1,E^*_i) = 0$
ϵ	$(\mu L^2)/D_s$	$(\mu L^2)/D_s$	$(\mu L^2)/D_{E_1}$
Dimensionless diffusion	$\chi_{E_i} = D_{E_i}/D_s, \chi_{c_i} = D_{c_i}/D_s$		

Table 2: The flux dynamics and the boundary conditions corresponding to (32) for each case of interest along with the the biological relevance. The parameters D_{E_i}, D_{c_i}, and D_s, are the enzyme, complex, and substrate diffusion coefficients, respectively, ϵ is a dimensionless parameter that captures the speed of diffusion (with respect to dilution). A species being spatially fixed translates to the flux being zero throughout the whole spatial domain.

We denote $\bar{E}_i(t)$, $\bar{S}(t)$, and $\bar{c}_i(t)$ to be the space averaged enzyme, substrate, and complex concentrations, respectively (e.g., $\bar{E}_i(t) = \int_0^1 E_i(t,x)dx$). The dynamics governing these space averaged variables are derived

by integrating (32) in space and applying the boundary conditions and are given by:

$$\frac{d\bar{E}_i(t)}{dt} = \bar{\alpha}_i(t) - \frac{1}{\eta_i}\big[\frac{\tilde{a}_i}{\tilde{d}_i}[\int_0^1 E_i(t,x)S(t,x)dx] - \bar{c}_i(t)\big] - (\gamma_i+1)(\bar{E}_i(t)+\bar{c}_i(t)) \tag{33a}$$

$$\frac{d\bar{c}_i(t)}{dt} = \frac{1}{\eta_i}\big[\frac{\tilde{a}_i}{\tilde{d}_i}[\int_0^1 E_i(t,x)S(t,x)dx] - \bar{c}_i(t)\big] \tag{33b}$$

$$\frac{d\bar{S}(t)}{dt} = \bar{\alpha}_s(t) - \sum_{j=1}^{n}\frac{1}{\eta_j}\left[\frac{\tilde{a}_j}{\tilde{d}_j}[\int_0^1 E_j(t,x)S(t,x)dx] - \bar{c}_j(t)\right] - (\gamma_s+1)(\bar{S}(t)+\sum_{j=1}^{n}\bar{c}_j(t)) \tag{33c}$$

where overbars denote spatially averaged variables. We make the follow assumptions necessary to state our main result

Assumption 3. Consider (32), for $i = 1,\dots,n$, assume that

I the functions $\alpha_i(t,x)$ and $\alpha_s(t,x)$ are smooth in both arguments

II there exists a smooth functions $\underline{\alpha}_i(x)$ and $\tilde{\alpha}_i(x)$ such that $0 \le \underline{\alpha}_i(x) \le \alpha_i(t,x) \le \tilde{\alpha}_i(x), \forall t \ge 0, \forall x \in \bar{\Omega}$

III there exists a smooth function $\tilde{\alpha}_s(x)$ such that $0 \le \alpha_s(t,x) \le \tilde{\alpha}_s(x), \forall t \ge 0, \forall x \in \bar{\Omega}$

IV the functions $v_{E,i}(x)$, $v_S(x)$, and $v_{c_i}(x) = v_{E,i}(x)v_S(x)$ (as in Table 2) are strictly greater than zero, are bounded above by unity, and are smooth

Assumptions 3-I-III and the compactness of $\bar{\Omega}$, ensure that the production terms are uniformly bounded in time space. The following assumption makes mathematically precise what it means for fixed (non-diffusing) species to be spatially localized. Assumption 3-IIII is automatically satisfied in a biological context because this functions represent the fraction of volume available to a molecule within the chromosome mesh to diffuse [13].

Assumption 4. (Localization of spatially fixed species) Assume that there exists $x_i, x_s \in (0,1)$ and $L_i, L_s > 0$ such that for $t \ge 0$

- for Case II: $\alpha_i(t,x) \le L_i\delta$, and $E_i(0,x) + c_i(0,x) \le \frac{L_i\delta}{\gamma_i+1}$, for all $x \notin [x_i-\delta, x_i+\delta]$
- for Case III: $\alpha_s(t,x) \le L_s\delta$, and $S(0,x) + \sum_{j=1}^{n} c_j(0,x) \le \frac{L_s\delta}{\gamma_s+1}$, for all $x \notin [x_s-\delta, x_s+\delta]$,

where $\delta > 0$ is such that $[x_i-\delta, x_i+\delta] \subset [0,1]$ and $[x_s-\delta, x_s+\delta] \subset [0,1]$ and Cases II-III correspond to those described in Table 2. Furthermore, assume that $\bar{\alpha}_i(t) = \int_0^1 \alpha_i(t,x)dx$ and $\bar{\alpha}_s(t) = \int_0^1 \alpha_s(t,x)dx$ are independent of δ.

The latter part of Assumption 4 ensures that the spaced averaged production rates are independent of localization. Biologically, this is consistent with the fact that the total amount of DNA in the cell is independent of where the DNA is concentrated.

Assumption 5. (Bounded initial conditions) For $i = 1,\dots,n$, let $\bar{E}_i(t)$, $\bar{S}(t)$, and $\bar{c}_i(t)$ be as in (33), and $\tilde{\alpha}_i(x)$, $\tilde{\alpha}_s(x)$, and $\underline{\alpha}_i(x)$ as in Assumption 3, assume that $\bar{E}_{i,*} \le \bar{E}_i(0)$, $\bar{E}_i(0) + \bar{c}_i(0) \le \bar{E}^*_{i,T}$, and that $\bar{S}(0) + \sum_{j=1}^{n}\bar{c}_j(0) \le S^*_T$ where $\bar{E}_{i,*} = \frac{\bar{\alpha}_i}{\gamma_i+1+\tilde{a}_i S^*_T}$, $\bar{E}^*_{i,T} = \frac{\bar{\alpha}^*_i}{\gamma_i+1}$, $\bar{S}^*_T = \frac{\bar{\alpha}^*_s}{\gamma_s+1}$, $\bar{\underline{\alpha}}_i = \int_0^1 \underline{\alpha}_i(x)dx$, $\bar{\alpha}^*_i = \int_0^1 \tilde{\alpha}_i(x)dx$, and $\bar{\alpha}^*_s = \int_0^1 \tilde{\alpha}_s(x)dx$.

The following definition will provide the candidate reduced model that approximates (33) well when diffusion is fast ($\epsilon \ll 1$) and the production of spatially fixed species is localized to a small region (Assumption 4 holds for $\delta \ll 1$).

Definition 7. (Reduced spaced-averaged dynamics) For $i = 1,\dots,n$, let $\hat{\bar{E}}_i(t)$, $\hat{\bar{S}}(t)$, and $\hat{\bar{c}}_i(t)$ follow

$$\frac{d\hat{\bar{E}}_i(t)}{dt} = \bar{\alpha}_i(t) - \frac{1}{\eta_i}\big[\hat{\bar{E}}_i(t)\hat{\bar{S}}(t)\frac{\tilde{a}_i\theta^*_i}{\tilde{d}_i} - \hat{\bar{c}}_i(t)\big] - (\gamma_i+1)(\hat{\bar{E}}_i(t)+\hat{\bar{c}}_i(t) \tag{34a}$$

$$\frac{d\hat{\bar{c}}_i(t)}{dt} = \frac{1}{\eta_i}\big[\hat{\bar{E}}_i(t)\hat{\bar{S}}(t)\frac{\tilde{a}_i\theta^*_i}{\tilde{d}_i} - \hat{\bar{c}}_i(t)\big] \tag{34b}$$

$$\frac{d\bar{S}(t)}{dt} = \bar{\alpha}_s(t) - \sum_{j=1}^{n}\frac{1}{\eta_j}\left[\hat{\bar{E}}_j(t)\hat{\bar{S}}(t)\frac{\tilde{a}_j\theta^*_j}{\tilde{d}_j} - \hat{\bar{c}}_i(t)\right] - (\gamma_s+1)(\hat{\bar{S}}(t)+\sum_{j=1}^{n}\hat{\bar{c}}_j(t)) \tag{34c}$$

where $\hat{\bar{E}}_i(0) = \bar{E}_i(0)$, $\hat{\bar{S}}(0) = \bar{S}(0)$, $\hat{\bar{c}}_i(0) = \bar{c}_i(0)$, and

$$\theta_i^* = \begin{cases} \int_0^1 \hat{v}_{E_i}(x)\hat{v}_S(x)dx & \text{for Case I} \\ \hat{v}_S(x_i) & \text{for Case II} \\ \hat{v}_{E_i}(x_s) & \text{for Case III} \end{cases}, \tag{35}$$

where x_i and x_s are as in Assumption 4 and Case I-III correspond to those described in Table 2.

Theorem 4. *Let $\epsilon > 0$ be defined for Case I-III by Table 2, $\bar{E}_i(t)$, $\bar{c}_i(t)$, and $\bar{S}(t)$ be given by (33), and $\hat{\bar{E}}_i(t)$, $\hat{\bar{S}}(t)$, and $\hat{\bar{c}}_i(t)$ be as in Definition 7, and suppose Assumption 4 holds for $\delta > 0$, then, there exists $\epsilon^* > 0$ such that for all $\epsilon < \epsilon^*$ and $t \geq 0$, we have that*

$$\bar{E}_i(t) = \hat{\bar{E}}_i(t) + \mathcal{O}\left(\frac{\epsilon}{1-\epsilon/\epsilon^*}\right) + \mathcal{O}(\delta), \quad \bar{c}_i(t) = \hat{\bar{c}}_i(t) + \mathcal{O}\left(\frac{\epsilon}{1-\epsilon/\epsilon^*}\right) + \mathcal{O}(\delta), \quad \bar{S}(t) = \hat{\bar{S}}(t) + \mathcal{O}\left(\frac{\epsilon}{1-\epsilon/\epsilon^*}\right) + \mathcal{O}(\delta).$$

Road map of proof: The rest of this section is dedicated towards proving Theorem 4. We first apply Theorem 3 to show that the spatial profile of a freely diffusing species converges to its available volume profile exponentially fast in the time scale associated with diffusion. If the localization assumption holds, then (33) has the form by described by Definition 7, but with additional "disturbance" terms of order ϵ and δ. We proceed to demonstrate the system described in Definition 7 is contracting (Definition 5) and apply the robustness property of contracting systems (Lemma 2) to show closeness between its solutions and those of (33).

The following result will define a positively invariant and compact subset of $\mathbb{R}^{2n+1}$ such that solutions to (32) are constrained within this set for all times and spatial values. Such a positively invariant set is necessary to apply Theorem 3 to (32).

Claim 1. Consider the system given by (32) where the flux terms are specified in Table 2 along with Assumptions 3 and let $\hat{\gamma} = \min(\gamma_1, \ldots, \gamma_n, \gamma_s)$, $\Gamma = \max_{x\in\Omega}\left(\sum_{j=1}^n \tilde{\alpha}_j(x) + \tilde{\alpha}_S(x)\right)/(\hat{\gamma}+1)$,

$$\boldsymbol{z}(t,x) = [E_1(t,x), \ldots, E_n(t,x), c_1(t,x), \ldots, c_n(t,x), S(t,x)],$$

$$\vec{n} = [1, \ldots, 1, 2, \ldots, 2, 1] \in \mathbb{R}^{2n+1}, \text{ and}$$

$$\chi = \{\boldsymbol{z} \in \mathbb{R}^{2n+1} : \boldsymbol{z}^i \geq 0, \forall i \text{ and } \boldsymbol{z}^T\vec{n} \leq \Gamma\},$$

then, $\boldsymbol{z}(t,x) \in \chi, \forall t \geq 0, \forall x \in \bar{\Omega}$.

Proof: The proof follows [48], which is based on the maximum principle for parabolic systems and requires showing that the vector field of the reaction dynamics of (32) points inward at the boundaries of χ. The spatial differential operator (if applicable depending on the case) for a general diffusing species $y(t,x)$ with available volume profile $v(x)$ in (32), is given by

$$\mathcal{L} = \frac{d}{dx}\left[v^2(x)\frac{d}{dx}\left(\frac{y(t,x)}{v(x)}\right)\right] = v(x)\frac{\partial^2 y(t,x)}{\partial x^2} - y(t,x)\frac{\partial^2 v(x)}{\partial x^2},$$

which is not in the standard form assumed in [48], therefore, the following coordinate transformations needs to be made:

- Case I: $u_{E_i}(t,x) = E_i(t,x)/v_{E_i(x)}$, $u_{c_i}(t,x) = c_i/(t,x)v_{c_i}(x)$, and $u_s(t,x) = S(t,x)/v_S(x)$,
- Case II: $u_{E_i}(t,x) = E_i(t,x)$, $u_{c_i}(t,x) = c_i(t,x)$, and $u_s(t,x) = S(t,x)/v_S(x)$,
- Case III: $u_{E_i}(t,x) = E_i(t,x)/v_{E_i}(x)$, $u_{c_i}(t,x) = c_i(t,x)$, and $u_s(t,x) = S(t,x)$.

With the transformation $u(t,x) = y(t,x)/v(x)$ the differential operator $\mathcal{L}$ is given by

$$\frac{1}{v(x)}\mathcal{L} = v(x)\frac{\partial^2 y(t,x)}{\partial x^2} + 2\frac{\partial v(x)}{\partial x}\frac{\partial y(t,x)}{\partial x},$$

which is now in the correct form. This transformation is just a subtle technical point required to apply the result in [48] and does play a role in the rest of the proof. Let

$$f_{E_i}(t,x) = \alpha_i(t,x) - \frac{1}{\eta_i}\big[E_i(t,x)S(t,x)\frac{\tilde{a}_i}{\tilde{d}_i} - c_i(t,x)\big] - (\gamma_i+1)(E_i(t,x)+c_i(t,x)), \tag{36a}$$

$$f_{c_i}(t,x) = \frac{1}{\eta_i}\big[E_i(t,x)S(t,x)\frac{\tilde{a}_i}{\tilde{d}_i} - c_i(t,x)\big], \tag{36b}$$

$$f_s(t,x) = \alpha_s(t,x) - \sum_{j=1}^{n}\frac{1}{\eta_j}\big[E_j(t,x)S(t,x)\frac{\tilde{a}_j}{\tilde{d}_j} - c_j(t,x)\big] - (\gamma_s+1)(S(t,x)+\sum_{j=1}^{n}c_j(t,x)), \tag{36c}$$

and $\boldsymbol{f}(t,x) = [f_{E_1}(t,x),\dots,f_{E_n}(t,x),f_{c_1}(t,x),\dots,f_{c_n}(t,x),f_s(t,x)]^T$ is the vector field of the reaction dynamics. Now we check that the vector field points inwards at the boundaries of χ, note that for $\boldsymbol{z}(t,x)\in\chi, \forall x\in\bar{\Omega}$, and $i=1,\dots,n$

$$f_{E_i}(t,x)\big|_{E_i=0} = \alpha_i(t,x) + (d_i+\kappa_i+\gamma_s)c_i(t,x) \geq 0,$$

$$f_s(t,x)\big|_{S=0} = \alpha_S(t,x) + \sum_{j=1}^{n}(d_j+\kappa_j+\gamma_j)c_j(t,x) \geq 0,$$

$$f_{c_i}(t,x)\big|_{c_i=0} = \frac{1}{\eta_i}\big[E_i(t,x)S(t,x)\frac{\tilde{a}_i}{\tilde{d}_i}\big] \geq 0,$$

now to check the surface of the hyperplane $z^T\vec{n} = \Gamma$

$$\begin{aligned}
f^T\vec{n} &= \big[\sum_{j=1}^{n}\alpha_j(t,x) - (\gamma_j+1)(E_j(t,x)+c_j(t,x))\big] + \alpha_S(t,x) - (\gamma_s+1)(E_j(t,x)+\sum_{j=1}^{n}c_j(t,x)) \\
&\leq \big[\sum_{j=1}^{n}\tilde{\alpha}_j(x)\big] + \tilde{\alpha}_S(x) - (\hat{\gamma}+1)(\sum_{j=1}^{n}(E_j(t,x)+2c_j(t,x)) + S(t,x)) \\
&= \big[\sum_{j=1}^{n}\tilde{\alpha}_j(x)\big] + \tilde{\alpha}_S(x) - (\hat{\gamma}+1)\Gamma \\
&= \big[\sum_{j=1}^{n}\tilde{\alpha}_j(x)\big] + \tilde{\alpha}_S(x) - \max_{x\in\Omega}\big(\sum_{j=1}^{n}\tilde{\alpha}_j(x) + \tilde{\alpha}_S(x)\big) \\
&\leq 0.
\end{aligned}$$

■

Leveraging the framework of Definition 4, we decompose the system variables for freely diffusing species of (32) as follows:

Definition 8. (Decomposition of freely diffusing species)

$$\text{For Case I and Case III:} \quad E_i^{\perp}(t,x) = P^{\perp}_{v_{E_i}}(E_i(t,x)), \quad \text{such that } E_i(t,x) = \bar{E}_i(t)\hat{v}_{E_i}(x) + E_i^{\perp}(t,x), \tag{37a}$$

$$\text{For Case I:} \quad c_i^{\perp}(t,x) = P^{\perp}_{v_{c_i}}(c_i(t,x)), \quad \text{such that } c_i(t,x) = \bar{c}_i(t)\hat{v}_{c_i}(x) + c_i^{\perp}(t,x), \tag{37b}$$

$$\text{For Case I and Case II:} \quad S^{\perp}(t,x) = P^{\perp}_{v_S}(S(t,x)), \quad \text{such that } S(t,x) = \bar{S}(t)\hat{v}_S(x) + S^{\perp}(t,x). \tag{37c}$$

Lemma 3. *Let $E_i^{\perp}(t,x)$, $c_i^{\perp}(t,x)$, and $S^{\perp}(t,x)$ be as in Definition 8 and suppose Assumption 3 holds, then for $i=1,\dots,n$, there exists $\zeta>0$ such that*

$$||E_i^{\perp}(t,x)||_H = \mathcal{O}(e^{\zeta t/\epsilon}) + \mathcal{O}(\epsilon), \quad ||c_i^{\perp}(t,x)||_H = \mathcal{O}(e^{\zeta t/\epsilon}) + \mathcal{O}(\epsilon), \quad ||S^{\perp}(t,x)||_H = \mathcal{O}(e^{\zeta t/\epsilon}) + \mathcal{O}(\epsilon),$$

where $H = L^2(\Omega)$.

Proof: This results follows directly from Theorem 3 where Assumption 2 is satisfied by Claim 1 and Assumption 3. ■

Proposition 1. Suppose that Assumption 4 holds, then in Case II for $i = 1, \dots, n$, there exits $\hat{L}_i > 0$ such that for all $t \geq 0$

$$E_i(t,x) \leq \hat{L}_i \delta, \forall x \notin [x_i - \delta, x_i + \delta]$$

and for Case III there exits $\hat{L}_s > 0$ such that for all $t \geq 0$

$$S(t,x) \leq \hat{L}_s \delta, \forall x \notin [x_s - \delta, x_s + \delta]$$

where δ, x_i, x_s are as stated in the assumption.

Proof: For Case II, let $E_{i,T}(t,x) = E_i(t,x) + c_i(t,x)$, which satisfies

$$\frac{\partial E_{i,T}(t,x)}{\partial t} = \alpha_i(t,x) - (\gamma_i + 1) E_{i,T}(t,x). \tag{38a}$$

For $c \notin [x_i - \delta, x_i + \delta]$ we have that $E_i(t,c) \leq E_{i,T}(t,c) \leq \frac{\alpha_i(t,c)}{\gamma_i+1} \leq \frac{L_i}{\gamma_i+1}\delta, \forall t \geq 0$ and thus $\hat{L}_i = \frac{L_i}{\gamma_i+1}$.

Similarly, for Case III, let $S_T(t,x) = S(t,x) + \sum_{j=1}^{n} c_j(t,x)$, which satisfies

$$\frac{\partial S_T(t,x)}{\partial t} = \alpha_s(t,x) - (\gamma_s + 1) S_T(t,x). \tag{38b}$$

For $c \notin [x_s - \delta, x_s + \delta]$ we have that $S(t,c) \leq S_T(t,c) \leq \frac{\alpha_s(t,c)}{\gamma_s+1} \leq \frac{L_s}{\gamma_s+1}\delta, \forall t \geq 0$ and thus $\hat{L}_s = \frac{L_s}{\gamma_s+1}$. ■

The following claim will aid us in rewriting (33) in the form of the reduced dynamics given by (34) with additional "disturbance" terms of order ϵ and δ. The claim is written to handle Case I-III.

Claim 2. Let $H = L^2(\Omega)$ and consider $y_1(t,x), y_2(t,x) \in H$, suppose that $y_1(t,x), y_2(t,x) \geq 0, \forall t \geq 0, \forall x \in \bar{\Omega}$ and that there exists $y_1^*, y_2^* \in \mathbb{R}_+$ such that $||y_1(t,x)||_H \leq y_1^*, \forall t \geq 0$ and $||y_2(t,x)||_H \leq y_2^*, \forall t \geq 0$, let $\bar{y}_1(t) = \int_0^1 y_1(t,x)dx$ and $\bar{y}_2(t) = \int_0^1 y_2(t,x)dx$. Let $\hat{v}_1(x)$ and $\hat{v}_2(x)$ be smooth positive functions and denote $y_1^\perp(t,x) = y_1(t,x) - \bar{y}_1(t)\hat{v}_1(x)$ and $y_2^\perp(t,x) = y_2(t,x) - \bar{y}_2(t)\hat{v}_2(x)$.

1. Suppose that $||y_1^\perp(t,x)||_H = \mathcal{O}(\epsilon)$ and $||y_2^\perp(t,x)||_H = \mathcal{O}(\epsilon)$, then

$$\int_0^1 y_1(t,x)y_2(t,x)dx = \bar{y}_1(t)\bar{y}_2(t)\theta + \Delta(t), \quad \text{where} \quad \theta = \int_0^1 \hat{v}_1(x)\hat{v}_2(x)dx, \quad \text{and} \quad |\Delta(t)| = \mathcal{O}(\epsilon). \tag{39}$$

2. Suppose that $||y_1^\perp(t,x)||_H = \mathcal{O}(\epsilon)$ and that there exists $x^* \in (0,1)$ and $\delta > 0$ such that $[x^* - \delta, x^* + \delta] \subset [0,1]$ and $y_2(t,x) \leq \delta, \forall x \notin [x^* - \delta, x^* + \delta]$, then

$$\int_0^1 y_1(t,x)y_2(t,x)dx = \bar{y}_1(t)\bar{y}_2(t)\theta + \Delta(t), \quad \text{where} \quad \theta = \hat{v}_1(x^*), \quad \text{and} \quad |\Delta(t)| = \mathcal{O}(\epsilon) + \mathcal{O}(\delta) \tag{40}$$

Proof: To proof the first claim, notice that

$$\begin{aligned}
\int_0^1 y_1(t,x)y_2(t,x)dx &= \int_0^1 \big(\bar{y}_1(t)\hat{v}_1(x) + y_1^\perp(t,x)\big)\big(\bar{y}_2(t)\hat{v}_2(x) + y_2^\perp(t,x)\big)dx \\
&= \bar{y}_1(t)\bar{y}_2(t)\int_0^1 \hat{v}_1(x)\hat{v}_2(x)dx + \underbrace{\int_0^1 y_1^\perp(t,x)\big(\bar{y}_2(t)\hat{v}_2(x) + y_2^\perp(t,x)\big) + \bar{y}_1(t)\hat{v}_1(x)y_2^\perp(t,x)dx}_{\Delta(t)} \\
&= \bar{y}_1(t)\bar{y}_2(t)\theta + \Delta(t)
\end{aligned}$$

where $\theta = \int_0^1 \hat{v}_1(x)\hat{v}_2(x)dx$. Let $\hat{v}_1^* = \max_{x\in\bar{\Omega}}(\hat{v}_1(x))$ and leveraging the Cauchy Schwarz inequality in H,

$$\begin{aligned}
\big|\Delta(t)\big| &= \left|\int_0^1 y_1^\perp(t,x)\big(\bar{y}_2(t)\hat{v}_2(x) + y_2^\perp(t,x)\big) + \bar{y}_1(t)\hat{v}_1(x)y_2^\perp(t,x)dx\right| \\
&= \left|\langle y_1^\perp(t,x), y_2(t,x)\rangle_H + \langle \bar{y}_1(t)\hat{v}_1(x), y_2^\perp(t,x)\rangle_H\right| \\
&\leq \left|\langle y_1^\perp(t,x), y_2(t,x)\rangle_H\right| + \left|\langle \bar{y}_1(t)\hat{v}_1(x), y_2^\perp(t,x)\rangle_H\right| \\
&\leq ||y_1^\perp(t,x)||_H ||y_2(t,x)||_H + ||\bar{y}_1(t)\hat{v}_1(x)||_H ||y_2^\perp(t,x)||_H \\
&\leq ||y_1^\perp(t,x)||_H y_2^* + y_1^*\hat{v}_1^* ||y_2^\perp(t,x)||_H \\
&= \mathcal{O}(\epsilon).
\end{aligned}$$

For the second part of the claim, notice that

$$\bar{y}_2(t) = \int_0^{x^*-\delta} y_2(t,x)dx + \int_{x^*-\delta}^{x^*+\delta} y_2(t,x)dx + \int_{x^*+\delta}^1 y_2(t,x)dx = \int_{x^*-\delta}^{x^*+\delta} y_2(t,x)dx + \bar{y}_{2,\delta}(t)$$

where

$$|\bar{y}_{2,\delta}(t)| = \Big| \int_0^{x^*-\delta} y_2(t,x)dx + \int_{x^*+\delta}^1 y_2(t,x)dx \Big| \leq 2\delta.$$

Next,

$$\begin{aligned}
\int_0^1 y_1(t,x)y_2(t,x)dx &= \int_0^1 \big(\bar{y}_1(t)\hat{v}_1(x) + y_1^{\perp}(t,x)\big)y_2(t,x)dx \\
&= \int_0^1 \bar{y}_1(t)\hat{v}_1(x)y_2(t,x)dx + \int_0^1 y_1^{\perp}(t,x)y_2(t,x)dx \\
&= \int_0^1 \bar{y}_1(t)\hat{v}_1(x)y_2(t,x)dx + \Delta_1(t) \\
&= \bar{y}_1(t)\big[\int_0^{x^*-\delta} \hat{v}_1(x)y_2(t,x)dx + \int_{x^*-\delta}^{x^*+\delta} \hat{v}_1(x)y_2(t,x)dx + \int_{x^*+\delta}^1 \hat{v}_1(x)y_2(t,x)dx\big] + \Delta_1(t) \\
&= \bar{y}_1(t)\int_{x^*-\delta}^{x^*+\delta} \hat{v}_1(x)y_2(t,x)dx + \Delta_2(t) + \Delta_1(t) \\
&= \bar{y}_1(t)\hat{v}_1(c)\int_{x^*-\delta}^{x^*+\delta} y_2(t,x)dx + \Delta_2(t) + \Delta_1(t), \text{ for some } c \in [x^*-\delta, x^*+\delta] \\
&= \bar{y}_1(t)\bar{y}_2(t)\hat{v}_1(c) + \bar{y}_1(t)\hat{v}_1(c)\bar{y}_{2,\delta}(t) + \Delta_2(t) + \Delta_1(t) \\
&= \bar{y}_1(t)\bar{y}_2(t)\hat{v}_1(c) + \Delta_3(t) + \Delta_2(t) + \Delta_1(t) \\
&= \bar{y}_1(t)\bar{y}_2(t)\hat{v}_1(x^*) + \Delta_4(t) + \Delta_3(t) + \Delta_2(t) + \Delta_1(t) \\
&= \bar{y}_1(t)\bar{y}_2(t)\theta + \Delta(t),
\end{aligned}$$

where $\theta = \hat{v}_1(x^*)dx$, the existence of c is guaranteed by the mean-value theorem for integrals [49], and

$$|\Delta_1(t)| = \big|\int_0^1 y_1^{\perp}(t,x)y_2(t,x)dx\big| = \big|\langle y_1^{\perp}(t,x), y_2(t,x)\rangle_H\big| \leq ||y_2(t,x)||_H||y_1^{\perp}(t,x)||_H \leq y_2^*||y_1^{\perp}(t,x)||_H = \mathcal{O}(\epsilon),$$

$$\begin{aligned}
|\Delta_2(t)| &= \Big|\bar{y}_1(t)\big[\int_0^{x^*-\delta} \hat{v}_1(x)y_2(t,x)dx + \int_{x^*+\delta}^1 \hat{v}_1(x)y_2(t,x)dx\big]\Big| \\
&\leq y_1^*\hat{v}_1^*\Big|\int_0^{x^*-\delta} y_2(t,x)dx + \int_{x^*+\delta}^1 y_2(t,x)dx\Big| \\
&= y_1^*\hat{v}_1^*\Big|\bar{y}_{2,\delta}(t)\Big| \\
&\leq 2y_1^*\hat{v}_1^*\delta \\
&= \mathcal{O}(\delta),
\end{aligned}$$

$$|\Delta_3(t)| = |\bar{y}_1(t)\hat{v}_1(c)\bar{y}_{2,\delta}(t)| \leq 2y_1^*\hat{v}_1^*\delta = \mathcal{O}(\delta),$$

the following uses the smoothness $\hat{v}_1(x)$ to guarantee the existence of $L_v > 0$ such that for all $x_1, x_2 \in (0,1)$, we have that $|\hat{v}_1(x_2) - \hat{v}_1(x_1)| \leq L_v|x_2 - x_1|$, and hence

$$|\Delta_4(t)| = \big|\bar{y}_1(t)\bar{y}_2(t)(\hat{v}_1(c) - \hat{v}_1(x^*))\big| \leq y_1^*y_2^*\big|\hat{v}_1(c) - \hat{v}_1(x^*)\big| \leq 2y_1^*y_2^*L_v\delta = \mathcal{O}(\delta).$$

Finally,

$$\big|\Delta(t)\big| = \Big|\sum_{i=1}^4 \Delta_i(t)\Big| \leq \sum_{i=1}^4 \Big|\Delta_i(t)\Big| = \mathcal{O}(\epsilon) + \mathcal{O}(\delta).$$

■

Corollary 1. *By the results of Claim 1 (boundedness), Lemma 3, and Proposition 1,*

$$\int_0^1 E_i(t,x)S(t,x)dx = \bar{E}_i(t)\bar{S}(t)\theta_i^* + \Delta_i(t)$$

where θ_i^* is given by (35) for Case I-III and for $t \geq 0$

$$|\Delta_i(t)| = \begin{cases} \mathcal{O}(\epsilon) + \mathcal{O}(e^{-\zeta t/\epsilon}) & \text{for Case I} \\ \mathcal{O}(\epsilon) + \mathcal{O}(e^{-\zeta t/\epsilon}) + \mathcal{O}(\delta) & \text{for Case II and Case III} \end{cases}, \tag{41}$$

where ζ is as in Lemma 3.

Applying the result of Corollary 1, the the dynamics of (33) can be written as

$$\frac{d\bar{E}_i(t)}{dt} = \bar{\alpha}_i(t) - \frac{1}{\eta_i}\left[\bar{E}_i(t)\bar{S}(t)\frac{\tilde{a}_i\theta_i^*}{\tilde{d}_i} - \bar{c}_i(t)\right] - (\gamma_i+1)(\bar{E}_i(t)+\bar{c}_i(t)) + \Delta_i(t) \tag{42a}$$

$$\frac{d\bar{c}_i(t)}{dt} = \frac{1}{\eta_i}\left[\bar{E}_i(t)\bar{S}(t)\frac{\tilde{a}_i\theta_i^*}{\tilde{d}_i} - \bar{c}_i(t)\right] - \Delta_i(t) \tag{42b}$$

$$\frac{d\bar{S}(t)}{dt} = \bar{\alpha}_s(t) - \sum_{j=1}^n \frac{1}{\eta_j}\left[\bar{E}_j(t)\bar{S}(t)\frac{\tilde{a}_j\theta_j^*}{\tilde{d}_j} - \bar{c}_j(t)\right] - (\gamma_s+1)(\bar{S}(t)+\sum_{j=1}^n \bar{c}_j(t)) + \sum_{j=1}^n \Delta_j(t) \tag{42c}$$

such that θ_i^* and $\Delta_i(t)$ are as in Corollary 1. By the form of (42), it is clear that these dynamics are in the form of (34) with additional "perturbation" terms of order ϵ and δ. Now, we show that the dynamics (34) are contracting (Definition 5) and thus we can apply the robustness property of contracting systems (Lemma 2) to show that the solutions of (42) and (34) are close.

Next we define the spaced averaged total enzyme and substrate quantities and show that these are the same for (33) and (34). Furthermore, we will show the dynamics for these quantities are governed by uncoupled, linear, and contracting ODEs.

Definition 9. (Total spaced average enzyme and substrate concentrations) For (33), we define the total space averaged enzyme and substrate for $i = 1\ldots,n$ as $\bar{E}_{i,T}(t) = \bar{E}_i(t) + \bar{c}_i(t)$, $\bar{S}_T(t) = \bar{S}(t) + \sum_{j=1}^n \bar{c}_j(t)$, respectively, and similarly for (34), we define $\hat{\bar{E}}_{i,T}(t) = \hat{\bar{E}}_i(t) + \hat{\bar{c}}_i(t)$ and $\hat{\bar{S}}_T(t) = \hat{\bar{S}}(t) + \sum_{j=1}^n \hat{\bar{c}}_j(t)$, the dynamics of these quantities are given by

$$\frac{d\bar{E}_{i,T}(t)}{dt} = \bar{\alpha}_i(t) - (\gamma_i+1)\bar{E}_{i,T}(t), \quad \frac{d\bar{S}_T(t)}{dt} = \bar{\alpha}_s(t) - (\gamma_s+1)\bar{S}_T(t), \tag{43a}$$

$$\frac{d\hat{\bar{E}}_{i,T}(t)}{dt} = \bar{\alpha}_i(t) - (\gamma_i+1)\hat{\bar{E}}_{i,T}(t), \quad \frac{d\hat{\bar{S}}_T(t)}{dt} = \bar{\alpha}_s(t) - (\gamma_s+1)\hat{\bar{S}}_T(t). \tag{43b}$$

Remark 6. *For $i = 1,\ldots,n$, $\bar{E}_{i,T}(t) = \hat{\bar{E}}_{i,T}(t), \forall t \geq 0$ since it is assumed that $\bar{E}_{i,T}(0) = \hat{\bar{E}}_{i,T}(0)$. Similarly, $\bar{S}_T(t) = \hat{\bar{S}}_T(t), \forall t \geq 0$ since it is assumed that $\bar{S}_T(0) = \hat{\bar{S}}_T(0)$.*

Remark 7. *From the linear and uncoupled structure of (43), it is clear that the $\bar{E}_{i,T}(t)$ are contracting (Definition 5) with contraction rate $\lambda_i = \gamma_i+1$. Similarly, the $\bar{S}_T(t)$ dynamics are contracting with contraction rate $\lambda_s = \gamma_s + 1$.*

Claim 3. Suppose Assumption 5 holds, then for all $i = 1,\ldots,n$, then $\bar{E}_{i,*} \leq \hat{\bar{E}}_i(t) \leq \bar{E}_{i,T}^*, \forall t \geq 0$.

Proof: Let $\tilde{\alpha}_i(x)$ be as in Assumption 3 and let $\bar{\alpha}_i^* = \int_0^1 \tilde{\alpha}_i(x)dx$, and thus $\bar{\alpha}_i(t) \leq \bar{\alpha}_i^*$. Let $\hat{\bar{E}}_{i,T}(t)$ be given by (43) and $\hat{\bar{E}}_i^*(t)$ be given by

$$\frac{d\hat{\bar{E}}_i^*(t)}{dt} = \bar{\alpha}_i^* - (\gamma_i+1)\hat{\bar{E}}_i^*(t) \implies \hat{\bar{E}}_i^*(t) = \hat{\bar{E}}_i^*(0)e^{-(\gamma_i+1)t} + (1-e^{-(\gamma_i+1)t})\bar{E}_{i,T}^* \tag{44}$$

where $\hat{\bar{E}}_i^*(0) = \hat{\bar{E}}_{i,T}(0) = \bar{E}_{i,T}(0) \leq \bar{E}_{i,T}^*$, which implies $\hat{\bar{E}}_i^*(t) \leq \bar{E}_{i,T}^*, \forall t \geq 0$. Let $e_{i,T}(t) = \hat{\bar{E}}_i^*(t) - \hat{\bar{E}}_{i,T}(t)$ and thus

$$\dot{e}_{i,T}(t) = \underbrace{\bar{\alpha}_i^* - \bar{\alpha}_i(t)}_{\geq 0, \forall t \geq 0} - (\gamma_i+1)e_i(t),$$

which implies that $\mathbb{R}_+$ is a positively invariant set for the $e_{i,T}(t)$ dynamics. Since $e_{i,T}(0) = 0$ this implies that $e_{i,T}(t) \geq 0, \forall t \geq 0$ and thus $\hat{\bar{E}}_i(t) \leq \hat{\bar{E}}_{i,T}(t) \leq \hat{\bar{E}}^*_i(t) \leq \bar{E}^*_{i,T}, \forall t \geq 0$.

Let $\tilde{\alpha}_s(x)$ be as in Assumption 3 and let $\bar{\alpha}^*_s = \int_0^1 \tilde{\alpha}_s(x)dx$ and thus $\bar{\alpha}_s(t) \leq \bar{\alpha}^*_s$. Let $\hat{\bar{S}}_T(t)$ be given by (43), and let $\hat{\bar{S}}^*_T(t)$ be given by

$$\frac{d\hat{\bar{S}}^*_T(t)}{dt} = \bar{\alpha}^*_s - (\gamma_s + 1)\hat{\bar{S}}^*_T(t) \implies \hat{\bar{S}}^*_T(t) = \hat{\bar{S}}^*_T(0)e^{-(\gamma_s+1)t} + (1 - e^{-(\gamma_s+1)t})\bar{S}^*_T \tag{45}$$

where $\hat{\bar{S}}^*_T(0) = \hat{\bar{S}}_T(0) = \bar{S}_T(0) \leq \bar{S}^*_T$, which implies $\hat{\bar{S}}^*_T(t) \leq \bar{S}^*_T, \forall t \geq 0$. Let $e_{s,T}(t) = \hat{\bar{S}}^*_T(t) - \hat{\bar{S}}_T(t)$ such that

$$\dot{e}_{s,T}(t) = \underbrace{\bar{\alpha}^*_s - \bar{\alpha}_s(t)}_{\geq 0, \forall t \geq 0} - (\gamma_s + 1)e_s(t),$$

which implies that $\mathbb{R}_+$ is a positively invariant set for the $e_{s,T}(t)$ dynamics. Since $e_{s,T}(0) = 0$ this implies that $e_{s,T}(t) \geq 0, \forall t \geq 0$ and thus $\hat{\bar{S}}_T(t) \leq \hat{\bar{S}}^*_T(t) \leq \bar{S}^*_T, \forall t \geq 0$.

Let $\underline{\alpha}_i(x)$ be as in Assumption 3, let $\bar{\underline{\alpha}}_i = \int_0^1 \underline{\alpha}_i(x)dx$, and $\hat{\bar{E}}_{i,*}(t)$ such that $\hat{\bar{E}}_{i,*}(0) = \hat{\bar{E}}_i(0)$ and

$$\frac{d\hat{\bar{E}}_{i,*}(t)}{dt} = \bar{\underline{\alpha}}_i - (\gamma_i + 1)\hat{\bar{E}}_{i,*}(t) - \tilde{a}_i\hat{\bar{E}}_{i,*}(t)\bar{S}^*_T \implies \hat{\bar{E}}_{i,*}(t) = \hat{\bar{E}}_{i,*}(0)e^{-(\gamma_i+1+\tilde{a}_i\bar{S}^*_T)t} + (1 - e^{-(\gamma_i+1+\tilde{a}_i\bar{S}^*_T)t})\bar{E}_{i,*}, \tag{46}$$

where $\hat{\bar{E}}_{i,*}(0) = \hat{\bar{E}}_i(0) = \bar{E}_i(0) \geq \bar{E}_{i,*}$, which implies $\hat{\bar{E}}_{i,*}(t) \geq \bar{E}_{i,*}, \forall t \geq 0$. Let $e_i(t) = \bar{E}_i(t) - \hat{\bar{E}}_{i,*}(t)$ such that

$$\dot{e}_i(t) = \underbrace{\bar{\alpha}_i(t) - \bar{\underline{\alpha}}_i}_{\geq 0, \forall t \geq 0} - (\gamma_i + 1 + \tilde{a}_i\bar{S}^*_T)e_i(t) + \tilde{a}_i\hat{\bar{E}}_{i,*}(t)\underbrace{(\bar{S}^*_T - \bar{S}(t))}_{\geq 0, \forall t \geq 0},$$

which implies that $\mathbb{R}_+$ is a positively invariant set for the $e_i(t)$ dynamics. Since $e_i(0) = 0$ this implies that $e_i(t) \geq 0, \forall t \geq 0$ and thus $\bar{E}_i(t) \geq \hat{\bar{E}}_{i,*}(t) \geq \bar{E}_{i,*}, \forall t \geq 0$.

■

Let $\hat{\bar{\boldsymbol{c}}}(t) = [\hat{\bar{c}}_1(t), \ldots, \hat{\bar{c}}_n(t)]$ and $\boldsymbol{f}_c(t, \hat{\bar{\boldsymbol{c}}}) \in \mathbb{R}^n$ such that

$$\frac{d\hat{\bar{\boldsymbol{c}}}^i(t)}{dt} = \boldsymbol{f}^i_c(t, \hat{\bar{\boldsymbol{c}}}) = \frac{1}{\eta_i}\big[\hat{\bar{E}}_i(t)\hat{\bar{S}}(t)\frac{\tilde{a}_i\theta^*_i}{\tilde{d}_i} - \hat{\bar{c}}_i(t)\big] = \frac{1}{\eta_i}\big[\big(\bar{E}_{i,T}(t) - \hat{\bar{c}}_i(t)\big)\big(\bar{S}_T(t) - \sum_{j=1}^n \hat{\bar{c}}_j(t)\big)\frac{\tilde{a}_i\theta^*_i}{\tilde{d}_i} - \hat{\bar{c}}_i(t)\big]. \tag{47}$$

Similarly, we define $\bar{\boldsymbol{c}}(t) = [\bar{c}_1(t), \ldots, \bar{c}_n(t)]$

$$\frac{d\bar{\boldsymbol{c}}^i(t)}{dt} = \boldsymbol{f}^i_c(t, \bar{\boldsymbol{c}}) = \frac{1}{\eta_i}\big[\bar{E}_i(t)\bar{S}(t)\frac{\tilde{a}_i\theta^*_i}{\tilde{d}_i} - \bar{c}_i(t)\big] - \Delta_i(t) = \frac{1}{\eta_i}\big[\big(\bar{E}_{i,T}(t) - \bar{c}_i(t)\big)\big(\bar{S}_T(t) - \sum_{j=1}^n \bar{c}_j(t)\big)\frac{\tilde{a}_i\theta^*_i}{\tilde{d}_i} - \bar{c}_i(t)\big] - \Delta_i(t). \tag{48}$$

We now show that system (47) is contracting. From the discussion in Remark 7, we can treat $\bar{E}_{i,T}(t)$ and $\bar{S}_T(t)$ as time varying inputs to (47) when showing the dynamics are contracting (see hierarchal structures in [30]). We then show the solutions of (47) are close to those of (48) by the robustness property of contacting systems.

Lemma 4. *Let $\hat{\bar{\boldsymbol{c}}}(t)$ be given by (47) and $\bar{\boldsymbol{c}}(t)$ be given by (48), suppose that Assumptions 3, 4,5 hold for $\delta > 0$, then, there exists $\epsilon^* > 0$ such that for all $\epsilon < \epsilon^*$ and $t \geq 0$, we have that*

$$|\hat{\bar{\boldsymbol{c}}}(t) - \bar{\boldsymbol{c}}(t)| \leq |\Delta_c|,$$

where $\Delta_c = \mathcal{O}\left(\frac{\epsilon}{1-\epsilon/\epsilon^*}\right)$ for Case I (as in Table 2) and $\Delta_c = \mathcal{O}\left(\frac{\epsilon}{1-\epsilon/\epsilon^*}\right) + \mathcal{O}(\delta)$ for Cases II-III.

Proof: Consider the metric

$$\boldsymbol{P}(t) = \text{diag}([\frac{1}{\tilde{a}_1\theta^*_1\hat{\bar{E}}_1(t)}, \ldots, \frac{1}{\tilde{a}_n\theta^*_n\hat{\bar{E}}_n(t)}]^T) \tag{49}$$

with time derivative given by

$$\dot{\boldsymbol{P}}(t) = -\boldsymbol{P}(t)\text{diag}(\boldsymbol{v}_p), \quad \text{where} \quad \boldsymbol{v}^i_p = \frac{d\hat{\bar{E}}_i(t)}{dt}/\hat{\bar{E}}_i(t) = \bar{\alpha}_i(t)/\hat{\bar{E}}_i(t) - (\gamma_i+1) - \tilde{a}_i\theta^*_i\hat{\bar{S}}(t) + (\gamma_s + k_i + d_i)\frac{\hat{\bar{c}}_i(t)}{\hat{\bar{E}}_i(t)}.$$

The Jacobian is given by

$$\frac{\partial \boldsymbol{f}_c}{\partial \boldsymbol{c}} = -\text{diag}(\boldsymbol{v}_c) + \boldsymbol{\sigma}, \quad \text{where} \quad \boldsymbol{v}_c^i = \tilde{a}_i \theta_i^* \hat{\bar{S}}(t) + \tilde{d}_i,$$

and $\boldsymbol{\sigma}$ is a rank one matrix given by

$$\boldsymbol{\sigma} = [\tilde{a}_1 \theta_1^* \hat{\bar{E}}_1(t), \ldots, \tilde{a}_n \theta_n^* \hat{\bar{E}}_n(t)]^T [-1, \ldots, -1].$$

With the chosen metric $\boldsymbol{P}(t)$, we have that

$$\boldsymbol{P}\boldsymbol{\sigma} = -\underbrace{[1, \ldots, 1]^T [1, \ldots, 1]}_{\boldsymbol{\sigma}_1} \implies -n\boldsymbol{I}_{n,n} \leq \boldsymbol{\sigma}_1 \leq 0\boldsymbol{I}_{n,n}$$

since the symmetric rank one matrix $\boldsymbol{\sigma}_1$, has $n-1$ zero eigenvalues and the nontrivial eigenvalue is $\lambda_\sigma = -n$ for eigenvector $v_n = [1, \ldots, 1]^T$. Recalling the positivity of $\hat{\bar{E}}_i(t)$, $\hat{\bar{c}}_i(t)$, $\hat{\bar{S}}(t)$ (Claim 1), and $\bar{\alpha}_i(t)$, we have that

$$\begin{aligned}
1/2\left(\boldsymbol{P}(t)\frac{\partial \boldsymbol{f}_c}{\partial \boldsymbol{c}} + \frac{\partial \boldsymbol{f}_c^T}{\partial \boldsymbol{c}}\boldsymbol{P}(t)\right) + \dot{\boldsymbol{P}}(t) &= -\boldsymbol{P}\text{diag}(\boldsymbol{v}_p + \boldsymbol{v}_c) + \boldsymbol{P}\boldsymbol{\sigma} \\
&\leq -\boldsymbol{P}\text{diag}(\boldsymbol{v}_p + \boldsymbol{v}_c) \\
&\leq -\min_{i=1,\ldots,n}\left((\gamma_s + \kappa_i + d_i)(1 + \frac{\hat{\bar{c}}_i(t)}{\hat{\bar{E}}_i(t)}) + \bar{\alpha}_i(t)/\hat{\bar{E}}_i(t)\right)\boldsymbol{P} \\
&\leq -\min_{i=1,\ldots,n}\left(\gamma_s + \kappa_i + d_i\right)\boldsymbol{P} \\
&= -\xi\boldsymbol{P}.
\end{aligned}$$

Thus, by Theorem 2, the system (47) is contracting with contraction rate $\xi = \gamma_s + \min_{i=1,\ldots,n}\left(\kappa_i + d_i\right)$. Assumptions 3, 4 imply that (41) holds for $\Delta_i(t)$ in (48) and therefore theres exists $\zeta > 0$ such that for all $i = 1, \ldots, n$

$$|\Delta_i(t)| = \mathcal{O}(\epsilon) + \mathcal{O}(e^{-\zeta/\epsilon t}), \text{ for Case I and } \quad |\Delta_i(t)| = \mathcal{O}(\epsilon) + \mathcal{O}(e^{-\zeta/\epsilon t}) + \mathcal{O}(\delta) \text{ for Cases II-III}$$

Therefore, applying the result from Lemma 2 to the nominal system (47) and the perturbed system (48), recalling that $\bar{c}_i(0) = \hat{\bar{c}}_i(0)$, and letting $\epsilon^* = \zeta/\xi$ we have that

$$|\bar{c}_i(t) - \hat{\bar{c}}_i(t)| \leq M\mathcal{O}\left(\frac{\epsilon}{1 - \epsilon/\epsilon^*}\right), \text{ for Case I} \quad |\bar{c}_i(t) - \hat{\bar{c}}_i(t)| \leq M\left[\mathcal{O}\left(\frac{\epsilon}{1 - \epsilon/\epsilon^*}\right) + \mathcal{O}(\delta)\right], \text{ for Case II-III}$$

where M is an upper bound on the ratio of the biggest and smallest eigenvalues of $\boldsymbol{P}$. Let $r(t)$ be the ratio of the biggest and smallest eigenvalues of $\boldsymbol{P}(t)$. By Claim 3, there exists $\bar{E}_{i,*}, \bar{E}_{i,T}^* \in \mathbb{R}_+$ independent of ϵ and δ such that $\bar{E}_{i,*} \leq \hat{\bar{E}}_i(t) \leq \bar{E}_{i,T}^*, \forall t \geq 0$, and thus

$$r(t) = \frac{\max_{i=1,\ldots,n} \tilde{a}_i \theta_i^* \hat{\bar{E}}_i(t)}{\min_{i=1,\ldots,n} \tilde{a}_i \theta_i^* \hat{\bar{E}}_i(t)} \leq \frac{\max_{i=1,\ldots,n} \tilde{a}_i \theta_i^* \bar{E}_{i,T}^*}{\min_{i=1,\ldots,n} \tilde{a}_i \theta_i^* \bar{E}_{i,*}} \implies M = \frac{\max_{i=1,\ldots,n} \tilde{a}_i \theta_i^* \bar{E}_{i,T}^*}{\min_{i=1,\ldots,n} \tilde{a}_i \theta_i^* \bar{E}_{i,*}}. \tag{50}$$

■

Corollary 2. *Recall Definition 9 and Remark 6, we have that*

$$\bar{E}_i(t) = \bar{E}_{i,T}(t) - \bar{c}_i(t) = \bar{E}_{i,T}(t) - \hat{\bar{c}}_i(t) + \mathcal{O}(\Delta_c) = \hat{\bar{E}}_{i,T}(t) - \hat{\bar{c}}_i(t) + \mathcal{O}(\Delta_c) = \hat{\bar{E}}_i(t) + \mathcal{O}(\Delta_c)$$

and

$$\bar{S}(t) = \bar{S}_T(t) - \sum_{j=1}^n \bar{c}_j(t) = \bar{S}_T(t) - \sum_{j=1}^n \hat{\bar{c}}_j(t) + \mathcal{O}(\Delta_c) = \hat{\bar{S}}_T(t) - \sum_{j=1}^n \hat{\bar{c}}_j(t) + \mathcal{O}(\Delta_c) = \hat{\bar{S}}(t) + \mathcal{O}(\Delta_c)$$

Remark 8. *The result of Theorem 4 depends on Assumption 5 via Lemma 4 and Claim 3. This assumption ensured fixed values for the minimum and maximum eigenvlaues of (49) in the proof of Lemma 4 ((50)). However, notice from (45), (45), and (46) in the proof of Claim 3, that regardless of the initial conditions, we approach these bounds at a convergence rate $\underline{\gamma} = 1 + \min(\gamma_1, \ldots, \gamma_n, \gamma_s)$.*

1.4 Fast Diffusion, binding, and unbinding: $\epsilon \ll 1$ and $\eta_i \ll 1$

The result of Theorem 3, which was crucial to proof Theorem 4, assumed that that the timescale associated with diffusion is much faster than binding and unbinding between E_i and S ($\frac{\epsilon}{\eta_i} \ll 1$). However, this assumption may not always be valid. In this section we consider the case when $\frac{\epsilon}{\eta_i} = \mathcal{O}(1)$ and demonstrate why the result of Theorem 3 should remain unchanged ($||\boldsymbol{z}^{\perp}|| \to 0$). We consider the three cases from Table 2.

1.4.1 Case I

Recalling Definition 4, (43), and (37), the dynamics are given by:

$$\frac{d\bar{E}_{i,T}(t)}{dt} = \bar{\alpha}_i(t) - (\gamma_i + 1)\bar{E}_{i,T}(t) \tag{51a}$$

$$\frac{d\bar{S}_T(t)}{dt} = \bar{\alpha}_S(t) - (\gamma_S + 1)\bar{S}_T(t) \tag{51b}$$

$$\frac{d\bar{c}_i(t)}{dt} = \underbrace{\frac{1}{\epsilon}\left[\frac{\epsilon}{\eta_i}\left(\int_0^1 \left(E_i(t,x)S(t,x)dx\right)\frac{\tilde{a}_i}{\tilde{d}_i} - \bar{c}_i(t)\right)\right]}_{\text{fast dynamics}} \tag{51c}$$

$$\frac{\partial E_i^{\perp}(t,x)}{\partial t} = \underbrace{\frac{1}{\epsilon}\left[\chi_{E_i}\frac{d}{dx}\left[v_{E_i}^2\frac{d}{dx}\left[\frac{E_i^{\perp}}{v_{E_i}}\right]\right] - \frac{\epsilon}{\eta_i}P_{v_{E_i}}^{\perp}\left(E_i(t,x)S(t,x)\frac{\tilde{a}_i}{\tilde{d}_i} - c_i(t,x)\right)\right]}_{\text{fast dynamics}} + \alpha_i^{\perp}(t,x) - (\gamma_i+1)\big(E_i^{\perp}(t,x) + P_{v_{E_i}}^{\perp}(c_i)\big) \tag{51d}$$

$$\frac{\partial c_i^{\perp}(t,x)}{\partial t} = \underbrace{\frac{1}{\epsilon}\left[\chi_{c_i}\frac{d}{dx}\left[v_{c_i}^2\frac{d}{dx}\left[\frac{c_i^{\perp}}{v_{c_i}}\right]\right] + \frac{\epsilon}{\eta_i}P_{v_{c_i}}^{\perp}\left[E_i(t,x)S(t,x)\frac{\tilde{a}_i}{\tilde{d}_i} - c_i(t,x)\right]\right]}_{\text{fast dynamics}} \tag{51e}$$

$$\frac{\partial S^{\perp}(t,x)}{\partial t} = \underbrace{\frac{1}{\epsilon}\left[\frac{d}{dx}\left[v_s^2\frac{d}{dx}\left[\frac{S^{\perp}}{v_s}\right]\right] + \sum_{j=1}^{n}\frac{\epsilon}{\eta_j}P_{v_s}^{\perp}\left(E_j(t,x)S(t,x)\frac{\tilde{a}_j}{\tilde{d}_j} - c_j(t,x)\right)\right]}_{\text{fast dynamics}} + \alpha_S^{\perp}(t,x) - (\gamma_s+1)\big(S^{\perp}(t,x) + \sum_{j=1}^{n}P_{v_S}^{\perp}(c_j)\big) \tag{51f}$$

The quasi-steady state of the fast dynamics is given by the solution to:

$$0 = \int_0^1 \left(E_i(t,x)S(t,x)dx\right)\frac{\tilde{a}_i}{\tilde{d}_i} - \bar{c}_i(t), \tag{52a}$$

$$0 = \left[\chi_{E_i}\frac{d}{dx}\left[v_{E_i}^2\frac{d}{dx}\left[\frac{E_i^{\perp}}{v_{E_i}}\right]\right] - \frac{\epsilon}{\eta_i}P_{v_{E_i}}^{\perp}\left(E_i(t,x)S(t,x)\frac{\tilde{a}_i}{\tilde{d}_i} - c_i(t,x)\right)\right], \tag{52b}$$

$$0 = \left[\chi_{c_i}\frac{d}{dx}\left[v_{c_i}^2\frac{d}{dx}\left[\frac{c_i^{\perp}}{v_{c_i}}\right]\right] + \frac{\epsilon}{\eta_i}P_{v_{c_i}}^{\perp}\left[E_i(t,x)S(t,x)\frac{\tilde{a}_i}{\tilde{d}_i} - c_i(t,x)\right]\right], \tag{52c}$$

$$0 = \left[\frac{d}{dx}\left[v_s^2\frac{d}{dx}\left[\frac{S^{\perp}}{v_S}\right]\right] + \sum_{j=1}^{n}\frac{\epsilon}{\eta_j}P_{v_s}^{\perp}\left(E_j(t,x)S(t,x)\frac{\tilde{a}_j}{\tilde{d}_j} - c_j(t,x)\right)\right]. \tag{52d}$$

By the key fact that $v_{c_i} = v_{E_i}v_s$ [13], (52) is satisfied by

$$E_i^{\perp}(t,x) = 0, \quad c_i^{\perp}(t,x) = 0, \quad S^{\perp}(t,x) = 0 \tag{53}$$

which is identical to that given in Section 1.2 with the additional constraint that

$$\bar{c}_i(t) = \bar{E}_i(t)\bar{S}(t)\theta_i\frac{\tilde{a}_i}{\tilde{d}_i}, \tag{54}$$

where

$$\theta_i = \frac{\int_0^1 v_{E_i}(x) v_S(x) dx}{\big[\int_0^1 v_{E_i}(x) dx\big]\big[\int_0^1 v_S(x) dx\big]}.$$

To show that as $\epsilon \to 0^+$, the full dynamics remain arbitrarily close to this quasi-steady state after a fast transient, one could show that (53) is an exponentially stable equilibrium of the fast dynamics.

1.4.2 Case II

Recalling Definition 4, (37), and the total quantities from (38), the dynamics are given by:

$$\frac{\partial E_{i,T}(t,x)}{\partial t} = \alpha_i(t,x) - (\gamma_i + 1) E_{i,T}(t,x) \tag{55a}$$

$$\frac{d\bar{S}_T(t)}{dt} = \bar{\alpha}_S(t) - (\gamma_S + 1)\bar{S}_T(t) \tag{55b}$$

$$\frac{\partial c_i(t,x)}{\partial t} = \underbrace{\frac{1}{\epsilon}\left[\frac{\epsilon}{\eta_i}\big[E_i(t,x)S(t,x)\frac{\tilde{a}_i}{\tilde{d}_i} - c_i(t,x)\big]\right]}_{\text{fast dynamics}} \tag{55c}$$

$$\frac{\partial S^{\perp}(t,x)}{\partial t} = \underbrace{\frac{1}{\epsilon}\left[\frac{d}{dx}\left[v_s^2 \frac{d}{dx}\big[\frac{S^{\perp}}{v_s}\big]\right] + \sum_{j=1}^{n} \frac{\epsilon}{\eta_j} P^{\perp}_{v_s}\left(E_j(t,x)S(t,x)\frac{\tilde{a}_j}{\tilde{d}_j} - c_j(t,x)\right)\right]}_{\text{fast dynamics}} + \alpha_S^{\perp}(t,x) - (\gamma_s + 1)\big(S^{\perp}(t,x) + \sum_{j=1}^{n} P^{\perp}_{v_S}(c_j)\big) \tag{55d}$$

The quasi-steady state of the fast dynamics is given by the solution to:

$$0 = \left[\frac{\epsilon}{\eta_i}\big[E_j(t,x)S(t,x)\frac{\tilde{a}_j}{\tilde{d}_j} c_i\big]\right], \tag{56a}$$

$$0 = \left[\frac{d}{dx}\left[v_s^2 \frac{d}{dx}\big[\frac{S^{\perp}}{v_s}\big]\right] + \sum_{j=1}^{n} \frac{\epsilon}{\eta_j} P^{\perp}_{v_s}\left(E_j(t,x)S(t,x)\frac{\tilde{a}_j}{\tilde{d}_j} - c_j\right)\right], \tag{56b}$$

$$\tag{56c}$$

which is satisfied by

$$S^{\perp}(t,x) = 0 \tag{57}$$

which is identical to that given in Section 1.2 , however, we also have the following constraint

$$c_i(t,x) = E_i(t,x)\bar{S}(t)\hat{v}_s(x)\frac{\tilde{a}_i}{\tilde{d}_i}, \tag{58}$$

To show that as $\epsilon \to 0^+$, the full dynamics remain arbitrarily close to this quasi-steady state after a fast transient, one could show that (57) is an exponentially stable equilibrium of the fast dynamics.

1.4.3 Case III

Recalling Definition 4, (37), and the total quantities from (38), the dynamics are given by:

$$\frac{d\bar{E}_{i,T}(t)}{dt} = \bar{\alpha}_i(t) - (\gamma_i + 1)\bar{E}_{i,T}(t) \tag{59a}$$

$$\frac{\partial S_T(t,x)}{\partial t} = \alpha_S(t,x) - (\gamma_S + 1)S_T(t,x) \tag{59b}$$

$$\frac{\partial c_i(t,x)}{\partial t} = \underbrace{\frac{1}{\epsilon}\left[\frac{\epsilon}{\eta_i}\left[E_i(t,x)S(t,x)\frac{\tilde{a}_i}{\tilde{d}_i} - c_i(t,x)\right]\right]}_{\text{fast dynamics}} \tag{59c}$$

$$\frac{\partial E_i^{\perp}(t,x)}{\partial t} = \underbrace{\frac{1}{\epsilon}\left[\chi_{E_i}\frac{d}{dx}\left[v_{E_i}^2\frac{d}{dx}\left[\frac{E_i^{\perp}}{v_{E_i}}\right]\right] + \frac{\epsilon}{\eta_i}P_{v_{E_i}}^{\perp}\left(E_i(t,x)S(t,x)\frac{\tilde{a}_i}{\tilde{d}_i} - c_i(t,x)\right)\right]}_{\text{fast dynamics}} + \alpha_i^{\perp}(t,x) - (\gamma_i + 1)\big(E_i^{\perp}(t,x) + P_{v_{E_i}}^{\perp}(c_i)\big) \tag{59d}$$

The quasi-steady state of the fast dynamics is given by the solution to:

$$0 = \left[\frac{\epsilon}{\eta_i}\left[E_i(t,x)S(t,x)\frac{\tilde{a}_i}{\tilde{d}_i} - c_i\right]\right], \tag{60a}$$

$$0 = \left[\chi_{E_i}\frac{d}{dx}\left[v_{E_i}^2\frac{d}{dx}\left[\frac{E_i^{\perp}}{v_{E_i}}\right]\right] + \frac{\epsilon}{\eta_i}P_{v_{E_i}}^{\perp}\left(E_i(t,x)S(t,x)\frac{\tilde{a}_i}{\tilde{d}_i} - c_i\right)\right], \tag{60b}$$

$$\tag{60c}$$

which is satisfied for $i = 1, \ldots, n$ by

$$E_i^{\perp}(t,x) = 0 \tag{61}$$

which is identical to that given in Section 1.2, however, we also have the following constraint

$$c_i(t,x) = \bar{E}_i(t)S(t,x)\hat{v}_{E_i}(x)\frac{\tilde{a}_i}{\tilde{d}_i}, \tag{62}$$

To show that as $\epsilon \to 0^+$, the full dynamics remain arbitrarily close to this quasi-steady state after a fast transient, one could show that (61) is an exponentially stable equilibrium of the fast dynamics.

1.5 Bounds on Available Volume Profile

Following [13], we introduce a model of the available volume profiles of a freely diffusing species within the DNA mesh of the cell. Let $\rho(x)$ be the local density of DNA length such that $\int_0^1 \rho(x)dx = \bar{\rho}$, where $\bar{\rho}$ is the total length of the chromosome DNA divided by the total volume occupied by the chromosome and let $\hat{\rho}(x) = \frac{\rho(x)}{\bar{\rho}}$. For a species diffusing inside the cell with radius of gyration r, we model the available volume profile $v(x)$ as:

$$v(x) = e^{-\kappa\pi r^2\bar{\rho}\hat{\rho}(x)} = e^{-(r/r^*)^2\hat{\rho}(x)}, \tag{63}$$

where κ is an empirical coefficient (as discussed in [13]) and $r^{*2} = 1/(\kappa\pi\bar{\rho})$. As shown in Figure 7, we estimate the chromosome density as a step function.

$$\hat{\rho}(x) = \begin{cases} \dfrac{1}{1-\Delta x}, & x \in [0, 1-\Delta x] \\ 0, & x \in (1-\Delta x, 1] \end{cases} \implies \bar{v} = \int_0^1 v(x)dx = v_0(1-\Delta x) + \Delta x,$$

where $v_0 = e^{-\frac{(r/r^*)^2}{1-\Delta x}}$ and Δx is the distance between the end of the chromosome and the cell poles (see Figure 1). Thus,

$$\hat{v}(x) = \frac{v(x)}{\bar{v}(x)} = \begin{cases} 0 \le \dfrac{v_0}{v_0(1-\Delta x) + \Delta x} \le 1, & x \in [0, 1-\Delta x] \\ 1 \le \dfrac{1}{v_0(1-\Delta x) + \Delta x} \le \dfrac{1}{\Delta x}, & x \in (1-\Delta x, 1] \end{cases}$$

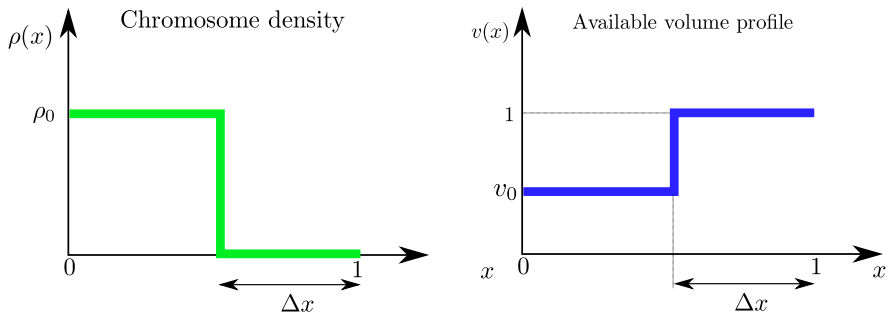

Figure 7: Idealization of the chromosome density which yields a simple estimate of the available volume profile. Here Δx is the distance between the end of the chromosome and the cell poles and $\rho_0 = \bar{\rho}/(1-\Delta x)$. Notice from (63), that $v_0 \to 0$ as $(r/r^*)^2 \to \infty$. This approximations are used to derive simple and biologically intuitive approximations for θ_i in (7b) for Case I-III.

.

For the E_i and S as described in (1) with available volume profiles $v_{E_i}(x)$ and $v_S(x)$, respectively, let $v_{0,E_i} = v_{E_i}(0)$ and $v_{0,S} = v_S(0)$. We summarize the bounds on θ_i as in (7b) of case I-III (as in Table 1) in the following list:

- For **case I**, this idealization implies that

$$\theta_i = \frac{v_{0,E_i} v_{0,S}(1-\Delta x) + \Delta x}{\left[v_{0,E_i}(1-\Delta x) + \Delta x\right]\left[v_{0,S}(1-\Delta x) + \Delta x\right]} \implies 1 \le \theta_i \le \frac{1}{\Delta x} \tag{64}$$

  The upper limit ($\frac{1}{\Delta x}$) is reached as v_{0,E_i} <u>and</u> $v_{0,S}$ approach zero. This limit can be achieved as the size of both species increases. The lower limit reached if v_{0,E_i} <u>or</u> $v_{0,S}$ approach one. The limit is achieve if any of the two species is sufficiently small. Since $\theta_i \ge 1$, it implies the binding is always equal to or greater than that predicted by well-mixed.

- For **case II and case III**, we further assume $\alpha_i(t,x)$ in case II and $\alpha_s(t,x)$ in case III are localized near inside or outside the chromosome. This implies that S and E_i are also localized within those regions. Therefore:

$$a_i = \begin{cases} \hat{v}_{0,S}, & \text{case II} \\ \hat{v}_{0,E_i}, & \text{case III} \end{cases}, \quad \theta_i = \begin{cases} 0 \le \dfrac{a_i}{a_i(1-\Delta x) + \Delta x} \le 1, & E_i\ (S) \text{ localized in chromosome in case II (case III)} \\ 1 \le \dfrac{1}{a_i(1-\Delta x) + \Delta x} \le \dfrac{1}{\Delta x}, & E_i\ (S) \text{ localized outside chromosome in case II (case} \end{cases} \tag{65}$$

  This implies that the binding may be very weak (even zero) when localization is near the chromosome and the size of the diffusing species is large (with respect to r^*). This implies that the binding may be strong (relative to a well-mixed model) when localization is near the poles and the size of the diffusing species is large (with respect to r^*).

Simulation Set ups: For all simulation on this paper we modeled the normalized chromosome density $\hat{\rho}(x)$ based on [13], thus

$$\hat{\rho}(x) \propto \frac{1}{1+e^{20(x-1/2)}},$$

where x is in its dimensionless form and the proportionality constant is chosen such that $\int_0^1 \hat{\rho}(x)dx = 1$.

1.6 Protein Production: Transcription and Translation

We consider n genes (D_i) being transcribed by RNAP (S) to form a DNA-RNAP complex ($c_{s,i}$) to produce mRNA (m_i) which is translated by ribosomes (R) to form mRNA-ribosome complex ($c_{m,i}$) which produces protein P_i. The mRNA's degrade at rate γ_i. The DNA, RNAP, and ribosomes are produced at rates

$\alpha_{D,i}$(t,x), $\alpha_s(t,x)$, $\alpha_r(t,x)$, respectively. We assume all species dilute at rate μ, the cells growth rate. The corresponding biochemical reactions are:

$$\underbrace{\mathrm{D_i + S \underset{d_{s,i}}{\overset{a_{s,i}}{\rightleftharpoons}} c_{s,i} \xrightarrow{\kappa_{s,i}} m_i + S + D_i}}_{\text{transcription, case II}}, \quad \underbrace{\mathrm{m_i + R \underset{d_{m,i}}{\overset{a_{m,i}}{\rightleftharpoons}} c_{m,i} \xrightarrow{\kappa_{m,i}} P_i + R + m_i}}_{\text{translation, case I}}$$

$$\emptyset \xrightarrow{\alpha_{D,i}} \mathrm{D_i}, \quad \emptyset \xrightarrow{\alpha_s} \mathrm{S}, \quad \emptyset \xrightarrow{\alpha_r} \mathrm{R}, \quad \mathrm{m_i} \xrightarrow{\gamma_i} \emptyset, \quad \mathrm{C_{m,i}} \xrightarrow{\gamma_i} \mathrm{R},$$

where γ_i is the mRNA degradation rate, $a_{s,i}$ and $d_{s,i}$ are the association and disassociation rate constants, respectively, between RNAP and the gene $\mathrm{D_i}$, $\kappa_{s,i}$ is the catalytic rate of formation of mRNA $\mathrm{m_i}$, $a_{m,i}$ and $d_{m,i}$ are the association and disassociation rate constants, respectively, between ribosomes and mRNA , $\kappa_{m,i}$ is the catalytic rate of formation of protein $\mathrm{P_i}$.

Spatial-temporal Dynamics: The dynamics corresponding to these biochemical reactions are given by:

$$\frac{\partial D_i(t,x)}{\partial t} = \alpha_{D,i}(t,x) - a_{s,i}S(t,x)D_i(t,x) + (d_{s,i} + \kappa_{s,i})c_{s,i}(t,x) - D_i(t,x), \tag{66a}$$

$$\frac{\partial c_{s,i}(t,x)}{\partial t} = a_{s,i}S(t,x)D_i(t,x) - (d_{s,i} + \kappa_{s,i})c_{s,i}(t,x) - c_{s,i}(t,x), \tag{66b}$$

$$\frac{\partial S(t,x)}{\partial t} = \mathcal{L}_s(S) + \alpha_s(t,x) + \sum_{i=1}^{n}\big[-a_{s,i}D_i(t,x)S(t,x) + (d_{s,i} + \kappa_{s,i})c_{s,i}(t,x)\big] - S(t,x), \tag{66c}$$

$$\frac{\partial m_i(t,x)}{\partial t} = \mathcal{L}_{m_i}(m_i) + \kappa_{s_i}c_{s,i}(t,x) - a_{m,i}m_i(t,x)R(t,x) + (\kappa_{m,i} + d_{m,i})c_{m,i}(t,x) - (1+\gamma_i)m_i(t,x), \tag{66d}$$

$$\frac{\partial c_{m,i}(t,x)}{\partial t} = \mathcal{L}_{c_i}(c_{m,i}) + a_{m,i}m_i(t,x)R(t,x) + (\kappa_{m,i} + d_{m,i})c_{m,i}(t,x) - (1+\gamma_i)m_i(t,x), \tag{66e}$$

$$\frac{\partial R(t,x)}{\partial t} = \mathcal{L}_R(R) + \alpha_R(t,x) + \sum_{j=1}^{n}\big[a_{m,j}m_j(t,x)R(t,x) + (\kappa_{m,j} + d_{m,j} + \gamma_{m,j})c_{m,j}(t,x)\big] - R(t,x). \tag{66f}$$

where the spatial variable has been normalized by L (cell-length) and the time variable has been normalized by $1/\mu$ the time scale associated with dilution. The flux dynamics and boundary conditions are given by,

$$\mathcal{L}_{m_i}(m_i) = -\frac{d}{dx}\big[J_{m_i}(x,m_i)\big], \quad J_{m_i}(x,m_i) = -\chi_{m_i}v_{m_i}(x)^2\frac{d}{dx}\big[v_{m_i}(x)^{-1}m_i\big], \quad J_{m_i}(x,m_i)\big|_{x=0,1} = 0,$$

$$\mathcal{L}_{c_i}(c_{m,i}) = -\frac{d}{dx}\big[J_{c_i}(x,c_{m,i})\big], \quad J_{c_i}(x,c_{m,i}) = -\chi_{c_i}v_{c_i}(x)^2\frac{d}{dx}\big[v_{c_i}(x)^{-1}c_{m,i}\big], \quad J_{c_i}(x,c_{m,i})\big|_{x=0,1} = 0,$$

$$\mathcal{L}_R(R) = -\frac{d}{dx}\big[J_R(x,R)\big], \quad J_R(x,R) = -\chi_R v_R(x)^2\frac{d}{dx}\big[v_R(x)^{-1}R\big], \quad J_R(x,R)\big|_{x=0,1} = 0,$$

$$\mathcal{L}_s(S) = -\frac{d}{dx}\big[J_s(x,S)\big], \quad J_s(x,S) = -\chi_s v_s(x)^2\frac{d}{dx}\big[v_s(x)^{-1}S\big], \quad J_s(x,S)\big|_{x=0,1} = 0.$$

where $v_{m_i}(x)$, $v_{c_i}(x)$, $v_R(x)$, and $v_s(x)$ are the available volume profiles for the mNA, mRNA-ribosome complex, ribosome, and RNAP, respectively and $\chi_{m_i} = D_{m_i}/(L^2\mu)$, $\chi_{c_i} = D_{c_i}/(L^2\mu)$, $\chi_R = D_R/(L^2\mu)$, D_{c_i}, and $\chi_s = D_s/(L^2\mu)$, D_s are dimensionless diffusion coefficients for the mNA, mRNA-ribosome complex, ribosome, and RNAP, respectively. The spaced average protein concentration $\bar{P}_i(t)$ is given by

$$\frac{d\bar{P}_i(t)}{dt} = \kappa_{m,i}\bar{c}_{m,i}(t) - \bar{P}_i(t), \quad \text{with} \quad \bar{c}_{m,i}(t) = \int_0^1 c_{m,i}(t,x)dx.$$

Values for dimensionless parameters:

We set all production rates with respect to that of RNAP such that $\bar{\alpha}_S = \int_0^1 \alpha_S(x)dx = 1$. All time scales relative to $\mu = 0.5$ 1/hr, consistent with the experiments [50] The total number of RNAP (N_{RNAP}) ranges

between 2,000 -10,000 we took it to be 5,000 [14]. The total number of ribosomes (N_{ribo}) was taken to be $10,000$ and since both RNAP and ribosomes and RNAP are stable, it implies $\bar{\alpha}_r = \int_0^1 \alpha_r(x)dx = \frac{N_{\text{ribo}}}{N_{\text{RNAP}}} = 2$. mRNA degradation is about 10 times faster than dilution [2], therefore, we took $\gamma_i = 10$ for all i. The rate of transcription (translation) is about 80 (40) times faster than dilution [2], thus we choose $\kappa_{s,i} = 80$ and $\kappa_{m,i} = 40$ for all i. We assumed that the DNA is on a high copy plasmid (500 copies) and thus $\bar{\alpha}_{D,i} = \int_0^1 \alpha_{D,i}(x)dx = \frac{N_{\text{DNA}}}{N_{\text{RNAP}}} = 0.1$.

The association and dissociation rate constants are varied as shown below to show that all of our results hold dispiite fast binding and unbinding but we maintain the ratio $d_{s,i}/a_{s,i} = d_{m,i}/a_{m,i} = 1$,for all i in all our simulations.

The length of the cell is about 3μm and thus $L = 1.5\mu$m [13]. The diffusion coefficient of RNAP is taken to be $D_s = 0.22\mu m^2/s$ [51] and thus $\chi_s = 704$. The diffusion coefficient of free ribosomes is taken to be $D_r = 0.4\mu m^2/s$ [13] and thus $\chi_r = 1280$. In [14], the diffusion coefficient of polysomes is $0.05 \pm 0.02\mu m^2/s$, and thus we take the diffusion coefficient of a free mRNA to be the upper bound $0.07\mu m^2/s$ and thus $\chi_{m,i} = 224$.

For the following, the spatial profiles for the production rates are given proportional to their functional form since the constant that fully specifies them is such that the production rate per-cell is as satisfies the above.

Additional simulation details for Figure 4-A in the main text: $\alpha_D(x) \propto e^{-20x}$ when DNA near mid cell and $\alpha_D(x) \propto e^{20(x-1)}$ when DNA at cell poles. The RNAP production was kept roughly spatially constant $\alpha_s(x) \propto e^{-.001x}$. The binding and unbinding coefficients for DNA-RNAP were $a_s = 1000$ and $d_s = 1000$.

Additional simulation details for Figure 4-B in the main text: $\alpha_D(x) \propto e^{-.001x}$ is chosen to be roughly constant. The RNAP production was kept roughly spatially constant $\alpha_s(x) \propto e^{-.001x}$. The ribosome production was kept roughly spatially constant $\alpha_r(x) \propto e^{-.001x}$. The RNAP radius of gyration was taken to be $r_s/r^* = 0.001$ such that its excluded volume effects were negligible. The binding and unbinding coefficients for DNA-RNAP were $a_s = 1000$ and $d_s = 1000$. The binding and unbinding coefficients for ribosome-mRNA were $a_m = 1000$ and $d_m = 1000$.

1.7 Transcription Factor Regulation

Intracellular signaling to control gene expression is often done via transcription factors (TFs). In this section we model a general transcription factor architecture where the repressor $\mathrm{P_r}$ dimerizes to form $\mathrm{c_1}$ (e.g., TetR dimerizes before targeting gene [33]) and then blocks the transcription of gene D that produces protein P. The biochemical reactions corresponding to this process are:

$$\emptyset \xrightarrow{\alpha} \mathrm{P_r}, \quad \underbrace{\mathrm{P_r} + \mathrm{P_r} \underset{\mathrm{d_1}}{\overset{\mathrm{a_1}}{\rightleftharpoons}} \mathrm{c_1},}_{\text{Case I}} \quad \underbrace{\mathrm{c_1} + \mathrm{D} \underset{\mathrm{d_2}}{\overset{\mathrm{a_2}}{\rightleftharpoons}} \mathrm{c_2},}_{\text{Case II}} \quad \mathrm{D} \xrightarrow{\kappa} \mathrm{P}, \tag{67}$$

where α is the production rate of $\mathrm{P_r}$, a_1 (d_1) is the association (disassociation) constant to form the $\mathrm{c_1}$ complex, a_2 (d_2) is the association (disassociation) constant to form the the $\mathrm{c_2}$ complex, and κ is the catalytic rate to produce protein P. Since the repressor $\mathrm{P_r}$, freely diffuses, the dimerization reaction belongs to Case I. The gene D is spatially fixed and it is repressed by the freely diffusing $\mathrm{c_1}$, thus this interaction falls under Case II. We assume that the total concentration of D is conserved, so that $D_T(x) = D(t,x) + c_2(t,x)$. The reaction diffusion equations corresponding to (67) are

$$\frac{\partial P_r(t,x)}{\partial t} = \chi_r \frac{d}{dx}\left[v_{P_r}^2(x)\frac{d}{dx}\left[\frac{P_r(t,x)}{v_{P_r}(x)}\right]\right] + \alpha(t,x) - \gamma_r P_r(t,x), \tag{68a}$$

$$\frac{\partial c_1(t,x)}{\partial t} = \chi_c \frac{d}{dx}\left[v_{c_1}^2(x)\frac{d}{dx}\left[\frac{c_1(t,x)}{v_{c_1}(x)}\right]\right] + a_1 P_r^2(t,x) - d_1 c_1(t,x) - a_2 c_1(t,x) D(t,x) + d_2 c_2(t,x), \tag{68b}$$

$$\frac{\partial c_2(t,x)}{\partial t} = a_2 c_1(t,x) D(t,x) - d_2 c_2(t,x), \tag{68c}$$

$$D(t,x) = D_T(x) - c_2(t,x), \tag{68d}$$

where $v_{P_r}(x)$ ($\chi_r = D_r/(L^2\mu)$) and $v_{c_1}(x)$ ($\chi_c = D_{c_1}/(L^2\mu)$) are the available volume profiles (dimensionless diffusion coefficients) of $\mathrm{P_r}$ and $\mathrm{c_1}$, respectively, and from (9), $v_{c_1}(x) = v_{P_r}^2(x)$. The boundary conditions

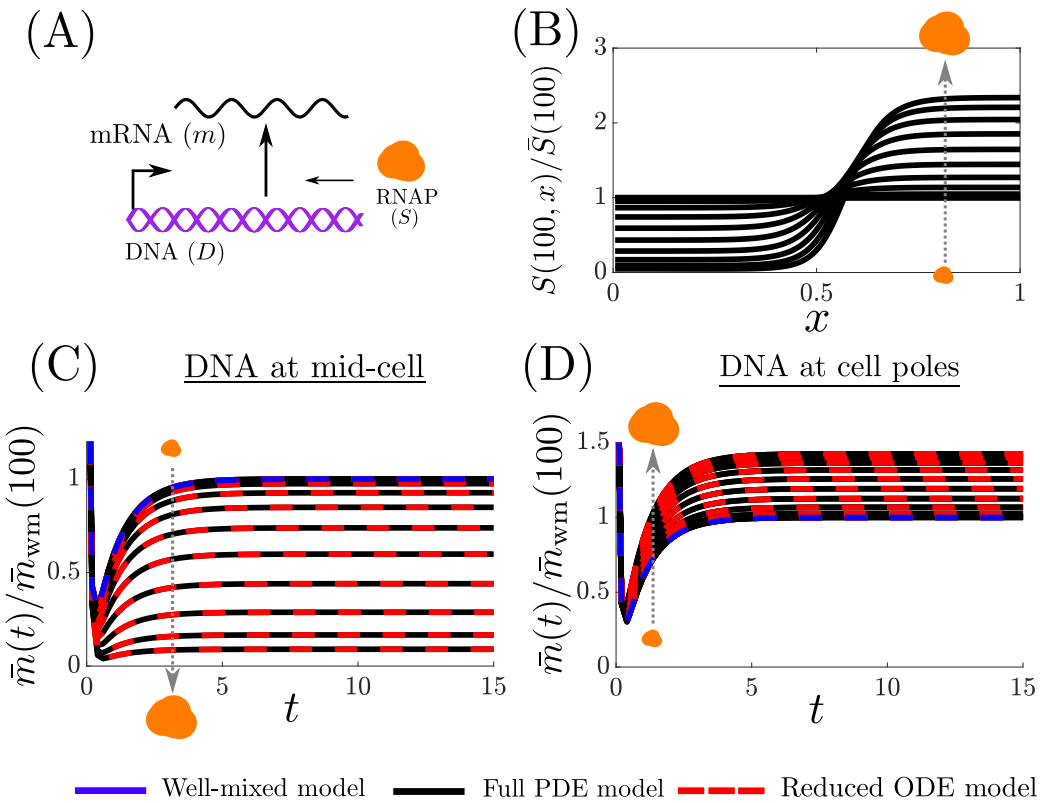

Figure 8: **RNAP steady state spatial profiles and space averaged mRNA transients** For the following we refer to the well-mixed model as (14) with (15) given by $\theta_{s,i} = 1$ and $\theta_{r,i} = 1$ for all i. Here time is nondimensionalized with the time scale associated with dilution. (A) DNA transcribed by RNAP (S) to form mRNA (m) (B) The steady state RNAP spatial profile predicted by (66), normalized by spatial averaged value. From the results on the main text this should mirror the normalized available volume profile, which it does (Remark 2). Note as the size of RNAP increases, it is further excluded from the chromosome. (C) The temporal space-average concentration of mRNA when the DNA is localized mid-cell for several sizes of RNAP for the well-mixed model, reduced ODE model (14) , and PDE (66). (D) The temporal space-average concentration of mRNA when the DNA is localized near the cell poles for several sizes of RNAP for the well-mixed model, reduced ODE model (14) , and PDE (66). The simulation set up and parameters are identical to those of Figure 4-A.

corresponding to (68) are

$$\left[v_{P_r}^2(x)\frac{d}{dx}\left[\frac{P_r(t,x)}{v_{P_r}(x)}\right]\right]_{x=0,1} = 0, \quad \left[v_{c_1}^2(x)\frac{d}{dx}\left[\frac{c_1(t,x)}{v_{c_1}(x)}\right]\right]_{x=0,1} = 0.$$

Values for dimensionless parameters: The growth rate we used to nondimensionalize the time scales was $\mu = 0.5$ 1/hr, consistent with the experiments [50]. The length of the cell is about 3μm and thus $L = 1.5\mu$m [13]. The diffusion coefficient of the transcription factor is taken to be $D_r = D_{c_1} = 0.4\mu m^2/s$ (that of LacI) [52] and thus $\chi_r = \chi_c = 1280$. The transcription factor was assumed to be stale thus $\gamma_r = \mu$. The total concentration of D given by $\bar{D}_T$ was used to nondimensionalize the other concentration variables such that $\bar{D}_T = 1$.

Additional simulation details for Figure 5 in the main text: $D_T(x) \propto e^{-20x}$ when DNA near mid cell and $D_T(x) \propto e^{20(x-1)}$ when DNA at cell poles. The transcription factor production was kept roughly spatially constant $\alpha_s(x) \propto e^{-.001x}$. The binding and unbinding coefficients were chosen to be $a_1 = a_2 = 1000$ and $d_1 = d_2 = 1000$ such that the dissociations constants $K_{d,1} = \frac{d_1}{a_1} = K_{d,2} = \frac{d_2}{a_2} = 1$.

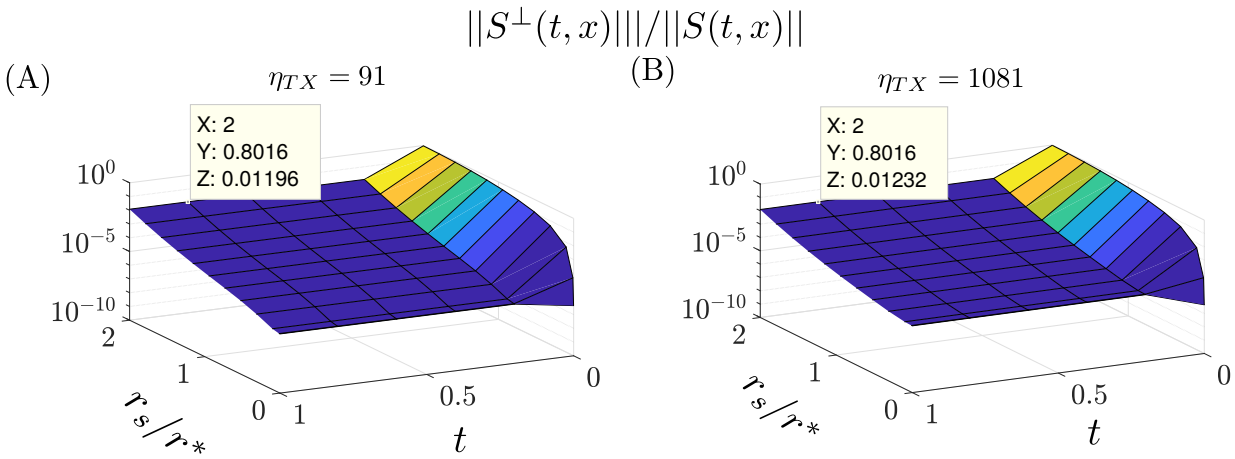

Figure 9: **The error in the RNAP approximation for several binding and unbinding speeds between DNA and RNAP** Let $S(t,x)$ be as in (66) and $S^{\perp}(t,x) = S(t,x) - \bar{S}(t)\hat{v}_s(x)$ be the a measure of the error in our approximation, where $||y(t,x)|| = (\int_0^1 (y^2(t,x)))^{1/2}$, and $\eta_{\mathrm{TX}} = 1/(\kappa_s + d_s + 1)$. The values of η_{TX} are varied by modifying d_s while maintaining $a_s/d_s = 1$. Here time is nondimensionalized with the time scale associated with dilution. (A) The relative error in time for several values of r_s for $\eta_{\mathrm{TX}} = 91 \implies d_s = 10$. (B) The relative error in time for several values of r_s for $\eta_{\mathrm{TX}} = 1081 \implies d_s = 1000$. For both values of η_{TX} the error is high at $t = 0$ since the initial RNAP spatial profile is chosen to be a constant but quickly decays to less than 2%. The rest of the simulation set up and parameters are identical to those of Figure 4-A.

1.8 Oscillator

Now we consider the repressor activator clock genetic circuit [36]. This circuit produces sustained oscillations if tuned within an appropriate parameter range [37, 1]. The circuit consists of two proteins $\mathrm{P_a}$ and $\mathrm{P_r}$. Protein $\mathrm{P_a}$, is an activator which dimerizes to form $\mathrm{P_{a,2}}$ and then binds to its own gene $\mathrm{D_a}$ to form complex $\mathrm{c_{a,1}}$ to initiate transcription. The dimer $\mathrm{P_{a,2}}$ also finds to the gene $\mathrm{D_r}$, which transcribes $\mathrm{P_r}$ to form complex $\mathrm{c_{a,2}}$ and initiates transcription. Protein $\mathrm{P_r}$, dimerizes to form $\mathrm{P_{r,2}}$ and then represses $\mathrm{P_a}$ by binding to $\mathrm{D_a}$ to form complex $\mathrm{c_r}$. The biochemical equations corresponding to this circuit are:

$$\underbrace{\mathrm{P_a} + \mathrm{P_a} \underset{\mathrm{d_1}}{\overset{\mathrm{a_1}}{\rightleftharpoons}} \mathrm{P_{a,2}},}_{\text{Case I, } \mathrm{P}_a \text{ diffuses}} \quad \underbrace{\mathrm{P_r} + \mathrm{P_r} \underset{\mathrm{d_2}}{\overset{\mathrm{a_2}}{\rightleftharpoons}} \mathrm{P_{r,2}},}_{\text{Case II, } \mathrm{P}_r \text{ diffuses}} \quad \underbrace{\mathrm{P_{a,2}} + \mathrm{D_a} \underset{\mathrm{d_3}}{\overset{\mathrm{a_3}}{\rightleftharpoons}} \mathrm{c_{a,1}}, \quad \mathrm{P_{r,2}} + \mathrm{D_a} \underset{\mathrm{d_5}}{\overset{\mathrm{a_5}}{\rightleftharpoons}} \mathrm{c_r},}_{\text{Case III, } \mathrm{P}_{a,2} \text{ and } \mathrm{P}_{r,2} \text{ diffuse and } \mathrm{D_a} \text{ fixed}} \quad \underbrace{\mathrm{P_{a,2}} + \mathrm{D_r} \underset{\mathrm{d_4}}{\overset{\mathrm{a_4}}{\rightleftharpoons}} \mathrm{c_{a,2}},}_{\text{Case II, } \mathrm{P}_{a,2} \text{ diffuse and } \mathrm{D_r} \text{ fixed}} \tag{69a}$$

$$\mathrm{D_a} \xrightarrow{\kappa_1} \mathrm{P_a}, \quad \mathrm{D_r} \xrightarrow{\kappa_2} \mathrm{P_r}, \quad \mathrm{P_a} \xrightarrow{\gamma_a} \emptyset, \quad \mathrm{P_r} \xrightarrow{\gamma_r} \emptyset, \quad \mathrm{c_{a,1}} \xrightarrow{\kappa_3} \mathrm{P_a}, \quad \mathrm{c_{a,2}} \xrightarrow{\kappa_4} \mathrm{P_r}, \tag{69b}$$

where a_i (d_i) for $i = 1, \ldots, 5$ are association (disassociation) rate constants, γ_a (γ_r) is the degradation rate of $\mathrm{P_a}$ ($\mathrm{P_r}$) κ_1 (κ_2) is the basal rate at which gene $\mathrm{D_a}$ ($\mathrm{D_r}$) is transcribed, and κ_3 (κ_4) is the rate at which the DNA-transcription-factor complexes are transcribed for $\mathrm{D_a}$ ($\mathrm{D_r}$). We assume that the total concentration of $\mathrm{D_a}$ is conserved, so that $D_{a,T}(x) = D_a(t,x) + c_{a,1}(t,x) + c_r(t,x)$. Similarly, we assume that the total concentration of $\mathrm{D_r}$ is conserved, so that $D_{r,T}(x) = D_r(t,x) + c_{a,2}(t,x)$. The spatiotemporal dynamics describing (69) are given by

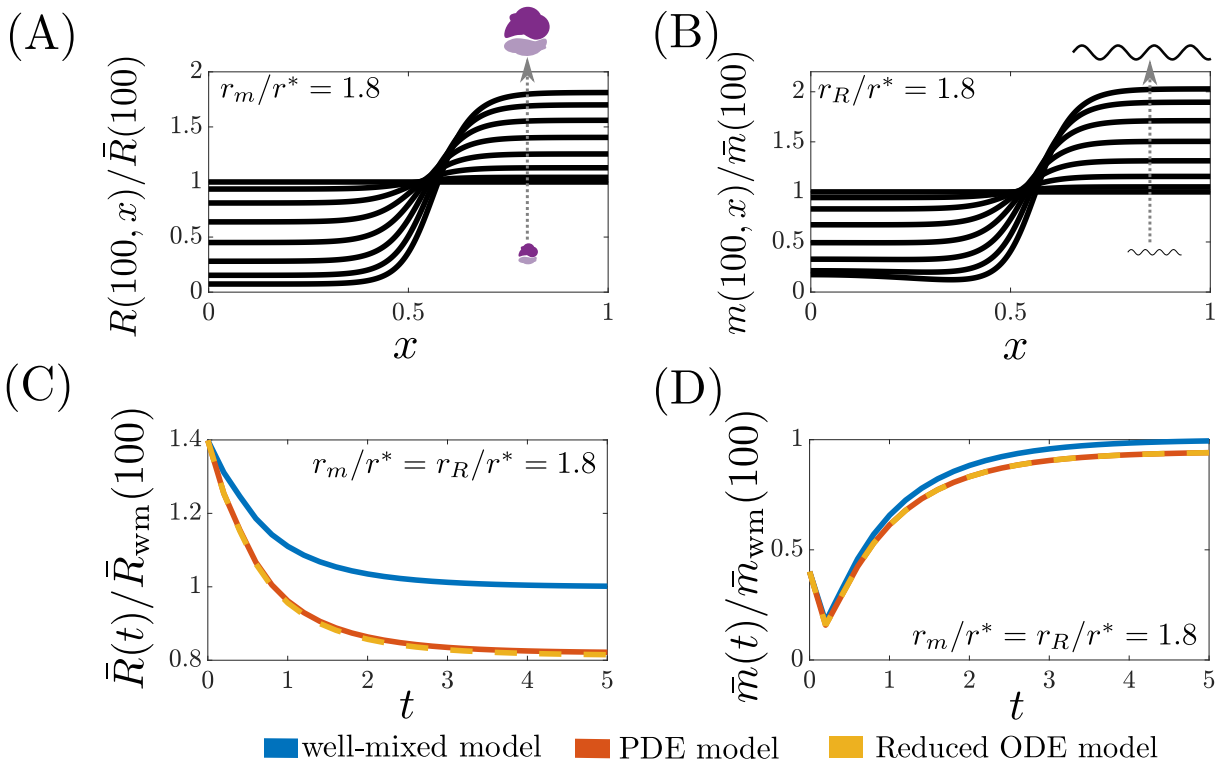

Figure 10: **Ribosome and mRNA steady state spatial profiles and space averaged transients** For the following we refer to the well-mixed model as (14) with (15) given by $\theta_{s,i} = 1$ and $\theta_{r,i} = 1$ for all i. Here time is nondimensionalized with the time scale associated with dilution. (A) The steady state ribosome spatial profile predicted by (66), normalized by spatial averaged value. From the results on the main text this should mirror the normalized available volume profile, which it does. Note as the size of the ribosome increases, it is further excluded from the chromosome. (B) The steady state mRNA spatial profile predicted by (66), normalized by spatial averaged value. From the results on the main text this should mirror the normalized available volume profile, which it does. Note as the size of the mRNA increases, it is further excluded from the chromosome. (C) The temporal space-averaged concentration of ribosomes normalized by the steady state of the well-mixed model for the reduced ODE model (14) and the PDE model (66) when $r_m/r^* = r_R/r^* = 1.8$. (D)The temporal space-averaged concentration of mRNA normalized by the steady state of the well-mixed model for the reduced ODE model (14) and the PDE model (66) when $r_m/r^* = r_R/r^* = 1.8$. The simulation set up and parameters are identical to those of Figure 4-B.

$$
\begin{aligned}
\frac{\partial P_a(t,x)}{\partial t} &= \chi_a \frac{d}{dx}\left[v_{P_a}^2(x)\frac{d}{dx}\left[\frac{P_a(t,x)}{v_{P_a}(x)}\right]\right] + \kappa_1 D_a(t,x) + \kappa_3 c_{a,1}(t,x) - \gamma_a P_a(t,x),\\
\frac{\partial P_r(t,x)}{\partial t} &= \chi_r \frac{d}{dx}\left[v_{P_r}^2(x)\frac{d}{dx}\left[\frac{P_r(t,x)}{v_{P_r}(x)}\right]\right] + \kappa_2 D_r(t,x) + \kappa_4 c_{a,2}(t,x) - \gamma_r P_r(t,x),\\
\frac{\partial P_{a,2}(t,x)}{\partial t} &= \chi_a \frac{d}{dx}\left[v_{P_{a,2}}^2(x)\frac{d}{dx}\left[\frac{P_{a,2}(t,x)}{v_{P_{a,2}}(x)}\right]\right] + a_1 P_a^2(t,x) - d_1 P_{a,2}(t,x)\\
&\quad - a_3 P_{a,2}(t,x) D_a(t,x) + d_3 c_{a,1}(t,x) - a_4 P_{a,2}(t,x) D_r(t,x) + d_4 c_{a,2}(t,x),\\
\frac{\partial P_{r,2}(t,x)}{\partial t} &= \chi_r \frac{d}{dx}\left[v_{P_{r,2}}^2(x)\frac{d}{dx}\left[\frac{P_{r,2}(t,x)}{v_{P_{r,2}}(x)}\right]\right] + a_2 P_r^2(t,x) - d_2 P_{r,2}(t,x)\\
&\quad - a_5 P_{r,2}(t,x) D_a(t,x) + d_5 c_r(t,x),\\
\frac{\partial c_{a,1}(t,x)}{\partial t} &= a_3 P_{a,2}(t,x) D_a(t,x) - d_3 c_{a,1}(t,x), \qquad \frac{\partial c_{a,2}(t,x)}{\partial t} = a_4 P_{a,2}(t,x) D_r(t,x) - d_4 c_{a,2}(t,x),\\
\frac{\partial c_r(t,x)}{\partial t} &= a_5 P_{r,2}(t,x) D_a(t,x) - d_5 c_r(t,x),\\
D_a(t,x) &= D_{a,T}(x) - c_{a,1}(t,x) - c_r(t,x), \quad D_r(t,x) = D_{r,T}(x) - c_{a,2}(t,x)
\end{aligned}
\tag{70}
$$

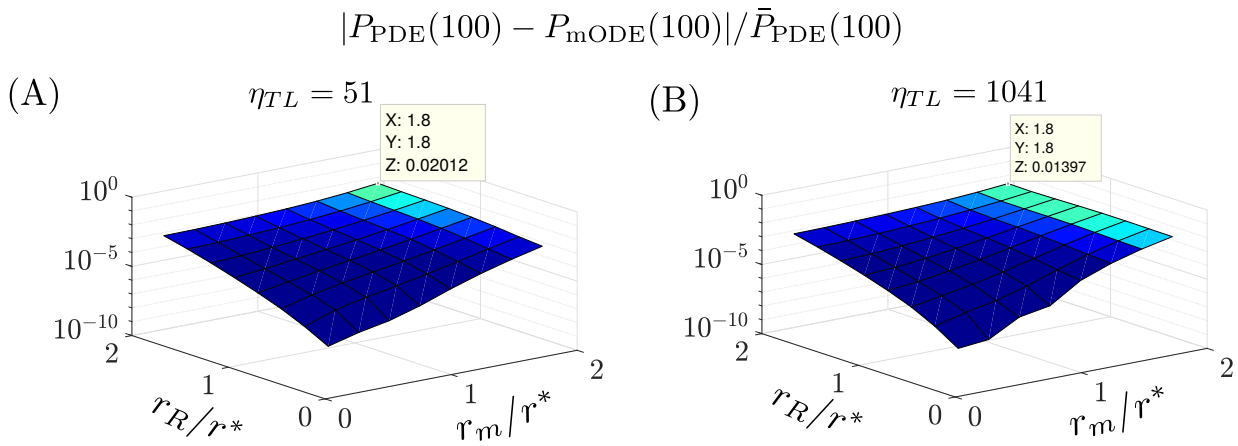

Figure 11: **PDE and reduced ODE model agree well in protein production example** Let $P_{\mathrm{PDE}}(100)$ be the steady state protein space averaged concentration predicted by (66) and $P_{\mathrm{ODE}}(100)$ be the steady state protein space averaged concentration predicted by (14). Let $\eta_{\mathrm{TL}} = 1/(\kappa_m + d_m + 1 + \gamma_m)$. The values of η_{TL} are varied by modifying d_m while maintaining $a_m/d_m = 1$. (A) The relative error for several values of r_m and r_s for $\eta_{\mathrm{TL}} = 51 \implies d_m = 10$. (B) The relative error for several values of r_m and r_s for $\eta_{\mathrm{TX}} = 1041 \implies d_m = 1000$. For both cases the relative error is less than 2.1% The rest of the simulation set up and parameters are identical to those of Figure 4-B.

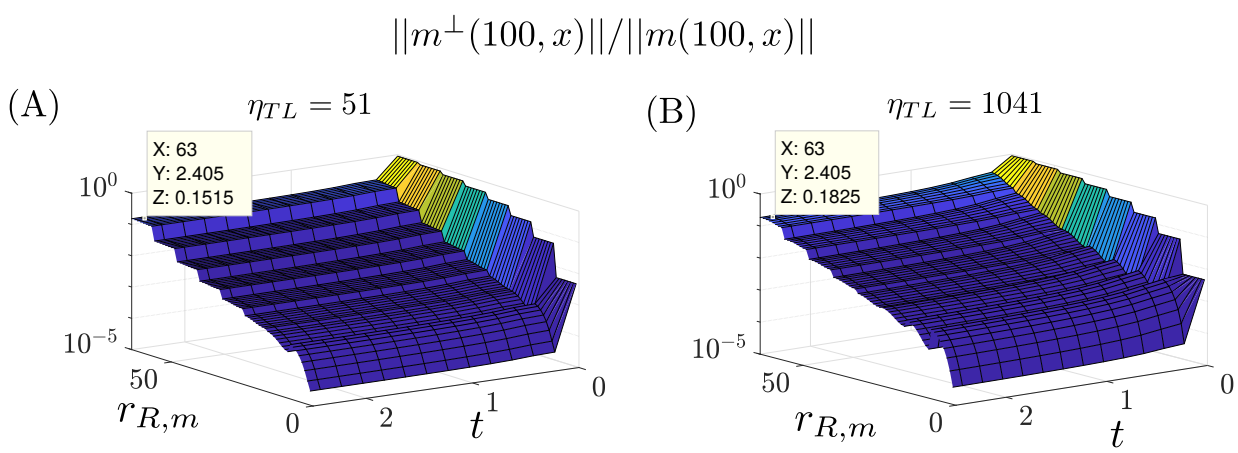

Figure 12: **The error in the mRNA approximation for several binding and unbinding speeds between mRNA and ribosome** Let $m(t, x)$ be as in (66) and $m^{\perp}(t, x) = m(t, x) - \bar{m}(t)\hat{v}_m(x)$ be the a measure of the error in our approximation, where $||y(t, x)|| = (\int_0^1 (y^2(t, x)))^{1/2}$, and $\eta_{\mathrm{TL}} = 1/(\kappa_m + d_m + 1 + \gamma_m)$. The values of η_{TL} are varied by modifying d_m while maintaining $a_m/d_m = 1$. Here r_R, m is a sequence corresponding to the mRNA and ribosome pairs from Figure 4-B. Here time nondimensionalized with the time scale associated with dilution. (A) The relative error in time for several values of r_R, m for $\eta_{\mathrm{TL}} = 51 \implies d_s = 10$. (B) The relative error in time for several values of r_R, m for $\eta_{\mathrm{TL}} = 1041 \implies d_s = 1000$. For both values of η_{TL} the error is high at $t = 0$ since the initial mRNA spatial profile is chosen to be a constant but quickly decays to less than 20%. The rest of the simulation set up and parameters are identical to those of Figure 4-B.

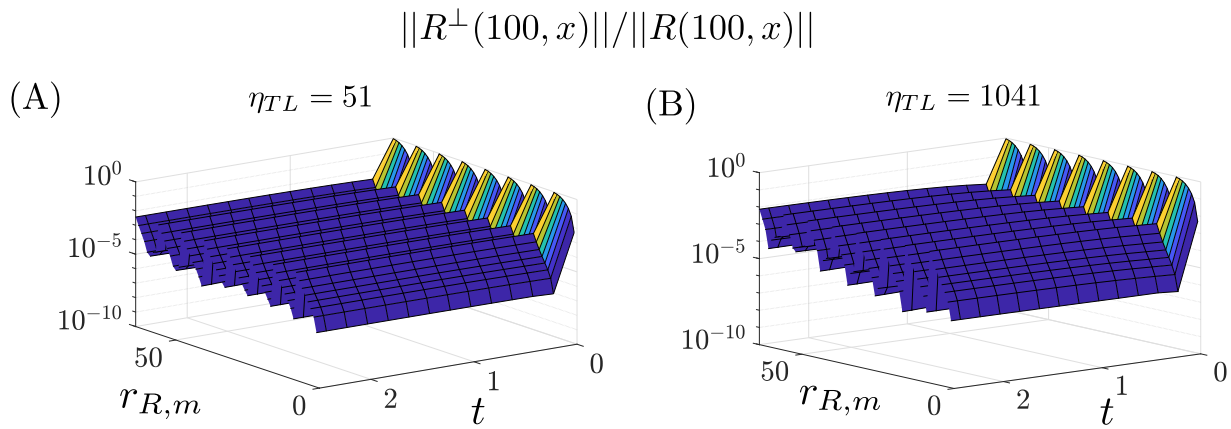

Figure 13: **The error in the ribosome approximation for several binding and unbinding speeds between mRNA and ribosome** Let $m(t,x)$ be as in (66) and $R^{\perp}(t,x) = R(t,x) - \bar{R}(t)\hat{v}_r(x)$ be the a measure of the error in our approximation, where $||y(t,x)|| = (\int_0^1 (y^2(t,x)))^{1/2}$, and $\eta_{\text{TL}} = 1/(\kappa_m + d_m + 1 + \gamma_m)$. The values of η_{TL} are varied by modifying d_m while maintaining $a_m/d_m = 1$. Here r_R, m is a sequence corresponding to the mRNA and ribosome pairs from Figure 4-B. Here time nondimensionalized with the time scale associated with dilution. (A) The relative error in time for several values of r_R, m for $\eta_{\text{TL}} = 51 \implies d_s = 10$. (B) The relative error in time for several values of r_R, m for $\eta_{\text{TL}} = 1041 \implies d_s = 1000$. For both values of η_{TL} the error is high at $t = 0$ since the initial mRNA spatial profile is chosen to be a constant but quickly decays to less than 1%. The rest of the simulation set up and parameters are identical to those of Figure 4-B.

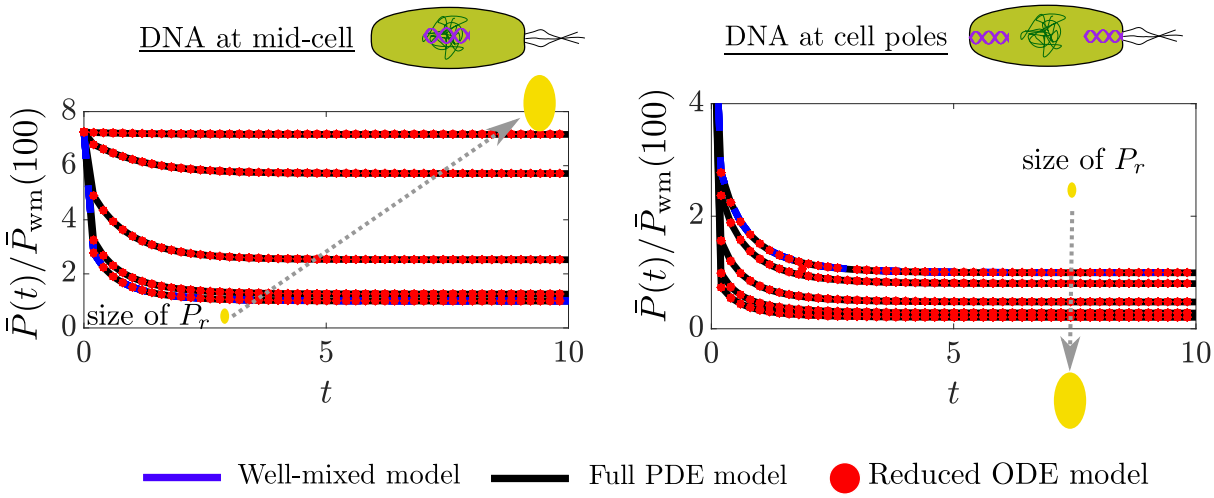

Figure 14: **Transcription factor regulation transient response** The transient response corresponding to Figure 5 in the main text when $\bar{P}_r/K = 2.5$

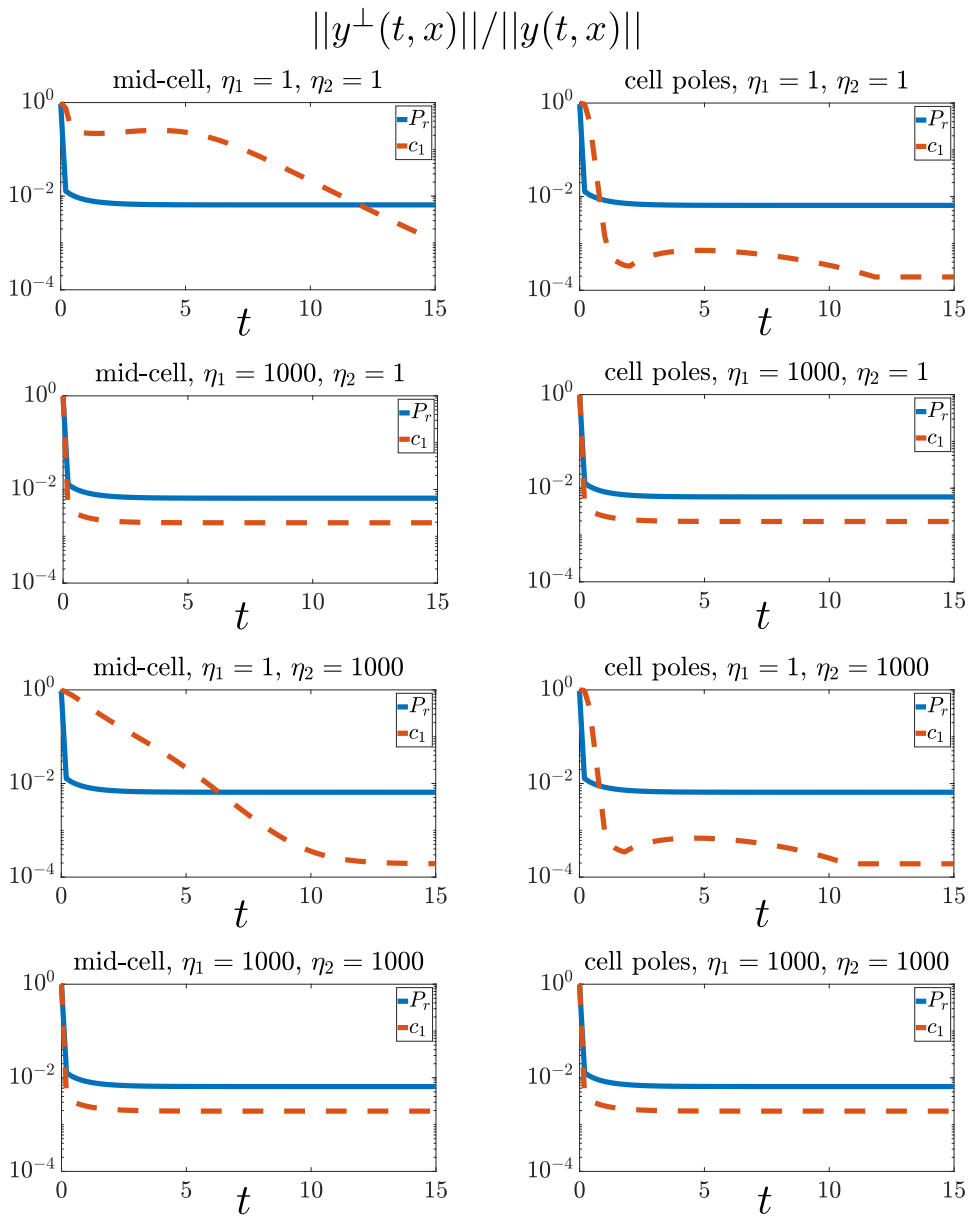

Figure 15: **Infinite dimensional dynamics decay in time independently of binding/unbinding speed** Let $y(t,x)$ be as in (68) (represents $P_r(t,x)$ or $c_1(t,x)$) and let $y^{\perp}(t,x) = y(t,x) - \bar{y}(t)v(x)$ be the a measure of the error in our approximation, where $v(x)$ is the available volume profile of the species. Let $||y(t,x)|| = (\int_0^1 (y^2(t,x)))^{1/2}$, $\eta_1 = d_1/\mu$, and $\eta_2 = d_2/\mu$ and recall that in the simulations we keep $d_1/a_1 = d_2/a_2 = 1$. We show $||y^{\perp}||/||y||$, the relative error for several values of η_1 and η_2 over dimensionless time (with respect to μ) both when the DNA is near mid-cell and the cell poles. The other simulation parameters are identical to those used to generate Figure 5 in the main text. For each time point shown, we took the max relative error with respect to the sizes of $\mathrm{P_r}$ used to generate Figure 5. The error is high at $t = 0$ since the initial spatial profiles were chosen to be a constant but note that they quickly decay.

where $v_{P_a}(x)$, $v_{P_r}(x)$, $v_{P_{a,2}}(x)$, and $v_{P_{r,2}}(x)$ are the available volume profiles of $\mathrm{P_a}$, $\mathrm{P_r}$, $\mathrm{P_{a,2}}$, and $\mathrm{P_{r,2}}$, respectively, $\chi_a = D_a/(L^2\mu)$ is the dimensionless diffusion coefficient of $\mathrm{P_a}$ and $\mathrm{P_{a,2}}$, $\chi_r = D_r/(L^2\mu)$ is the dimensionless diffusion coefficient of $\mathrm{P_r}$ and $\mathrm{P_{r,2}}$. From (9), $v_{P_{a,2}}(x) = v^2_{P_a}(x)$ and $v_{P_{r,2}}(x) = v^2_{P_r}(x)$. The boundary conditions corresponding to (70) are

$$\left[v^2_{P_a}(x)\frac{d}{dx}\left[\frac{P_a(t,x)}{v_{P_a}(x)}\right]\right]_{x=0,1} = 0, \quad \left[v^2_{P_r}(x)\frac{d}{dx}\left[\frac{P_r(t,x)}{v_{P_r}(x)}\right]\right]_{x=0,1} = 0,$$

$$\left[v^2_{P_{a,2}}(x)\frac{d}{dx}\left[\frac{P_{a,2}(t,x)}{v_{P_{a,2}}(x)}\right]\right]_{x=0,1} = 0, \quad \left[v^2_{P_{r,2}}(x)\frac{d}{dx}\left[\frac{P_{a,2}(t,x)}{v_{P_{r,2}}(x)}\right]\right]_{x=0,1} = 0.$$

Parameters for Figure 6 in the main text: The growth rate we used to nondimensionalize the time scales was $\mu = 0.5$ 1/hr, consistent with the experiments [50]. The length of the cell is about 3μm and thus $L = 1.5\mu$m [13]. The diffusion coefficient of the transcription factor is taken to be $D_a = D_r = 0.4\mu m^2/s$ (that of LacI) [52] and thus $\chi_a = \chi_r = 1280$. The following dimensionless parameters were chosen such that the well-mixed model displayed sustained oscillations: $a_1 = 220, d_1 = 1000, a_2 = 1000, d_2 = 1000, a_3 = 1000, d_3 = 1000, a_4 = 1000, d_4 = 1000, a_5 = 1000, d_5 = 1000, \kappa_3 = 250, \kappa_1 = .04, \kappa_4 = 30, \kappa_2 = .004, \gamma_a = 1, \gamma_r = 0.5$. Furthermore, we choose d_i and a_i for $i = 1, \ldots 5$ large, to demonstrate our results hold even for large binding and unbinding rates. The total concentration of $\mathrm{D_a}$ which is the same as $\mathrm{D_r}$ since we assume they are on the same plasmid, is given by $\bar{D}_T$ and it was used to nondimensionalize the other concentration variables such that $\bar{D}_T = 1$. The total DNA spatial profile was chosen as $D_T(x) \propto e^{50(x-1)}$ to model DNA at cell poles.

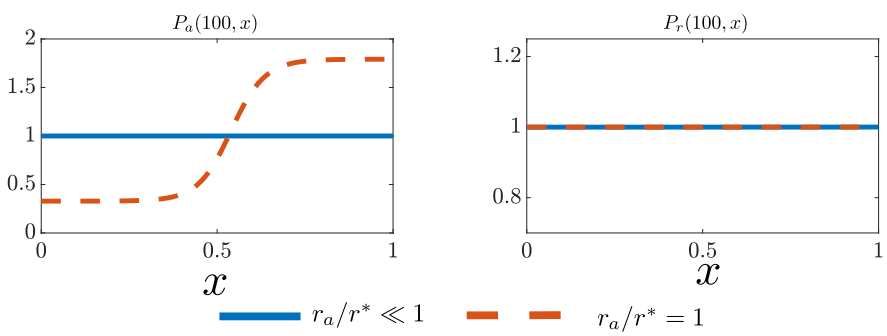

Figure 16: **The activator is excluded from the chromosome as its size increases** The steady state spatial profiles normalized by the average values for $\mathrm{P_a}$ and $\mathrm{P_r}$, that is $P_a(\infty,x)/\bar{P}_a(\infty)$ and $P_r(\infty,x)/\bar{P}_a(\infty)$ for the results of Figure 6 in the main text. As the size of $\mathrm{P_a}$ increases it is excluded from the chromosome. The repressor remains homogeneously distributed throughout the cell. The parameter values and simulation details are identical to those of Figure 6 in the main text.

1.9 Numerical Method Convergence Rate

For the simulation in Figure 4-A when the DNA is localize at the cell-poles and $r_s/r^* = 1$, we varied the number of spatial nodes used to discretize the spatial domain to demonstrate the convergence rate of our numerical scheme. Let N be the number of points used to discretize the spatial domain and let $\bar{m}_N(t)$ as the spaced average mRNA concentration for that given discretization. We considered when $N = 1024$ to be the true solution $m_{1024}(t)$ and thus define the following relative error

$$e_\infty = \max_{t\in[0,T]}\left|\frac{\bar{m}_N(t) - \bar{m}_{1024}(t)}{\bar{m}_{1024}(t)}\right|, \tag{71}$$

where we took its max value over the time interval of the simulation $t \in [0,T]$. The results from this numerical experiment are shown in Figure 17. The convergence rate of our numerical scheme is $\mathcal{O}(N^{-2})$ as expected for a second order finite difference numerical scheme.

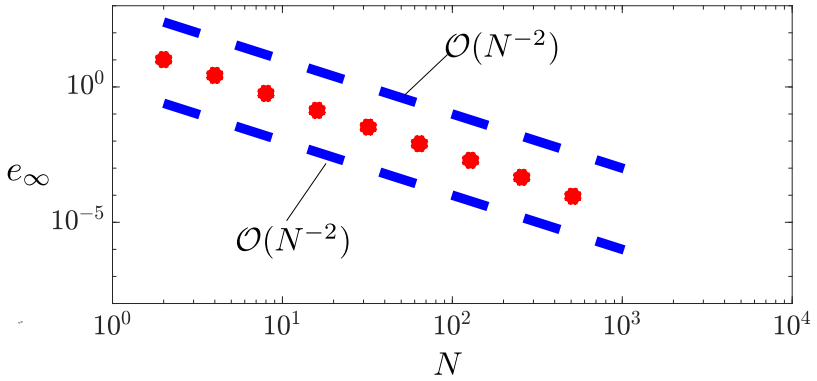

Figure 17: **Convergence rate of numerical scheme used to simulate PDEs in this work** For the simulation in Figure 4-A when the DNA is localize at the cell-poles and $r_s/r^* = 1$, we varied the number of spatial nodes used to discretize the spatial domain to demonstrate the convergence rate of our numerical scheme. Let N be the number of points used to discretize the spatial domain and let $\bar{m}_N(t)$ as the spaced average mRNA concentration for that given discretization. We considered when $N = 1024$ to be the true solution $m_{1024}(t)$ and the relative error e_∞ is given by (71). The relative error is given by the red markers and the blue dashed lines serve as references for $\mathcal{O}(N^{-2})$ convergence rates.